



Dissertation zur Erlangung des Doktorgrades
Der Fakultät für Chemie und Pharmazie
der Ludwig-Maximilian-Universität München

Dynamics of cortical actin in budding yeast
Saccharomyces cerevisiae

vorgelegt von
Haochen Yu
aus Chengdu, V.R.China

München, 2010

Tag der mündlichen Prüfung am 6. April 2010

Erster Gutachter: **Prof. Dr. Roland Beckmann**

Zweiter Gutachter: **Prof. Dr. Ralf-Peter Jansen**

Dissertation eingereicht in Fakultät für Chemie und Pharmazie am 22. Januar 2010

Erklärung

Diese Dissertation wurde im Sinne von § 13 Abs.3. bzw 4 der Promotionsordnung vom 29. Januar 1998 von Herrn *Dr. Roland Wedlich-Söldner* betreut und von Herrn *Prof. Ralf-Peter Jansen* vor der Fakultät für Chemie und Pharmazie vertreten.

Ehrenwörtliche Versicherung

Diese Dissertation wurde selbstständig, ohne unerlaubte Hilfe erarbeitet.

München, am

.....

Curriculum Vitae

Haochen Yu Alias: Jerry

Born on June 29th 1982, Chengdu, Sichuan, P.R.China

Bachelor of Applied Science with Honours (2nd upper Class, National University of Singapore)

Research Experience

Sept 2005 – PhD candidate in Max Planck Institute of Biochemistry, Martinsried, Germany. Project title: “The dynamics of cortical actomyosin in yeast.”
Advisors: Dr. Roland Wedlich-Söldner and Prof. Ralf-Peter Jansen.

May 2004 – Sept 2005 Assitant Research Officer in Mammalian Cell Biology group and Cell Dynamics group in Temasek Lifesciences Laboratory, Singapore. Project title: “Role of mammalian centrosomes in spindle positioning and orientation”. Advisors: Drs. Snezhana Oiliferenko and Maki Murata-Hori.

Higher Education

July 2000 – May 2004 B. Appl. Sc. (Hons 2nd class upper) in Department of Biological Sciences, National University of Singapore.

June 2003 – May 2004 Thesis work and dissertation in Cell Dynamics group in Temasek Lifesciences Laboratory. Project title: “Molecular characterization of fission yeast microtubule binding protein Mia1p” Advisor: Dr. Snezhana Oliferenko and Prof. Mohan Balasubramanian.

June 2002 – Nov 2002 Full-time Professional placement work in Laboratory of Marine Molecular Biotechnology in Department of Biological Sciences. National University of Singapore. Project title: “Molecular nature of innate immunity in marine crustacean” Advisor: Prof. Jeak Ling Ding.

Nov 2001 – Feb 2002 Full-time lab-intern in Laboratory of Molecular Genetics in Department of Biological Sciences. Project title: “Transcriptome profiling of human ES cells.” National University of Singapore.

Earlier Education

Oct 1999 – May 2000 Pre-university bridging programme, National University of Singapore and Stanford University.

Sept 1994 – Oct 1999 High-school education in Lie Wu Middle School, Chengdu, Sichuan, China.

Sept 1989 – July 1994 Primary education in Filial Primary School for University of Electronic Science and Technology of China, Chengdu, Sichuan, China.

Abbreviations

aa	Amino acid	LB	Luria-Bertani medium
ABP	Actin binding protein	MB	Medium budded
ADF	Actin depolymerization factor	MOPS	3-(N-morpholino) propanesulfonic acid
ADP	Adenosine-5'-diphosphate	MT	Microtubules
ANOVA	Analysis of variance	N	Sample size
Arp	Actin related protein	NA	Not applicable
ATP	Adenosine-5'-triphosphate	Nat	Nourseothricin
ATPase	Adenosine triphosphate hydrolase	NPF	Nucleation-promoting factor
bp	Base pair(s)	N-terminal	Amino terminal
CCD	Charge-coupled device	ORF	Open-reading frame
Cdc	Cell division cycle	PBS	Phosphate-buffered saline
ConA	Concanavalin A	PCR	Polymerase chain reaction
CTD	C-terminal cargo binding domain (Myo2)	PEG	Polyethylenglycol
C-terminal	Carboxyl terminal	Pfy	Profilin
ddH₂O	Double distilled water	Pi	phosphate
DAD	<u>di</u> aphanous <u>au</u> to <u>re</u> gulatory <u>do</u> main	RFP	Red fluorescent protein
DID	<u>di</u> aphanous <u>i</u> nhibitory <u>do</u> main	RNA	Ribonucleic acid
DMSO	Dimethylsulfoxide	rpm	round per minute (centrifugation)
DNA	Deoxyribonucleic acid	RT	Room temperature
DRF	Diaphanous related formin	SC	Synthetic complete
EDTA	Ethylenediaminetetraacetic acid	SD	Standard deviation
EGFP	Enhanced green fluorescent protein	SD	Synthetic drop-out
EGTA	Ethylene glycol tetraacetic acid	SDS	Sodium dodecyl sulfate
EM	Electron microscopy	SEM	Standard error of mean
ER	Endoplasmic reticulum	SNR	Signal/noise ration
F-actin	Filamentous actin	TAE	Tris-acetate-EDTA
FH	Formin homology	TBE	Tris-Borate-EDTA
Fig.	Figure	TE	Tris-EDTA
G-actin	Globular actin	TIRFM	Total internal reflection microscopy
GDP	Guanosine-5'-biphosphate	Tpm	Tropomyosin
GEN	Geneticin	Tris	Tris(hydroxymethyl)aminomethane
GFP	Green fluorescent protein	ts	temperature sensitive
GTP	Guanosine-5'-triphosphate	U	Unit (enzyme activity unit)
GTPase	Guanosine triphosphate hydrolase	UB	Unbudded
HYG	Hygromycin B	v/v	Volume over volume
IQ repeats	Isoleucine (I) and Glutamine (Q) repeats	w/v	Weight over volume
KAN	Kanamycin	YPD	Yeast extract (Y)-peptone (P)- Glucose (D)
LatB	Latrunculin B	YT	Yeast extract (Y)-tryptone (T)
LB	Large budded		

1. Introduction	1
1.1. Actin	1
1.2. Actin binding proteins	4
1.2.1. Arp2/3 complex and dendritic nucleation	6
1.2.2. Formins	6
1.3. Actin cytoskeleton in <i>S. cerevisiae</i>	9
1.3.1. <i>S.cerevisiae</i> as model organism	9
1.3.2. Organization of F-actin structures in <i>S. cerevisiae</i>	10
1.3.3. Formin-dependent actin regulation in <i>S. cerevisiae</i>	12
1.3.4. Structure and dynamics of actin cables	15
1.4. Myosin	16
1.4.1. Myosin as molecular motor	16
1.4.2. Myosins in <i>S. cerevisiae</i>	17
1.4.3. Myo2 in <i>S. cerevisiae</i>	18
1.4.4. Smy1	19
1.5. Experimental set-up	20
1.5.1. Technical challenges in studying actin cable dynamics in <i>S. cerevisiae</i>	20
1.5.2. Total internal reflection microscopy	21
1.6. Objectives of investigation	22
2. Results	23
2.1. Actin cable dynamics in control cells	23
2.1.1. Abp140-GFP exhibits rapid blinking behaviour	23

2.1.2. Actin cables form a highly dynamic network on the cell cortex	24
2.1.3. Individual actin cables exhibit versatile behaviours	26
2.1.4. Actin cable network undergoes rapid remodelling	27
2.2 Actin dynamics in formin and formin-related mutants	30
2.2.1. Bni1 drives actin assembly in unpolarized cells	30
2.2.2. Fast cable motility is independent of actin polymerization	33
2.3. Myo2 drives fast cable motility	35
2.3.1. Actin cable dynamics in <i>myo2</i> temperature sensitive mutants	35
2.3.2. Speed of cable motility is dependent on Myo2 neck length	37
2.4. Interaction of actin cables with cortical Bni1 and Myo2	39
2.4.1. Bni1 and Myo2 dots are distinct from actin patches	39
2.4.2. Cortical Bni1 associates with actin cables	40
2.4.3. Cortical Myo2 associates with actin cables	41
2.4.4. Dynamics of cortical Bni1 dots	42
2.4.5. Dynamics of cortical Myo2 dots	44
2.4.6. Smy1 is a component of Myo2 dots	46
2.5. Actin cable organization in budded cells	48
2.5.1. Cable dynamics in polarized cells	48
2.5.2. Cable dynamics in large budded cells	51
2.6. The physiological role of fast cable motility	53
2.6.1. Physiological role of Bni1-driven actin dynamics	53
2.6.2. Physiological role of Myo2-driven actin motility	54
3. Discussion	56

3.1. Dynamics of actin cable network	56
3.2. Interplay of two formins	58
3.3. A novel role for myosins	60
3.4. Actin dynamics and cell polarization	62
3.5. Outlook	65
4. Summary	67
5. Materials and methods	69
5.1 Materials	69
5.1.1. Strains	69
5.1.2. Kits used	75
5.1.3. Enzymes and proteins	75
5.1.4. Nucleic acids	76
5.1.5. Chemicals	80
5.1.6. Other materials	83
5.1.7. Buffers and solutions	84
5.1.8. Media	86
5.2. Microbiological and genetic methods	89
5.2.1. <i>Escherichia coli</i>	89
5.2.2. <i>S. cerevisiae</i>	90
5.3. Molecular biological and genetic techniques	94
5.3.1. Handling nucleic acids	94
5.3.2. <i>in vitro</i> modification of DNA	95
5.3.3. Analyses of DNA	95
5.3.4. Polymerase chain reaction (PCR)	96
5.4. Microscopy	98

5.4.1. Epifluorescent microscopy	98
5.4.2. TIRF microscopy	99
5.4.3. Image processing and analyses	100
5.5. Cell biological methods	103
5.5.1. Polarization assay	103
5.5.2. Mating projection (shmoo) assay	104
6. Literature	105

List of figures

Figure	Page	Figure	Page
1-1	2	2-8	34
1-2	4	2-9	36
1-3	5	2-10	38
1-4	8	2-11	39
1-5	10	2-12	40-41
1-6	11-12	2-13	41-42
1-7	14	2-14	43
1-8	16	2-15	45
1-9	18	2-16	47
1-10	19	2-17	49-50
1-11	21	2-18	52
2-1	23	2-19	54
2-2	24-25	2-20	55
2-3	25-26	3-1	57
2-4	26	3-2	62
2-5	28	3-3	65
2-6	30	5-1	92
2-7	32	5-2	102

List of tables

Table	Page	Table	Page
2-1	29	5-1	69
2-2	33	5-2	75
2-3	34	5-3	76
2-4	37	5-4	78
2-5	38	5-5	80
2-6	43	5-6	83
2-7	46	5-7	84
2-8	50	5-8	86
2-9	52		

Acknowledgements

I owe my deepest gratitude to Dr. Roland Wedlich-Söldner, who generously provided me with the opportunity to carry out this work in his lab, whose guidance and support in every possible way enabled me to carry it from the beginning to the end.

This thesis would also not be possible without the support of Prof. Ralf-Peter Jansen, who kindly took over the role of faculty representative, and whose patient advices injected vigour and clarity in me during difficult periods in my years as a doctorate student.

I am also indebted to Dr. Alvaro Crevenna, who helped me all the way along the development of this work in discussing the results, collaborating in data analyses and in being a wonderful friend in all domains of life.

I am grateful for Ms. Gisela Beck for her excellent and unfailing technical support.

Heartfelt thanks also go to all current and former members of laboratory of cellular dynamics and cell patterning, Max-Planck Institute of Biochemistry, for forging a relaxed yet dynamic research atmosphere.

I would like to also thank Carlos Acevedo-Rocha and Akos Dobay, whose openness and intelligence helped me to explore and enrich my intellectual and spiritual life.

My deep gratitude also goes to Gosia, Juli, Monica, Salima, Daidi, Jena and Sozui, whose unfailing love, friendship and guidance enabled me to walk through the dark hours.

Lastly, I would like to honour my parents and my late grandparents, who sew the seeds of knowledge and curiosity in me years ago, which drove me to reach this point, which will keep driving me to go beyond it.

1. Introduction

1.1. Actin

Eukaryotic non-muscle actin plays vital roles in many cellular processes, such as cell migration, cell division, endocytosis and intracellular transport. The actin cytoskeleton is composed of flexible, thin actin filaments (around 7 nm in diameter), also known as microfilaments. A single actin filament is a right-handed double helix consisting of two proto-filaments. Each proto-filament is a polymer assembled from globular actin monomers in a head-to-tail manner (Fig. 1-1A). Actin in its filamentous form is referred to as *F-actin*, whereas the globular actin monomer is referred to as *G-actin*. Actin monomer is an enzyme ATPase, which can be found in any of the four different forms depending on the stage of ATP hydrolysis. These four forms are: the nucleotide-free form, the ATP-bound form, the ADP-Pi bound form and the ADP bound form. Only the nucleotide-bound forms of G-actin are able to be incorporated into filaments (Fig. 1-1B).

Since actin proteins serve many essential physiological functions, it is not surprising that the actin gene is present in all eukaryotic systems and is highly conserved throughout evolution. 80.2% of the nucleotide sequences of actin gene are identical between human *Homo sapiens* and yeast *Saccharomyces cerevisiae*, whereas 95% of polypeptide sequences were conserved. Besides its ubiquitous presence in eukaryotes, recent studies also revealed that actin homologues exist in prokaryotic systems (for review see Carballido-Lopez, 2006). Although these proteins share relatively low sequence homology with actin, crystal structures indicated a high structural homology. Like actin, these proteins also polymerize into filamentous structures, which in turn are essential for the regulation of cell morphology (Carballido-Lopez et al., 2006).

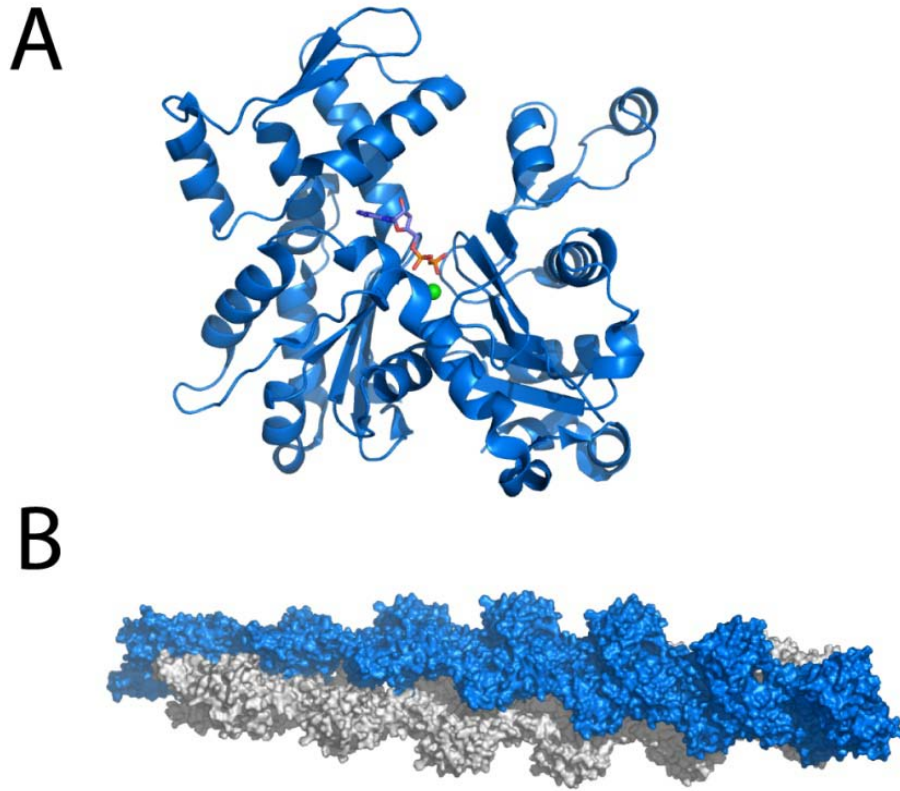


Figure 1-1.

Molecular model of G-actin and F-actin. (A) Molecular model of G-actin. Shown is the ribbon model of G-actin (blue) bound to an ADP molecule (red) and a divalent cation (green). (B) Molecular model of an F-actin filament showing a single turn of the helix. The two protofilaments are coloured in blue and white. Each protofilament is a polymer of single actin proteins which are organized in a linear, head-to-tail manner. A single turn of the double helix spans 13 subunits of G actin, which is about 37nm in length. (images adapted with modification from Wikipedia, under GFDL license)

The mechanisms of F-actin polymerization were elucidated mostly by *in vitro* experiments on purified actin (Carrier, 1991; Pollard, 1986). In general, polymerization of an F-actin filament occurs in two phases. The first phase is the *nucleation* phase, in which actin dimers and trimers are formed. Dimerization and trimerization are thermodynamically unfavourable, making

nucleation the rate-limiting step of polymerization. The actin trimers serve as nucleators for the subsequent rapid additions of G-actin subunits, or the *elongation* phase of actin polymerization. The additions of actin monomers during elongation are thermodynamically favourable. The rate of filament elongation is directly proportional to the concentration of available monomers. Actin subunits are incorporated into the proto-filaments with fixed orientation. Therefore actin filaments have intrinsic polarity. One end is termed the *barbed end* (+) and the other the *pointed end* (-). These terms were originally derived from electron microscopy (EM) images using myosin S1 as a marker for F-actin, whereby myosin heads are differentially localized along the filament due to its directionality (Hayashi and Ip, 1976). Monomers can be associated with or dissociated from either ends of the filament (Fig. 1-2).

Earlier experiments on actin polymerization dynamics have shown that the rate of association or dissociation at either end of the filament is associated with the monomer concentration (Pollard, 1984, 1986). Once the polymerization is initiated by addition of ATP, the reactions continue to occur until the monomer concentration reaches a level that produces equal rates of association and dissociation. This concentration is termed *critical concentration*. The critical concentration of ADP-actin is about 20 times higher than that of ATP-actin. The critical concentration of ATP-actin at pointed end is about 5 times higher than that at barbed end. The net results of these differences are such that for incorporation of monomers, ATP-actin is preferred over ADP-actin, whereas the barbed end is preferred over pointed end. ADP-subunits are therefore more likely to be exposed at pointed end. At steady state, in the presence of ATP, the actin monomer concentration falls between the critical concentrations at the two ends. Though the polymer and monomer concentration remain constant, net addition of subunits at barbed end and net loss of subunits at pointed end result are equalized. Actin filament therefore migrates towards the barbed end without changing its length. This process is termed *treadmilling* (see book chapter in Pollard, 2008). Upon addition to the filament, incorporated actin monomer slowly hydrolyzes the ATP to produce ADP-Pi and later on inorganic phosphate is released. Thus, the older the actin filament is, the more ADP-bound subunits it contains. The transition of ATP-bound form of subunits towards to ADP-bound forms is termed *filament aging*.

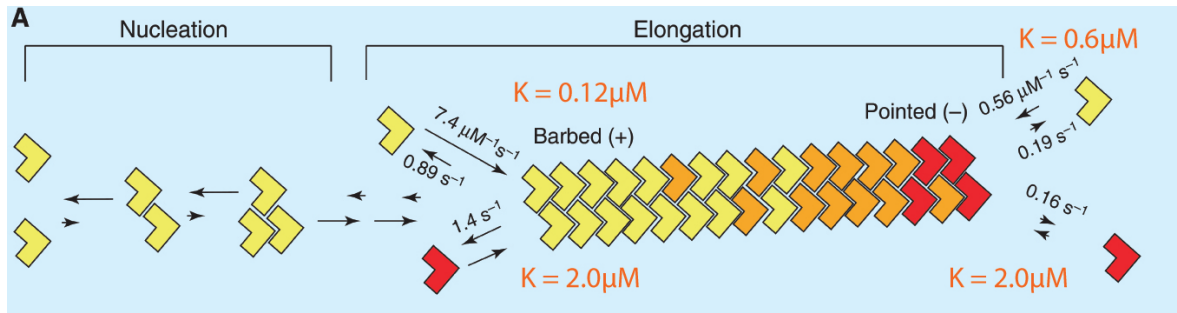


Figure 1-2.

Polymerization cycle of F-actin. The two stages of F-actin polymerization are represented here schematically. Yellow L-shapes represent ATP-bound subunits. Red Ls represent ADP bound form, orange Ls represent ADP-Pi bound form. Association and dissociation rates are represented here as on / off rate of monomers. K is critical concentration of the actin monomers. (adapted with modification from Nicholson-Dykstra et al., 2005)

1.2. Actin-binding proteins and nucleators

In living cells, the dynamics of F-actin differs substantially from that *in vitro*. This is because F-actin dynamics is tightly regulated *in vivo* via numerous actin binding proteins (ABPs). ABPs can either bind to G-actin monomer or F-actin filament. Figure 1-3 provides some examples of ABPs and their functions in non-muscle cells. G-actin binding proteins are able to regulate actin assembly by controlling the cellular concentration of monomers (Fig.1-3A). One example of such proteins is profilin, which promotes F-actin assembly by sequestration of monomers from the cytoplasmic pool to polymerization machinery (see section 1.2.2.).

ABPs can also bind to the ends or the sides of actin filaments. End-binding proteins either promote or inhibit the elongation of filament. End-binding proteins include capping proteins, which bind to the barbed end of F-actin. This binding blocks the addition and removal of actin monomers. Therefore it limits the length of actin filament at the same time protects it from depolymerization (e.g. capping proteins, Fig. 1-3B). Some side-binding proteins can induce bundling of actin (e.g. actinin, Fig. 1-3C) or crosslinking of filaments (e.g. filamin, Fig. 1-3D) through their abilities to bind actin and to dimerize or multimerize. Other side-binders influence the stability of filaments. One of the most important side-binder is the actin depolymerization factor (ADF)/cofilin. Cofilin binds to the side of filament by insertion between two subunits.

This binding induces an additional twist on the filament. This additional twist modifies the lattice of filament, which makes the filament prone to disassembly (Fig. 1-3E, for review see Bamburg, 1999). Another important class of side binders are the tropomyosins. These are helical proteins which form an additional double helix over the lattice of actin filament. This kind of binding stabilizes to filament by protecting it from severing (Fig. 1-3F, Xu et al., 1999).

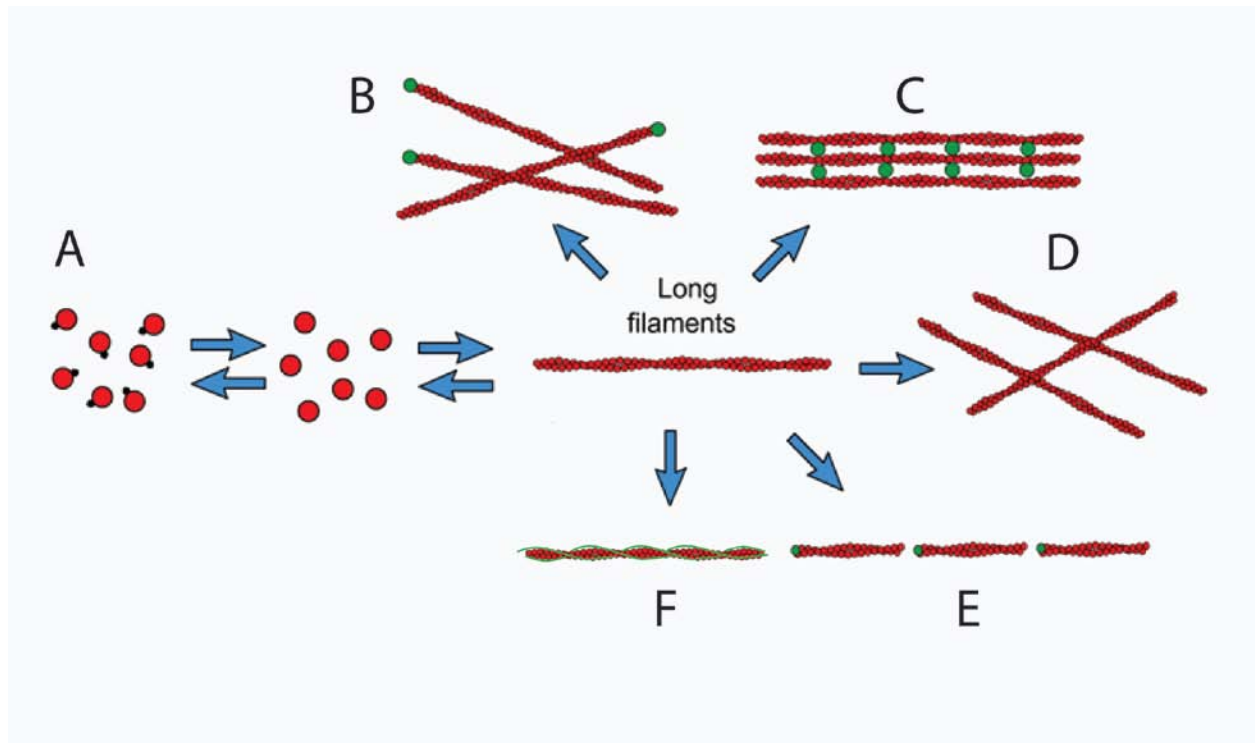


Figure 1-3.

Organization of F-actin via actin bind proteins. Shown are examples of (A) monomer sequestration, (B) capping of filaments, (C) parallel or anti-parallel bundling of filaments, (D) filament crosslinking, (E) filament severing and (F) longitudinal stabilization of filament.

Besides these regulatory functions some actin-binding proteins are able to promote F-actin assembly by acting as nucleators for polymerization. Up to now three classes of such nucleators molecules have been identified, namely the actin related protein 2/3 (Arp2/3, Frankel and Mooseker, 1996) complex, the formins (Goode and Eck, 2007) and

the recently discovered Spire (Quinlan et al., 2005). In reference to the context of this work, only the first two classes of nucleators will be discussed.

1.2.1. Arp2/3 complex and dendritic nucleation

Arp proteins are a class of proteins that share significant sequence homology with actin (for review see Frankel and Mooseker, 1996). Arp2, Arp3 and 5 other subunits (ARPC1-5) form the Arp2/3 complex. Arp2 and Arp3 resemble actin structurally and bind to actin monomers. They can be incorporated at the pointed end of a filament. Binding of a single actin monomer to Arp2/3 forms a stable complex that mimics an F-actin trimer. This molecular mimicry overcomes the thermodynamically unfavourable dimerization and trimerization of subunits, thus promotes nucleation. It was shown Arp2/3 complex could also bind to the side of a filament with a fixed orientation, forming a branching point. Furthermore, the lengths of the Arp2/3 nucleated filaments are limited by activity of capping protein and ADF/cofilin. Therefore Arp2/3 dependent actin assembly creates a tree-like structure of short F-actin filaments. These structures can be observed both in yeast actin patches and lamellipodia of mammalian cells. This mode of actin polymerization is called *dendritic nucleation* (Fig.1-4A, for review see Pollard, 2007).

1.2.2. Formins

Formins are a class of multi-domain proteins that assemble actin filaments independent of Arp2/3 complex (Evangelista et al., 2002b; Kovar et al., 2003; Li and Higgs, 2003; Sagot et al., 2002b). Formins have been identified as a superfamily of homologous genes in wide range of animals, fungi, plants and protists. In mammals, formins are highly diverse, with fifteen homologous alleles of seven different classes. A typical formin contains regulatory domains and formin homology (FH) domains, FH1, FH2 and FH3. Among these, FH2 is the defining feature shared by all formins. Within diverse superfamily members, the best studied formins are the diaphanous-related formins (DRFs), which include the mammalian mDial and the yeast Bni1 and Bnr1 (Goode and Eck, 2007).

A DRF contains a FH1 and a FH2 domain. FH1 is a proline-rich (PR) domain which recruits profilin-bound G-actin. FH2 binds to actin and anchors the protein to the barbed end of actin filament (for review see Evangelista et al., 2003). DRF contains regulatory domains that consist

of an autoinhibitory unit and Rho-GTPase binding domain. Autoinhibition is mediated through intramolecular interaction between diaphanous inhibitory domain (DID) at the N-terminus and diaphanous autoregulatory domain (DAD) at the C-terminus. The GTPase binding domain (GBD) is located N-terminal of DAD and sometimes partially overlaps with it. Therefore the binding of GTP bound Rho-proteins disrupts the intramolecular interaction of DID and DAD, which in turn causes the activation of the formin protein (Lammers et al., 2005). Furthermore, it is also known that DRFs function as homodimers. The dimerization of DRF is mediated by the dimerization domain (DD) and coiled-coil (CC) domain (Fig. 1-4B, Pring et al., 2003).

Unlike Arp2/3, formin mediates the assembly of unbranched actin filaments. It is believed that FH2 dimer nucleates actin assembly by binding directly and stabilizing the actin polymerization intermediates (dimers and trimers, Xu et al., 2004). After filament nucleation, most FH2 domains maintain high affinity to actin and persistently associate with the barbed end. Formin can move processively along the growing barbed end by a stepping mechanism, while allowing rapid addition of subunits. This is called the *processive capping* mechanism (Fig. 1-4C, Romero et al., 2004). FH1 domain promotes the rate of filament elongation by interaction with profilin-bound actin monomers. The interaction of FH1 and profilin presumably limits the diffusion of actin monomers close to the barbed end, thus increases the efficiency of formin. Furthermore, multiple PR motifs exist in some FH1 domains, suggesting multiple interactions with profilin (Kovar et al., 2003). Indeed, recent study showed that the efficiency of formin Bni1 decreases with the reduction of PR motifs (Paul and Pollard, 2008).

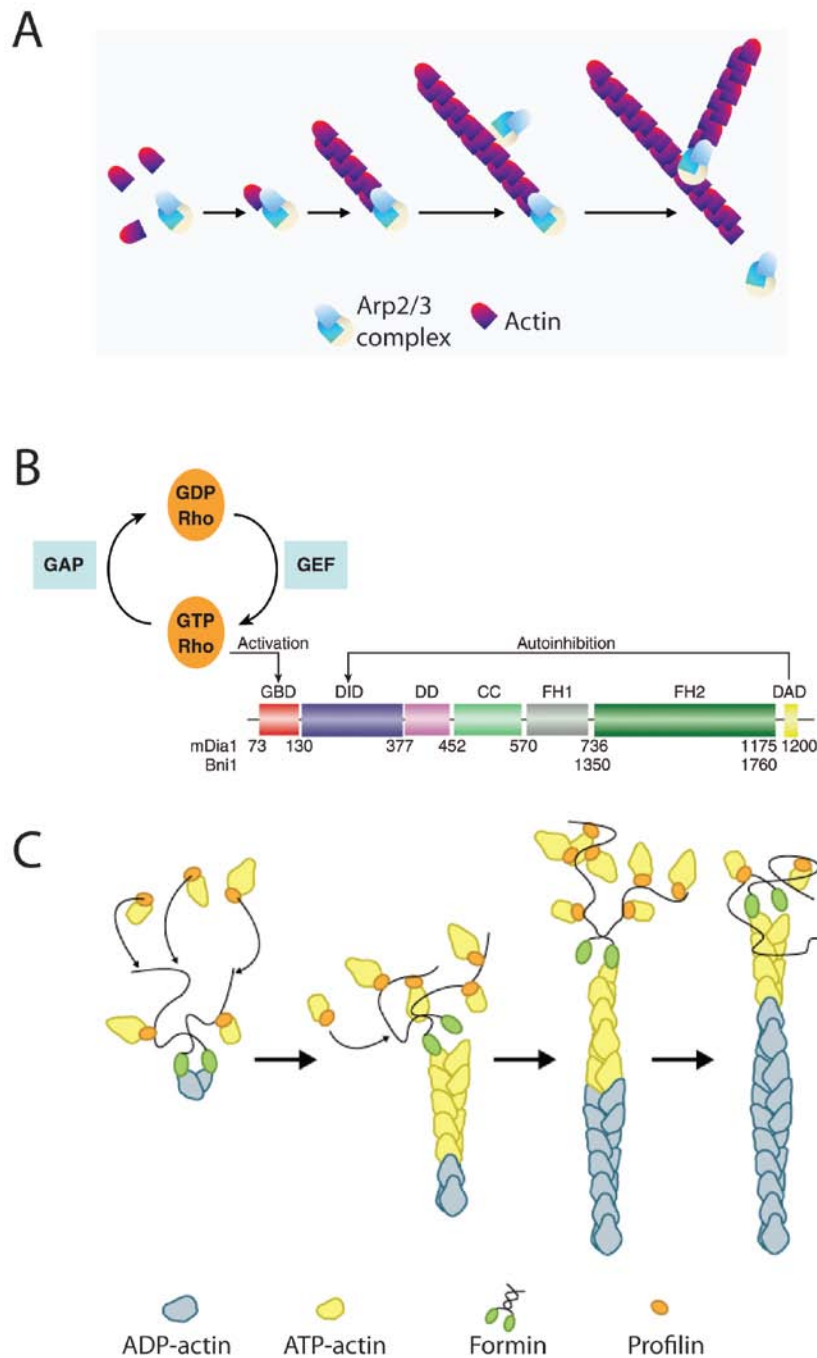


Figure 1-4.

F-actin assembly mediated by Arp2/3 complex and formin. (A) Simplified model of dendritic nucleation by Arp2/3 complexes. (B) Domain organization and Rho-GTPase dependent regulation of DRF family formins. (adapted with modification from Goode and Eck, 2007) (C) Model of nucleation and elongation of F-actin mediated by formin and profilin. This process is also known as the *processive capping* mechanism. Green

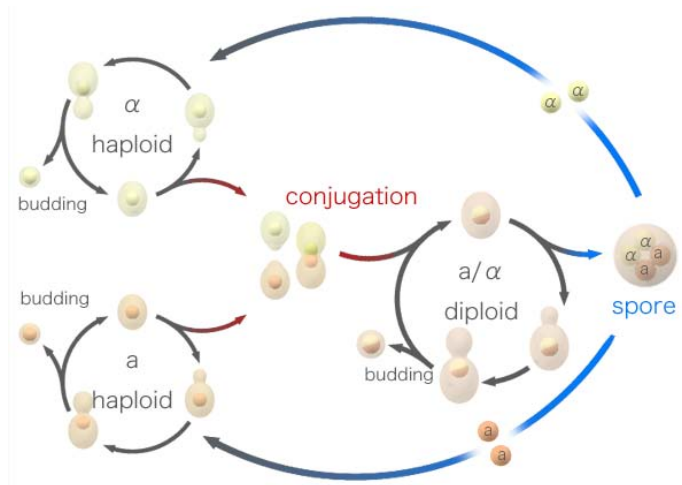
ovals represent FH2 domains, which associate with actin barbed end. Curved lines represent the relatively unstructured FH1 domain, which recruits actin via interaction with profilin. Elongation is achieved as formin continuously steps on the nascent barbed end in coordination with the addition of new subunits.

1.3. The actin cytoskeleton in *S. cerevisiae*

1.3.1. *S. cerevisiae* as model organism

S. cerevisiae or budding yeast is widely used as a eukaryotic model organism for molecular biology and cell biology. *S. cerevisiae* is unicellular and can propagate in either diploid or haploid forms. Under optimum or low-stress conditions both diploids and haploids undergo a simple lifecycle of vegetative growth (budding). The doubling time of wildtype (wt) yeast is approximately 2.5 hrs under such conditions. Such a short life-cycle is ideal for genetic and biochemical experiments. The haploid yeast cells are either of **a** or **α** mating type. Two haploid cells of different mating types can exchange genetic materials through mating (also known as conjugation). Under nutrient deficiency or stress, each diploid cell undergoes meiosis to generate four spores (tetrads), which are then able to propagate as haploid cells in vegetative growth (Fig. 1-5).

S. cerevisiae is also known for its genetic malleability. Standardized tools for genetic manipulation have been extensively developed (Janke et al., 2004; Longtine et al., 1998; Sikorski and Hieter, 1989). The physiology and genetics of *S. cerevisiae* cells have been intensively studied and well characterized. The genome of *S. cerevisiae* has also been fully sequenced and well annotated (<http://www.yeastgenome.org/>). In the past two decades, *S. cerevisiae* has become increasingly important in cell biology, especially in the field of cytoskeletal dynamics and cell polarity. Many insights leading to the fundamental breakthroughs in our understanding of actin dynamics were gained through investigations in this model organism (for review see Pruyne et al., 2004).

**Figure 1-5.**

Life cycle of *S. cerevisiae*. *S. cerevisiae* cells exist both in diploid and haploid forms. The transition from haploid to diploid form is called conjugation. The transition from diploid to haploid form is called sporulation. (Image adapted from Wikipedia under GFDL license)

1.3.2. Organization of F-actin structures in *S. cerevisiae*

F-actin in budding yeast is organized in three types of structures: actin patches, actin cables and actomyosin rings.

Actin patches are foci of F-actin structures on the yeast cell cortex. They are named as such because they appear as patch-like structures when visualized with Rhodamine-phalloidine under epifluorescent microscope (Fig. 1-6). EM study showed that they are endocytic structures containing dendritic networks of actin filaments dependent on Arp2/3 complex, as described above (section 1.2.1., Fig. 1-5A, Young et al., 2004). These dendritic actin networks polymerize around the sites of endocytosis and are associated with endocytic coat proteins such as clathrin. Actin patches are coupled with type I myosin Myo3 and Myo5, which produce the force needed for membrane invagination (Evangelista et al., 2000; Geli and Riezman, 1996). At later stages of the endocytosis, vesicles are pinched off from the cell membrane and transported along actin cables, whereas actin patches disassemble (Huckaba et al., 2004; Kaksonen et al., 2003). Fluorescence-labelled Abp1 was often used to measure the dynamics of actin patches. The average lifespan of Abp1 patch is between 10s~20s depending on the genetic background of the cell and experimental conditions (Kaksonen et al., 2005).

Actin cables are linear, unbranched filamentous structures that are assembled by yeast formins Bni1 and Bnr1, as well as profilin Pfy1 (Fig. 1-6, Evangelista et al., 2002b; Sagot et al., 2002a;

Sagot et al., 2002b). In polarized cells, these actin cables become bundled and are used as tracks for type V Myosin-dependent polarized transport during cell growth (see sections 1.3.3. and 1.3.4. for detailed explanation on functions of yeast formins and regulation of actin cables).

Actomyosin rings are ring-like structures containing actin, type II Myosin, septin and other factors. They are present transiently at the budneck region between the mother and the daughter cell and are involved in cytokinesis (Fig. 1-6, Bi et al., 1998; Lippincott and Li, 1998; Longtine et al., 1996).

The yeast actin cytoskeleton undergoes extensive reorganization throughout the vegetative cell cycle (Amberg, 1998; Karpova et al., 1998). As shown in Fig. 1-6, in an unbudded cell actin cables and patches are distributed randomly (Fig. 1-6A). During budding, actin cables become bundled and are polarized towards the budding site (Fig. 1-6B). Later on, actin patches become highly concentrated in the growing daughter cell (Fig. 1-6C, D). As the daughter cell grows larger, actin cables and patches are again depolarized and re-organized in both mother and daughter cells. Actin rings are present at the budneck only transiently at this stage (Fig. 1-6E).

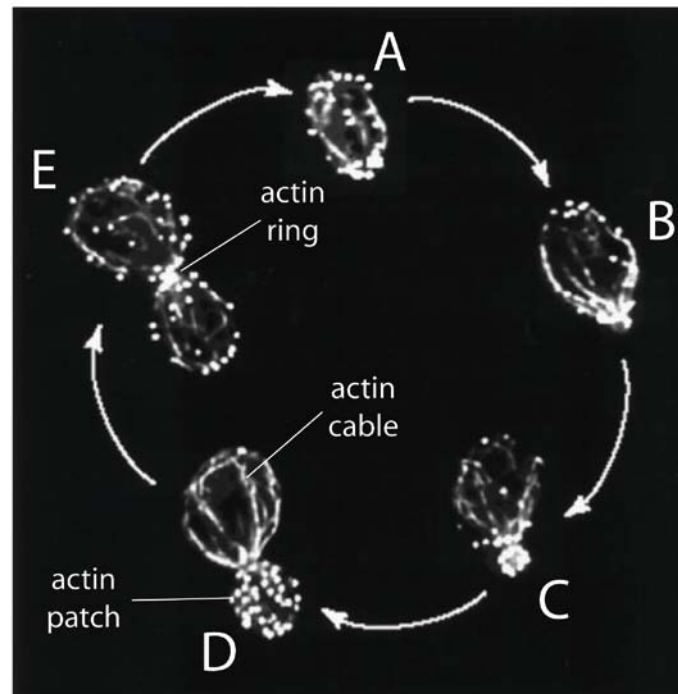


Figure 1-6.

Reorganization of *S. cerevisiae* actin cytoskeleton throughout the cell cycle. Yeast cells were fixed and stained with rhodamine phalloidine to visualize all F-actin structures. Shown here are actin organization in (A) an unbudded cell, (B) a polarized cells with an emerging bud, (C) a polarized cells with a small bud, (D) a polarized cells with a large bud and (E) a cell undergoing cytokinesis with the actin cables and patches depolarizing in both mother and daughter cells. Actin ring is present transiently at the budneck (adapted with modification from Amberg, 1998)

1.3.3. Formin-dependent actin regulation in *S. cerevisiae*

Actin cable assembly is independent of Arp2/3 complex, but dependent on the yeast formins Bni1 and Bnr1, as well as on profilin Pfy1 (Evangelista et al., 2002b; Sagot et al., 2002a; Sagot et al., 2002b). Disruption of both formins and Pfy1 caused a complete loss of actin cables, cells failed to polarize and eventually died. Bni1 and Bnr1 are similar in their domain organization, but are differentially regulated by Rho-GTPases (Fig. 1-7A, Dong et al., 2003). Besides profilin, Bud6 was also identified as a potent co-factor promoting the Bni1, Bnr1 dependent actin polymerization (Kikyo et al., 1999; Moseley et al., 2004). Once assembled, the maintenance of cables is dependent on yeast tropomyosins Tpm1 and Tpm2, which bind along the length of actin filaments, thereby stabilizing the lattice of actin filaments (Pirani et al., 2006; Vibert et al., 1993; Xu et al., 1999).

In unpolarized cells, actin cables are oriented randomly along the cell cortex. Once the cell becomes polarized, the actin cables are bundled and re-oriented along the mother-daughter axis. At this stage, almost all Bni1 and Bnr1 proteins are concentrated at the polarization sites. Bni1 localizes to the budtip, whereas Bnr1 is restricted to the budneck (Buttery et al., 2007; Fujiwara et al., 1998). As formins are persistently associated with the barbed ends of actin filament, these localization patterns enable the cell to build arrays of actin filaments with their barbed ends pointing towards the polarization sites. Furthermore, actin cables in polarized cells appear as thick bundles, which are presumably arrays of bundled cables (Karpova et al., 1998). It was suggested that the fimbrin Sac6 and its cofactor Scp1 are responsible for the bundling of actin

cables, as these proteins bundle actin *in vitro* (Goodman et al., 2003). However, to date no *in vivo* data is available to support this claim. The oriented cable bundles are utilized as tracks for polarized transport using type V myosins as motors (Fig.1-7B, Pruyne et al., 1998).

Previous studies showed different dynamical and biochemical properties of Bni1 and Bnr1. In addition to budtip-localization in the daughter cells, Bni1 was observed to form “cytoplasmic” puncta in the mother cells. Movements of these puncta from daughter to mother cells were also detected. In contrast, Bnr1 was shown to be restricted to the budneck region, probably by interacting with the septin ring (Buttery et al., 2007; Kikyo et al., 1999). A recent study on polarized cells showed that Bnr1 was inhibited via displacement from barbed ends by Bud14. Deletion of Bud14 caused extensive stabilization of actin cables in mother cells. Actin cables in *bud14Δ* cells appear long and bend (Chesarone et al., 2009). Interestingly, *in vitro* data suggested that Bnr1 has a higher nucleation activity and a higher affinity to actin than Bni1. Also, Bnr1 but not Bni1, was shown to bundle actin filaments (Wen and Rubenstein, 2009). These data suggest that Bni1 and Bnr1 play differential roles in the regulation of actin dynamics, probably through a mechanism involving spatial and temporal interplays of the two proteins. The understanding on how these interplays take place *in vivo* is of critical importance in resolving the mechanism of formin-driven actin dynamics.

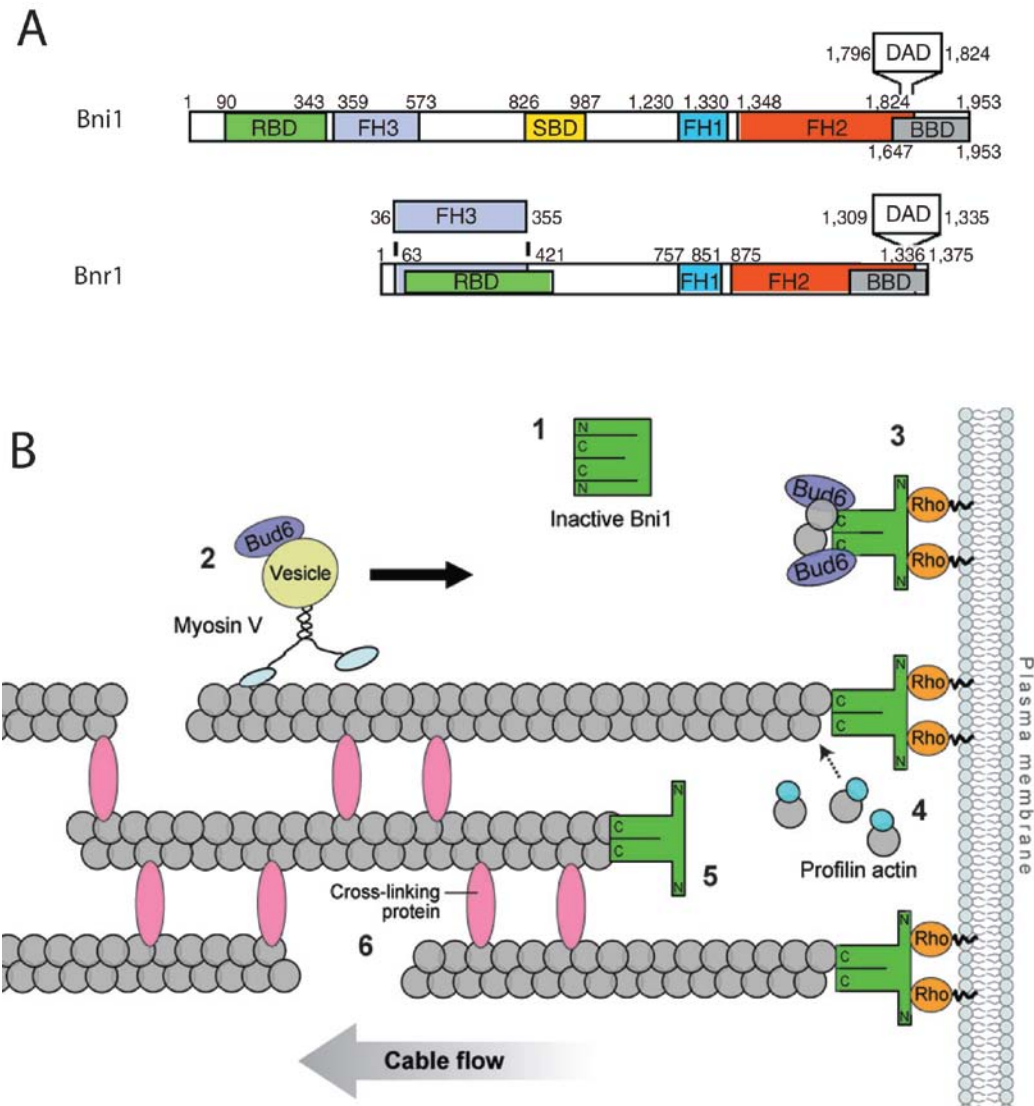


Figure 1-7.

Yeast formins. (A) Schematic representation of the primary structures of yeast formins Bni1 and Bnr1. Shown are Rho-GTPase binding domains (RBD), formin-homology domains (FH1, 2, 3), Dia-autoregulatory domain (DAD), Bud6 binding domain (BBD), Spa2-binding domain (SBD, adapted from Evangelista et al., 2002b). (B) Assembly of actin cables by yeast formin Bni1. [1] Inactive Bni1 diffuse throughout cytoplasm. [2] Bud6 is delivered to polarization site by Myosin V. [3] Bni1 binds to GTP-bound GTPase on the cell membrane and becomes activated. Bud6 binds to the COOH-terminus of Bni1 and promotes filament assembly. [4] Bni1 recruits profilin-actin complexes. [5] Bni1 dissociates with GTPase, but remains on the barbed end of the filament. [6] Bundling of unbranched filaments via cross-linkers such as fimbrin/Sac6. (Adapted from Goode and Eck, 2007)

1.3.4. Structure and dynamics of actin cables

To function as tracks for polarized transport, actin cables must be continuous structures that are consistently polarized towards the sites of cell growth. However, it was first proposed by Karpova and colleagues that an actin cable could be an array of short actin filaments instead of a single continuous filament (Karpova et al., 1998). This model was supported by later experiments on rapid actin turn-over under treatment of actin-depolymerizing drug Latrunculin A (LatA). It was shown that the actin cables disappear within 60 seconds upon addition of LatA. This was considered to be too fast for the depolymerization of single actin filament (Okada et al., 2006). On the other hand, EM studies on actin cables in fission yeast *Schizosaccharomyces pombe* showed such a bundled structure (Kamasaki et al., 2005). However, no such data exists for actin cables in *S. cerevisiae*. Therefore, the exact architecture of the actin cables remains unknown.

Most of studies on actin organization in yeast were carried out using immuno-fluorescent images, which could only provide indirect information on actin dynamics. Up to now, only two studies have been published on the dynamics of actin cables in living cells (Huckaba et al., 2006; Yang and Pon, 2002). Both studies used GFP fused to Abp140 – an actin binding protein of unknown function – to visualize actin cables *in vivo*. The earlier work described the organization of polarized bundles of actin cables and provided an estimation of the extension rates of these bundles (Yang and Pon, 2002). The more recent work proposed a possible mechanism for the regulation of actin motility through the competition of type II myosin and tropomyosin (Huckaba et al., 2006). However, due to technical limitations, neither of these studies provided convincing mechanistic explanations for the measurements on cable dynamics. Furthermore, conclusions on the regulation of dynamics were drawn based on relatively low number of observations, ignoring different cell cycle stages. Finally, dynamics of unbundled actin cables in unpolarized cells were completely overlooked in these studies, although previous data clearly showed their existence (Karpova et al., 1998). Therefore, in order to thoroughly understand the mechanism of actin cable regulation, a much more comprehensive approach is needed.

1.4. Myosins

1.4.1. Myosin as molecular motor

As mentioned above, myosins are molecular motors that use actin filaments as tracks for movements. Myosins are multi-domain proteins that are found in all eukaryotic systems. The myosin superfamily is highly diverse, containing about twenty different classes. The classification of myosins is based on sequence homologies in the motor domains. Different classes of myosins localize differently in cells and perform distinct functions (for review see Mermall et al., 1998).

Despite this diversity, the fundamental mechanism of myosin function is conserved, namely it is an F-actin dependent molecular motor (mechano-chemical transduction reaction). All myosin proteins contain a so-called “head domain”, which is an enzyme ATPase that can bind to actin filaments. The head domain is usually followed by a flexible “neck” domain, allowing the movement of the head domain. The binding and hydrolysis of ATP on the head domain induce a conformational change on myosin, which produces a “power stroke” towards the barbed end of actin filament, utilizing the neck domain as a lever arm. This power stroke is tightly coupled with the binding and release of actin, enabling the myosin to move directionally along an actin filament (Fig. 1-8, for review see Tyska and Warshaw, 2002).

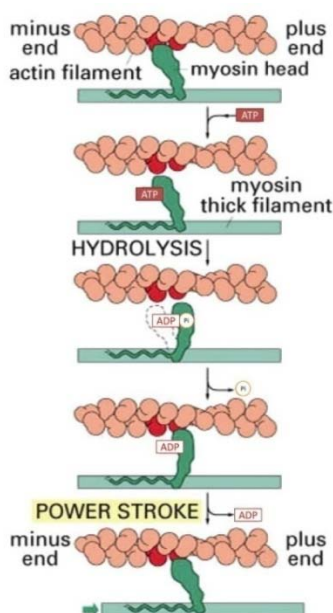


Figure 1-8.

Mechano-chemical transduction of myosin heads.

Nucleotide-free myosin head is tightly bound to the actin filaments. ATP binding releases the myosin head from actin. Hydrolysis of ATP into ADP induces a conformational change which drives the myosin head towards the plus end (barbed end) of actin filament, at the same time enables myosin to restore the binding to actin. The release of ADP from the head domain restores the myosin to the original conformation, which produces the power stroke. Notice that barbed end is marked as plus end whereas pointed is marked as minus in this figure. (Adapted from book chapter in Alberts, 2007)

In addition to transport functions, myosin motors also contribute to actin remodelling by organizing actin filaments. The generation and roles of type II myosin dependent contractile forces during muscle contraction (Yanagida, 2007) and cytokinesis have been intensely studied (Matsumura, 2005; Zhou and Wang, 2008). Recently, budding yeast myosin II has been implicated in retrograde actin flow (Huckaba et al., 2006). In addition, there were several reports of unconventional myosins reorganizing actin filaments using via their motor function (McConnell and Tyska, 2007; Tokuo et al., 2007; Zot and Pollard, 1993). However, all the results acquired were not based on direct observation of actin-myosin interaction. Therefore, direct evidence for Myosin-dependent actin motility is still missing.

1.4.2. Myosins in *S. cerevisiae*

In *S. cerevisiae*, 5 myosin genes of 3 different classes have been identified. These are the type I MYO3, MYO5, the type II MYO1 and the type V MYO2, MYO4. The type I myosins act in a coordinated manner with the actin polymerization machinery in actin patches, generating the forces during endocytic internalization (Evangelista et al., 2000; Sun et al., 2006). The type II myosin Myo1 is involved in cytokinesis as a component of actomyosin ring (for review see Moseley and Goode, 2006). The type V myosins are the motors that are responsible of polarized transport of secretory vesicles, RNA and organelles (for review see Pruyne et al., 2004).

Among three classes of myosins, only type V myosins interact with actin cables. The two MyoV, Myo2 and Myo4 have similar domain structures. Both use polarized actin cables as tracks for transport. Yet the cargo identities of the two motors are distinct. Myo2 mediates the transport of secretory vesicles (Schott et al., 1999), mitochondria (Altmann et al., 2008), peroxisomes (Hoepfner et al., 2001), mitotic spindles (Hwang et al., 2003), vacuoles (Catlett and Weisman, 1998) and trans-Golgi network (Rossanese et al., 2001). Myo4 mediates the transport of ER (Estrada et al., 2003) and mRNA (Fig. 1-9, Munchow et al., 1999). In cell physiology, Myo2 is a key regulator of cell polarization and vectorial transport. Therefore it is essential for cell survival (Johnston et al., 1991). Myo4 is not an essential gene. But it is required for mating type switch in haploid cells (Jansen et al., 1996).

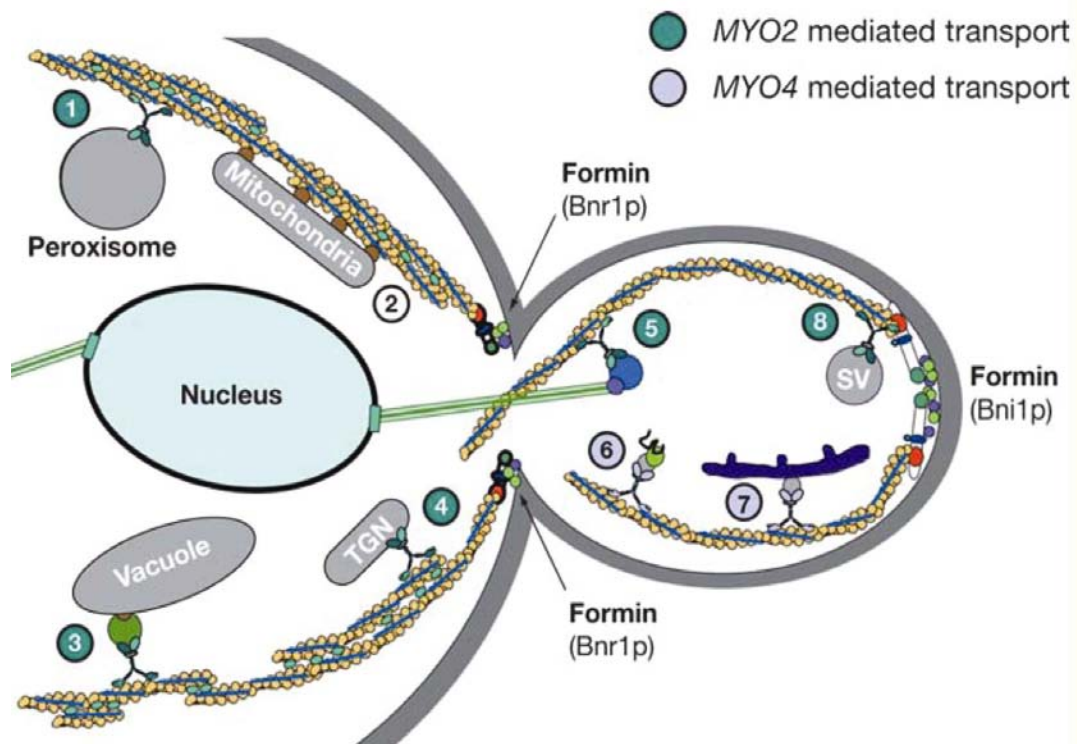


Figure 1-9.

MyoV functions in *S. cerevisiae*. Respectively: Myo2-dependent transport of peroxisomes (1), mitochondria (2), vacuoles (3), trans-golgi network (4), mitotic spindle (5) and secretory vesicles (8). Myo4-dependent transport of mRNA (6) and ER (7). (adapted from Pruyne et al., 2004)

1.4.3. Myo2 in *S. cerevisiae*

The type V myosin Myo2 was first identified as an essential myosin that is responsible for vectorial transport of secretory vesicles (Johnston et al., 1991). It consists of four major domains, namely the N-terminal motor domain, the neck IQ domain, the coiled-coil domain and the C-terminal globular tail domain (CTD, see Fig. 1-10). Disruption of the motor domain abolished vectorial transport, and caused the accumulation of secretory vesicles in mother cells (Govindan et al., 1995; Johnston et al., 1991; Pruyne et al., 1998). The IQ domain contains 6 IQ (Isoleucine, Q-glutamine) motifs. These IQ motifs bind to the regulatory myosin light-chain Mlc1 and the calmodulin Cmd1. It was proposed that these interactions activate and stabilize Myo2 *in vivo*, thus increasing its efficacy in transport (Brockerhoff et al., 1994; Stevens and Davis, 1998).

Modification on the number of IQ domains affected the speed of vectorial transport, suggesting that IQ domains function to stabilize the lever-arm of the motor (Schott et al., 2002). The coiled-coil domain spans up to 500 amino acids and is considered to be essential for the dimerization of Myo2 (Dunn et al., 2007). The CTD is a globular domain that binds to different cargos with high specificity (for review, see Weisman, 2006). Disruption of the CTD alone abolished cargo transport, without affecting the budtip localization of Myo2, suggesting that the motor function was unaffected (Schott et al., 1999).

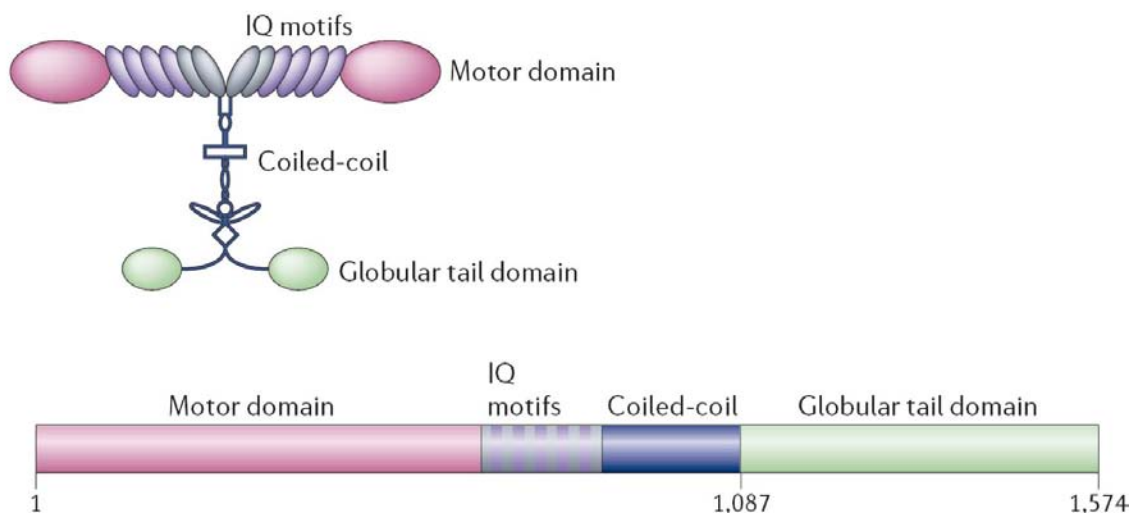


Figure 1-10.

Domain structure of Myo2. Myo2 contain four domains: motor domain (pink), IQ domain (purple), coiled coil (blue) and globular tail domain (green) (adapted with modification from Weisman, 2006)

1.4.4. Smy1

Smy1 was first described as a suppressor of a *myo2-66*, a mutant of Myo2 that lost its motor function at restrictive temperature (Lillie and Brown, 1992). Smy1 and Myo2 were found to colocalize at the polarization site of bud-tips, and interact physically through their C-terminal globular domains (Beningo et al., 2000; Lillie and Brown, 1994). Amino acid sequence showed that Smy1 is related to the microtubule-based molecular motor kinesin. Surprisingly, Smy1 does

not seem to function as a kinesin (Hodges et al., 2009; Lillie and Brown, 1998). Instead, it has multiple genetic and physical interactions with other actin-related or polarity proteins, such as formin Bnr1, profilin Pfy1, polarisome components Bem1 and Bem2 (Kamei et al., 1998; Marcoux et al., 2000; Tong et al., 2004). Despite these interactions, deletion of SMY1 caused no visible phenotypes or even reduced fitness of cells under vegetative growth conditions (Lillie and Brown, 1994, unpublished observations). A previous report showed that *smy1Δ* cells are defective in formation of mating projections (Bidlingmaier and Snyder, 2002). Recent *in vitro* data showed that Smy1 binds and slides along F-actin through electrostatic interactions. This sliding ability increases the processivity of MyoV bound to it (Hodges et al., 2009). Despite these data, it is still unclear in what these interactions mean *in vivo*. Direct observation on the role of Smy1 in actin dynamics is needed in this respect.

1.5. Experimental set-up

1.5.1. Technical challenges in studying actin cable dynamics in *S. cerevisiae*

Despite the fact that yeast actin cables were discovered over 20 years ago, there is little data available on their dynamic behaviours throughout the cell cycle. Previous measurements of actin cable dynamics were focused on cable bundles in polarized cells (Huckaba et al., 2006; Yang and Pon, 2002). Therefore, these measurements cannot be considered as a comprehensive characterization of actin cables. Furthermore, these studies provided little mechanistic understanding of cable dynamics. This lack of data was due to several factors: **1)** Abp140-GFP, the only fluorescent marker for observation of actin cables in live *S. cerevisiae* cells is only weakly associated with actin (Riedl et al., 2008). **2)** Yeast cells are small (5~10 μm in diameter) compared to other model organisms used in cell biology. Therefore extremely high spatial resolution is required to distinguish different structures. **3)** Yeast cell have poor optical properties due to their spherical shape. **4)** Signal to noise ratios (SNR) are low in conventional wide-field microscopy.

1.5.2. Total internal reflection microscopy

To overcome these technical difficulties, yeast cells were imaged with Total internal reflection microscopy (TIRFM, Axelrod et al., 1983). Instead of passing the laser perpendicular into the sample as in wide-field imaging, the incidence angle of the laser is set at or below a critical angle, at which the laser light is totally reflected by the glass-sample interface. An evanescent electromagnetic wave is generated close to the surface of reflection. This evanescent wave has the same energy level as the incidental light and it decays exponentially over distance. It can therefore excite the fluorophores within the thin section of 100~150 nm close to the sample-glass interface (Fig. 1-11). Using this method, extremely high SNR and spatial resolution are achieved, since no interferences are produced by other parts of sample. Furthermore, since only the bottom surface of the cell is illuminated, photo-bleaching and photo-damage can be kept to a minimum.

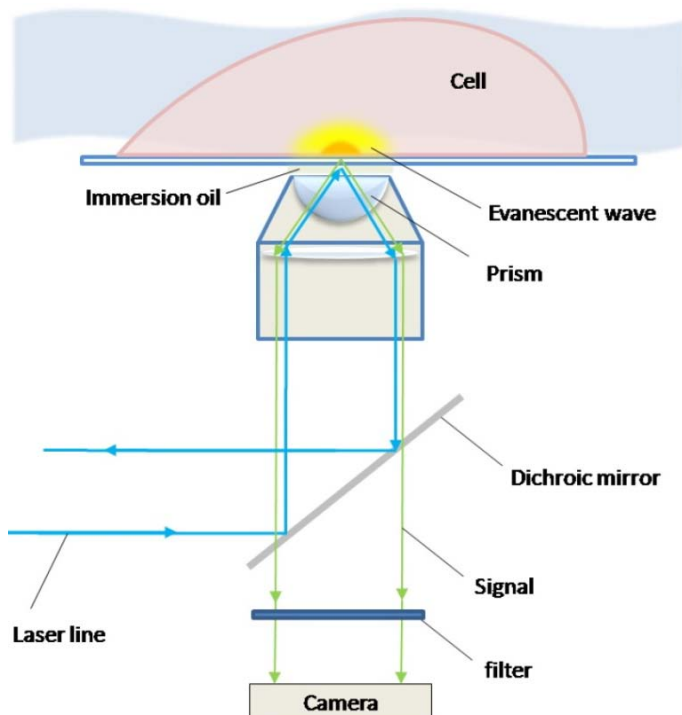


Figure 1-11.

Schematic representation of a TIRFM setup. Laser light is subjected to the sample using a prism, which introduces an incident angle at which a total reflection of the incidental light occurs. The resulting evanescent wave illuminates the fluorophores in the thin section close to the sample-glass interface.

1.6. Objectives of investigation

The objectives of this work were first to apply the improved spatio-temporal resolution on our TIRFM set-up to the visualization of actin cables. Using this imaging method, actin dynamics in large numbers of cells can be visualized and quantified in order to comprehensively characterize actin dynamics in various cell cycle stages. Combining the data gained from such quantitative characterizations with powerful yeast genetics, the molecular mechanisms regulating cellular actin organization and dynamics can be investigated. The ultimate goal of this work was to establish a molecular model for cortical actin cable dynamics.

2. Results

2.1. Actin cable dynamics in control cells

2.1.1. Abp140-GFP exhibits rapid blinking behaviour

S. cerevisiae cells intended for investigation of actin dynamics were labelled with Abp140-GFP using transformation technique based on homologous DNA recombination (by fusion of GFP to the C-terminus of Abp140. GFP fusions were generated by direct tagging at the genomic locus, see methods). Successfully labelled strains were immobilized on glass slides treated with Concanavalin A (ConA, see method section 5.4.2.) and observed using TIRFM. We have shown that Abp140 binds to F-actin with low affinity (Riedl et al., 2008). To confirm this in yeast cells, Abp140-GFP was imaged with a low exposure time of 56ms. As expected, Abp140-GFP labelled actin cables in a highly transient manner, exhibiting rapid intensity fluctuations (Fig. 2-1).

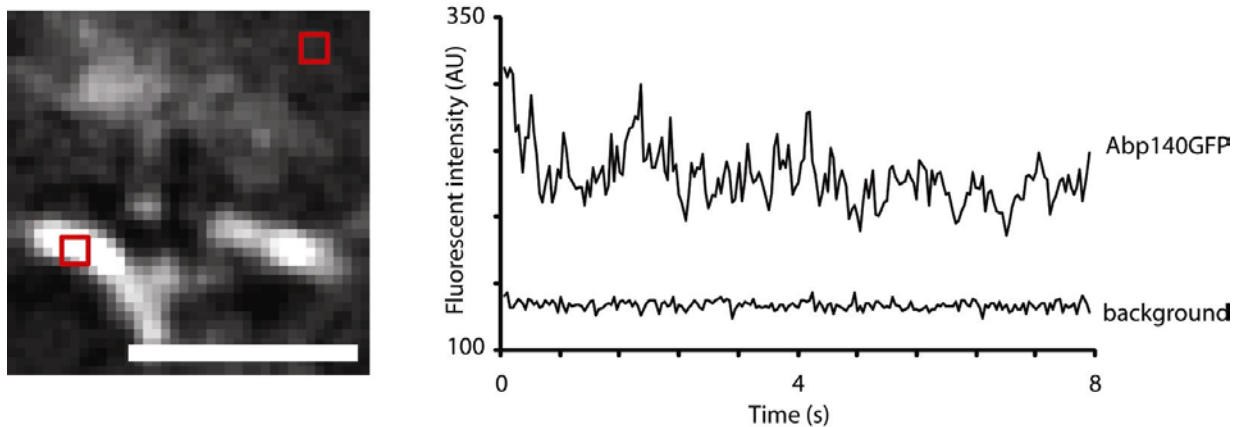


Figure 2-1

Fluctuations of Abp140-GFP signal. Wildtype cells labelled with Abp140GFP (JYY44) were imaged using TIRFM. Shown is a polarized cell with relatively static actin cables. Image sequence acquired at 56 ms/frame. Average intensities of indicated areas (red rectangles) were plotted against time. Bars = 2 μ m. for all figures.

2.1.2. Actin cables form a highly dynamic network on the cell cortex

We previously showed that Abp140 binds to actin via its N-terminal 17 amino and that this peptide binds to both G and F actin (Riedl et al., 2008). In yeast cells, Abp140 labels both actin cables and actin patches (Yang and Pon, 2002). Actin patches are punctate endocytic structures, which appear and disappear on the cell cortex. Actin cables are linear structures which move along the cell cortex. These observations were confirmed here using epifluorescent microscopy (Fig. 2-2). Therefore, Abp140 labelled actin cables and patches reliably.

It was previous reported that actin cables were mostly present on the cell cortex, and they extended into the bud tip in polarized cells. To test these observations, cells labelled with Abp140 (1-60)-GFP were observed in 3D using a wide-field fluorescent microscope. Actin cables appeared to be restricted to the cell cortex despite extensive buckling (Fig. 2-2A). Images acquired using time-lapse 3D microscopy showed that actin cables in the mother cells always terminated at the bud neck. Actin cables in the bud were generally short and randomly oriented (Fig. 2-2B). These observations are contrary to the previous belief that actin cables penetrate the budneck and are continuous from the mother cell till the budtip (Pruyne et al., 2004).

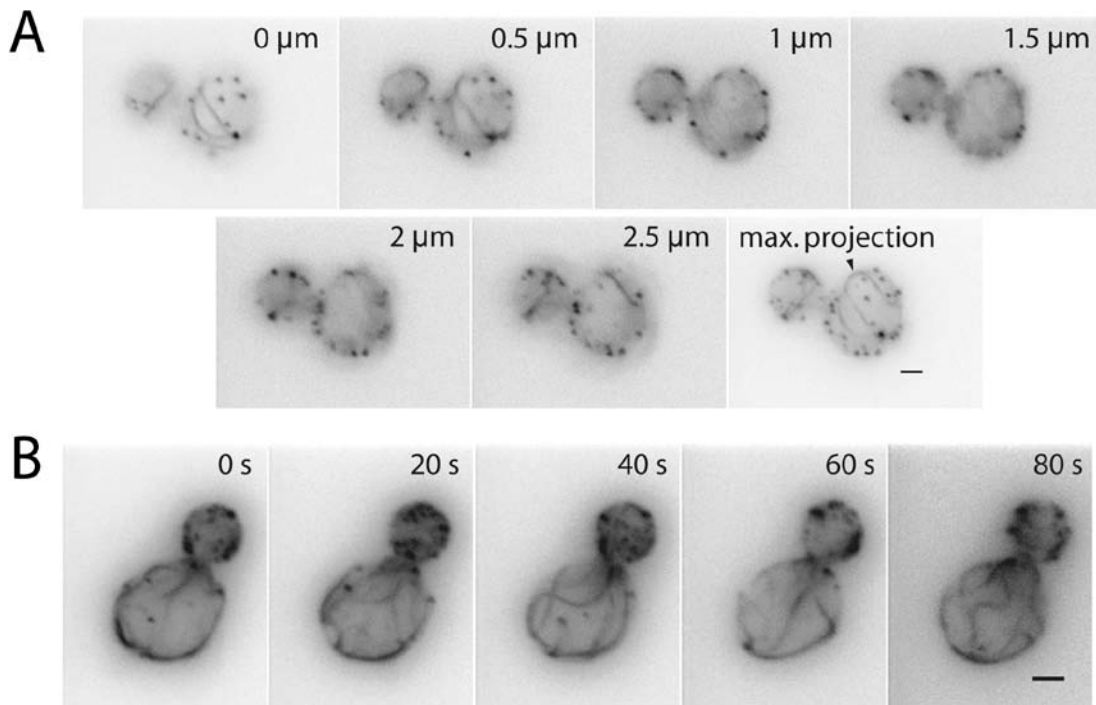
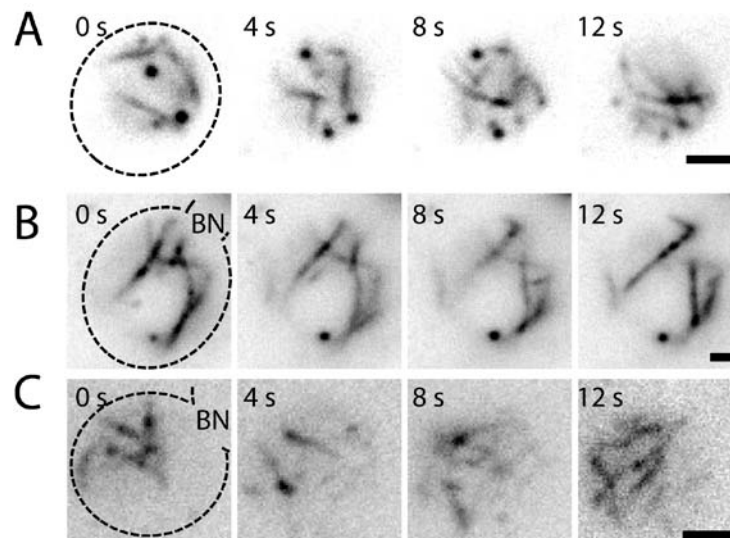


Figure 2-2

Organization of actin cables. (A) 3-dimensional organization of cables labelled with Abp140(1-60)-GFP. Z-positions are given for each frame. Arrowhead indicates buckling of an actin cable. Note that the cable was only visible in the bottom and top frames. (B) 4-D series of a cell labeled as in A. Images shown are maximum projections of individual z-stacks. Strain used JYY180. Scale bar = 2 μm (always).

In order to characterize the reorganization of actin cables during the cell cycle, cells were divided into three categories based on the size of daughter cells. These categories were unpolarized/unbudded cells (**UB**), polarized/small-medium budded cells (**MB**) and large budded cells (**LB**). Actin dynamics in control cells (JYY141) from each category was followed using TIRFM. Strikingly, actin cables were organized into highly dynamic networks in all cell cycle stages. In UB cells cables reorganized within a few seconds, were randomly distributed, often short and moved independently from each other (Fig. 2-3A). During polarized growth in MB cells cables were more stable, oriented mostly along the mother-bud axis, grew longer and often assembled into larger bundles (Fig. 2-3B). In LB cells these bundles were again disassembled and cables moved faster and were more randomly oriented (Fig. 2-3C).

**Figure 2-3.**

Cables dynamics through the cell cycle. Endogenous Abp140 was tagged with GFP in control cells (JYY141) and actin cables were imaged by TIRFM. (A-C) Actin

reorganization in an UB (A), MB (B) and LB (C) cell. Dotted lines represent the cell boundaries.

2.1.3. Individual actin cables exhibit versatile dynamic behaviours

Cortical actin cables exhibited several types of dynamic behaviours. We typically observed extension, retraction, fast translational motility, partial bundling and buckling of cables. The extension behaviours were frequently observed and were similar to previously described (Fig. 2-4A; Yang and Pon, 2002). Retraction was also frequently observed as an actin cables disappeared from the illuminated area (Fig. 2-4B). Cables were also observed moving across the cell surface without changing their length, a process we termed “translational motility” (Fig. 2-4C). Partial bundling and buckling usually occurred mostly with longer cables, especially in polarized cells (Fig. 2-4D, E).

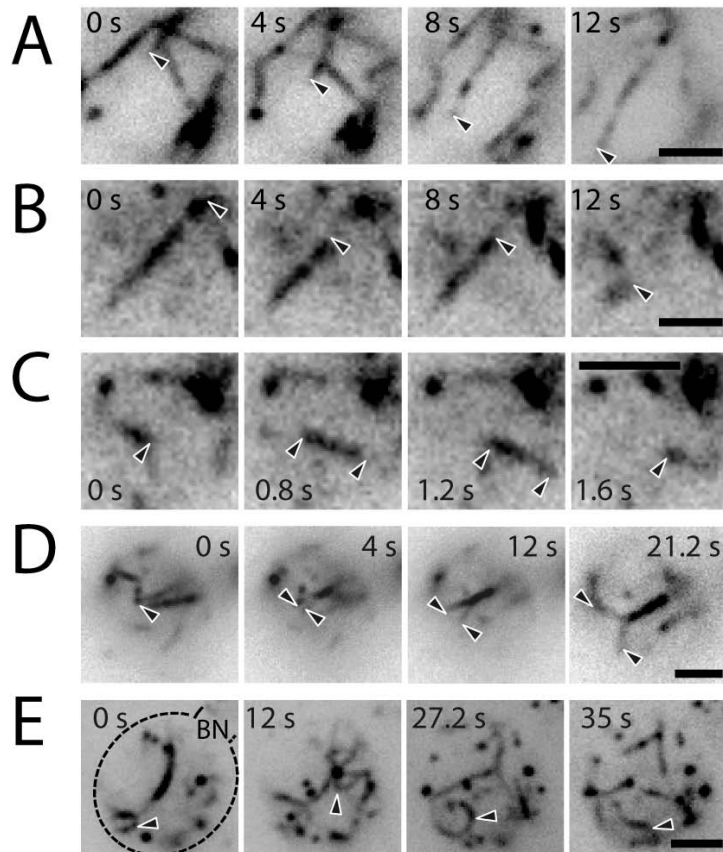


Figure 2-4.

The versatile, dynamic behaviours of actin cables. Shown are examples of (A) cable extension (B) cable retraction (C) fast translational motility (D) cable bundling (E) cable buckling. Arrowheads indicate the ends of cables or the centre of the buckle. Strain used JYY141.

2.1.4. The actin cable network undergoes rapid remodelling

To obtain a quantitative characterization of cable dynamics, a large number of individual cables were traced while they moved through the field of view. Since in TIRFM only part of the cell cortex was visible, it was usually not possible to observe both ends of a cable at the same time. Therefore, it was at first not possible to directly differentiate cable growth from translational motility. Henceforth, we refer to the movement of leading cable ends as extension, and the movement of trailing ends as retraction.

Cable extension rates were highest in UB cells, greatly slowed down in polarized MB cells and partially recovered in LB cells. Strikingly, when the histograms of extension rates were fitted against Gaussian distributions, two populations of cables with clearly separable extension rates were apparent in UB and LB cells (Fig. 2-5A, table 2-1). The faster population ($> 2 \mu\text{m/s}$, mean 2 in table 2-1) was nearly absent from polarized cells. Cable retraction rates were on average slightly faster than extensions but remained relatively constant throughout the cell cycle, with faster rates above $2 \mu\text{m/s}$ (Fig. 2-5B). This indicated that actin cables underwent constant, rapid remodelling throughout the cell cycle (Fig. 2-5B, table 2-1). Finally, the overall number of extension or retraction events was halved in polarized versus unpolarized cells, indicating a general reduction of cable dynamics in polarized cells. The numbers of extensions are higher than retractions in each cell cycle stages (Fig. 2-5C, table 2-1).

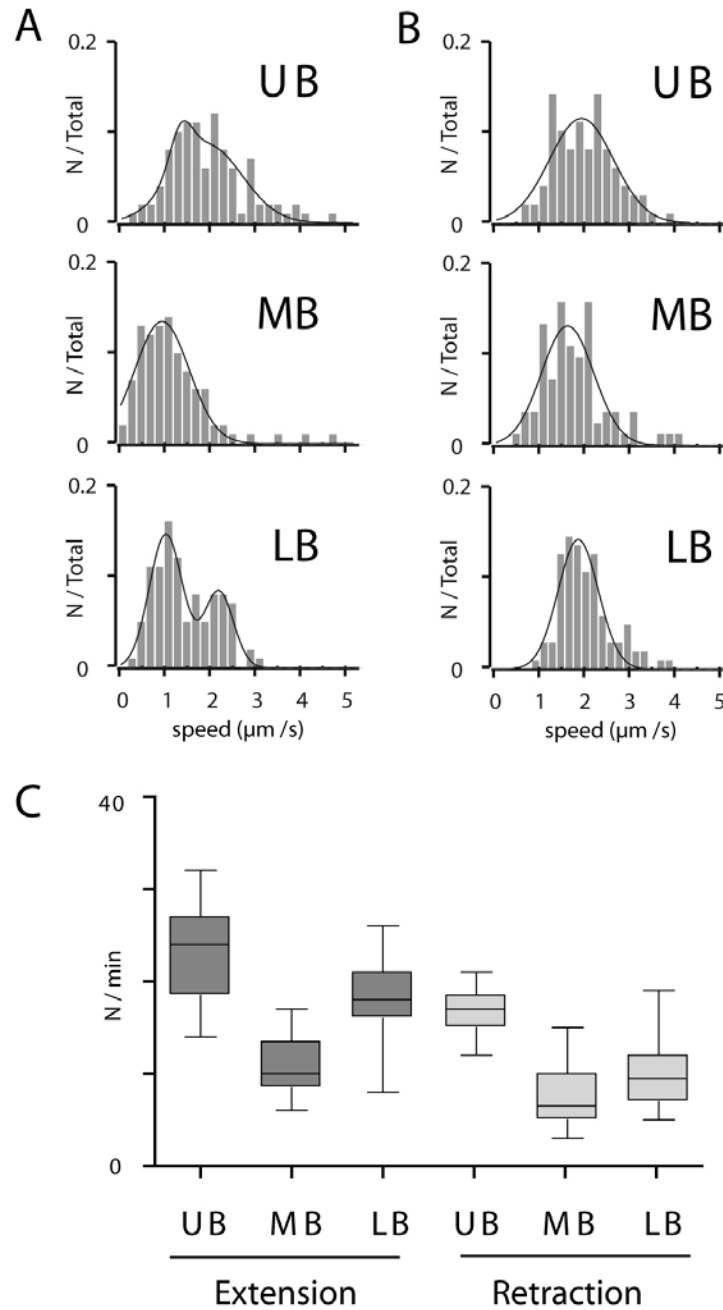


Figure 2-5.

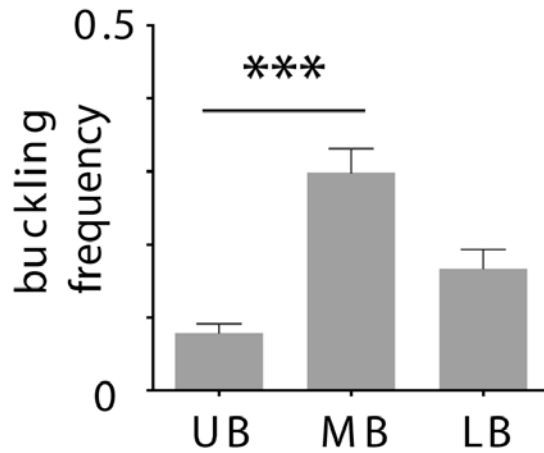
Dynamics of actin cables in control strain. The extension rates (A) and retraction rates (B) of actin cables were measured in image stacks from UB, MB and LB cells. At least 80 actin cables were tracked for each condition. Measurements were plotted into histograms. Lines represent the Gaussian fits of the data. (C) Frequencies of extension and retraction events in each cell per minute. Box plots: middle line = median, upper line of the box = 75%; lower line of the box = 25%; upper whisker = 100%; lower whisker = 0 %. Error bars: SEM. Strain used, JYY141.

Table 2-1. Measurements of actin cable dynamics in control strain¹

Speed of actin cable leading ends (extension)						
Strain	Mean 1 ($\mu\text{m/s}$)	SD1	Mean 2 ($\mu\text{m/s}$)	SD2	R²	N (cables/cells)
control UB	1.36	0.42	1.93	0.74	0.85	100/18
control MB	0.96	0.65	NA	NA	0.95	100/19
control LB	1.04	0.51	2.21	0.48	0.93	100/20
Speed of actin cable trailing ends (retraction)						
Strain	Mean 1 ($\mu\text{m/s}$)	SD1	Mean 2 ($\mu\text{m/s}$)	SD2	R²	N (cables/cells)
control UB	1.94	0.71	NA	NA	NA	100/20
control MB	1.64	0.64	NA	NA	NA	82/20
control LB	1.72	0.58	NA	NA	NA	96/20
Extension events, (N/min/cell)						
Strain	Mean		SEM		N (cells)	
control UB	22.9		1.15		21	
control MB	11.1		0.77		20	
control LB	15.8		0.94		21	
Retraction events, (N/min/cell)						
Strain	Mean		SEM		N (cells)	
control UB	16.7		0.64		16	
control MB	7.8		0.82		20	
control LB	9.8		0.84		20	

In addition to cable extension rate, the buckling rate was also used as a parameter for assessment of actin cable dynamics. The assumption was that as the cable increases in length, it tends to buckle due to geometric constraints on the highly curved cell surface (5-10 μm diameter for *S. cerevisiae* mother cells, Okada et al., 2006). Buckling rates were calculated by dividing number of buckling events over the number of cables. Counting was done within 1 min of imaging time. A high frequency of cable buckling was observed in MB cells (0.3 ± 0.032 , N = 21). In contrast, buckling was rare in UB cells (0.078 ± 0.013 , N = 20). LB cells exhibited a medium level in buckling frequency (0.16 ± 0.027 , N = 20, mean \pm SEM, Fig. 2-6).

¹ Means were given from those of the fitted curves. SD is the standard deviation. SEM is the standard error of means. R² measures the goodness of the fit. N is the sample size, NA, not applicable.

**Figure 2-6.**

Buckling rate of actin cables in control strain. Buckling rate was measured as the number of buckling events divided by the total number of cables emerged in a cell during the elapsed time of a image stack (60s). Bars represent standard error of mean (SEM). Asterisks: $p < 0.0001$ (Mann-Whitney test).

2.2. Actin dynamics in formin and formin-related mutants

2.2.1. Bni1 drives actin cable assembly in unpolarized cells

With the resolution offered by TIRFM it was now possible to utilize genetic tools to investigate the molecular basis for the various cable extension rates. Yeast actin cables are formin polymerized structures (Evangelista et al., 2002a; Sagot et al., 2002b). We first confirmed that no Abp140-GFP labelled cables were present in the absence of both yeast formins, Bni1 and Bnr1. Also, almost all cables were disassembled in the profilin ts mutant *pfy1-4* and in the tropomyosin ts mutant *tpm2Δ tpm1-2* (Evangelista et al., 2002b, Fig. 2-7A).

In order to differentiate the role of each formin, cable dynamics were imaged after deleting either of the two formins. In UB *bni1Δ* cells (JYY22), the number of actin cables was reduced by 83 % compared to control cells (Fig. 2-7B, C, table 2-2). Surprisingly, the extension rate of remaining cables was increased to an average of 2.5 $\mu\text{m/s}$ - close to the faster populations described above (Fig. 2-7B, Table 2-2). The prominent peak in control cells at $\sim 1.4 \mu\text{m/s}$ was completely lost, indicating that this peak largely represented Bni1-mediated polymerization. A few cables also showed slower extension rates around 0.7 $\mu\text{m/s}$ (Fig 2-7C, arrowhead). In *bnr1Δ* UB cells (JYY24), a 26 % decrease in cable number was observed that covered the 17% cables left in *bni1Δ* cells (Fig. 2-7B, D, table 2-2). No striking change was observed in the extension rate and organization of actin cables apart from a reduction of slow extensions $< 1 \mu\text{m/s}$ (Fig. 2-7D).

These data leads to the hypothesis that Bni1 and Bnr1 drive cable assembly with different extension rate, Bni1 drives faster extension at 1-1.4 $\mu\text{m/s}$, whereas Bnr1 dependent cable extension is slower at around 0.7 $\mu\text{m/s}$. This model provides the cell with a mechanism to switch between two modes of cable dynamics by switching between different formins, as proposed above (see introduction section 1.3.3.).

To further confirm this hypothesis, the roles of known formin regulators on cable dynamics were assayed. Deletion of the Bni1 nucleation co-factor Bud6 (Moseley et al., 2004) caused a 51% reduction of cable numbers in UB cells (JYY168, Fig. 2-7E, table 2-2) with a reduction of extension rates typical of Bni1 (1.4 $\mu\text{m/s}$) (Fig. 2-8E). This indicates that Bud6 function is not limited to the budtip of polarized cells, as previously described (Amberg et al., 1997; Kikyo et al., 1999). Bud14 is required to terminate cable elongation by Bnr1 at the bud neck in polarized cells (Chesarone et al., 2009). Unexpectedly, deletion of Bud14 also caused stabilization of actin cables in UB cells. This was reflected in the reduced number numbers (Fig. 2-7B, table 2-2) and drastically reduced extension rates (Fig. 2-7F). Actin cables in *bud14 Δ* UB cells (JYY160) were also bundled and mostly polarized towards one or multiple sites (Fig. 2-7F). Based on previous results, it is likely that this change in cable dynamics was caused by untimely activation of Bnr1 in UB cells. Consistent with this hypothesis, Bnr1-GFP, which is entirely cytoplasmic in control UB cells (JYY7), localized to the cell cortex in multiple caps or patches that were associated with cable ends in *bud14 Δ* UB cells (JYY166, Fig. 2-7G, H).

Taken together, these data demonstrate that Bni1 and Bnr1 drive actin cable assembly with different kinetics in unpolarized cells. Bni1 is the major generator of actin cables in UB cells. Bud6 participates in actin dynamics, most probably by activating Bni1. Timely inactivation of Bnr1 by Bud14 is required to allow fast remodelling of the cable network.

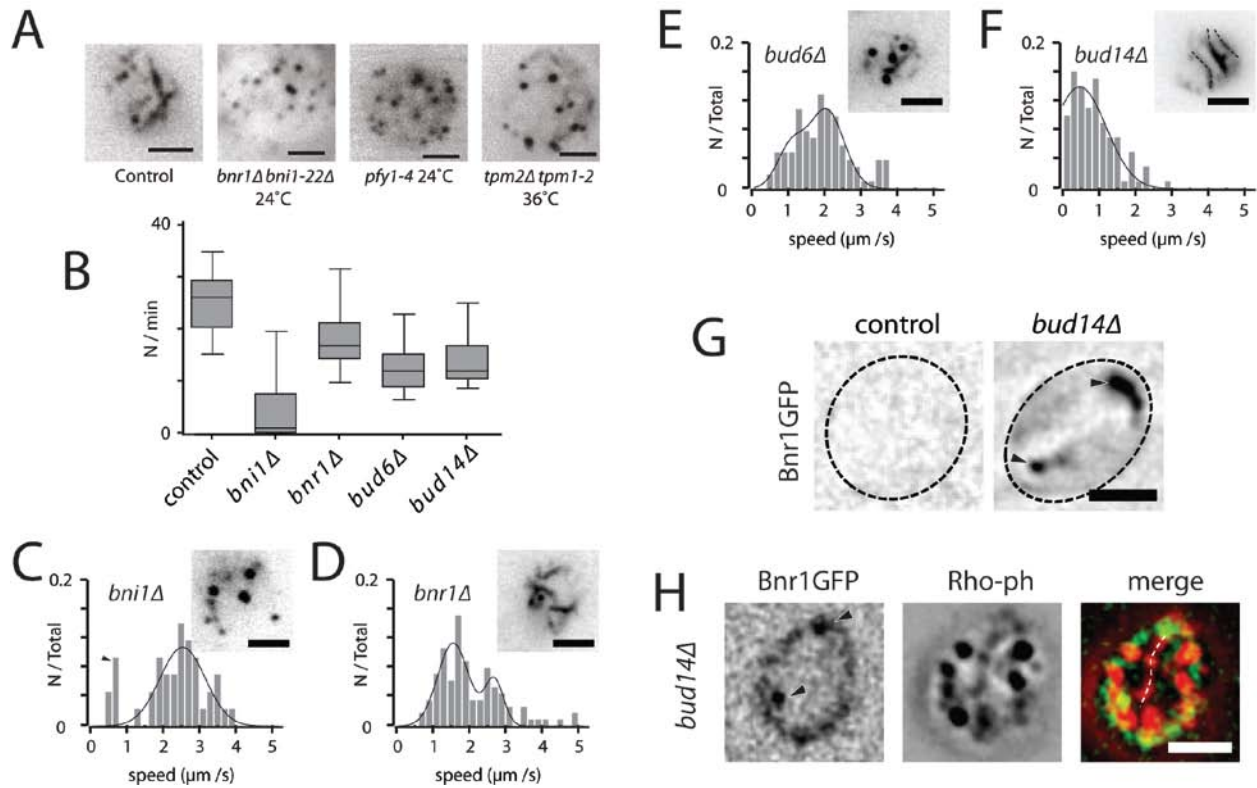


Figure 2-7

Dynamics of actin cables in UB cells of mutants affecting formin functions. (A) Organization of actin cable network in control, *bnr1Δ bni1-22Δ* mutant, *pfy1-4* mutant and *tpm2Δ tpm1-2* mutant cells. (B) Number of cables that emerged in UB cells of the indicated strains within one minute of imaging. Box plots are as in Fig. 2-5. (C-F) Organization and extension rate of actin cables in UB cells of the following mutants: (C) *bni1Δ* arrowhead indicates population of cables exhibiting very slow cable extension rate, (D) *bnr1Δ*, (E) *bud6Δ* and (F) *bud14Δ*. Insets show example TIRFM images of cable organization in respective strains. Polarized cables in (E) are marked with dotted lines. Cable extension rates are presented as histograms and fitted with Gaussian distributions. (F) Localization of Bnr1-GFP in control and *bud14Δ* UB cell. Arrowheads show polarization sites. Dotted lines mark the cell boundaries. (G) Polarization of actin cable (dotted line) towards Bnr1-GFP dots in UB cell of *bud14Δ* mutant. Cells expressing Bnr1-GFP were fixed and stained with 3 μM rhodamine-phalloidin. Arrowheads indicate Bnr1-GFP dots. Images were smoothed for better visualization.

Table 2-2. Measurements of actin cable dynamics in UB cells of formin and formin-related mutants

Cable numbers (N/min/cell)						
Strain	Mean	SEM	N (cells)			
control UB	22.9	1.15	21			
<i>bni1Δ</i> UB	3.8	1.07	25			
<i>bnr1Δ</i> UB	17	1.15	20			
<i>bud6Δ</i> UB	11.2	0.83	23			
<i>bud14Δ</i> UB	12.7	1.04	20			
Extension rates						
Strain	Mean 1 (μm/s)	SD 1	Mean 2 (μm/s)	SD 2	R ²	N (cables/cells)
control UB	1.36	0.42	1.93	0.74	0.85	100/18
<i>bni1Δ</i> UB	2.54	1.13	NA	NA	0.81	42/25
<i>bnr1Δ</i> UB	1.56	0.55	2.68	0.43	0.81	100/20
<i>bud6Δ</i> UB	1.07	0.52	2.06	0.59	0.85	100/30
<i>bud14Δ</i> UB	0.52	0.72	NA	NA	0.93	100/20

2.2.2. Fast cable motility is independent of actin polymerization

The data presented above showed that, intriguingly, fast cable extension rates $> 2 \mu\text{m/s}$ were not affected by deletion or deregulation of either formin, except in *bud14Δ*, where all cables become bundled and immobilized (Figure 2-7B, D). Furthermore, this high-speed population corresponded mostly to cables undergoing *translational motility* (Fig. 2-4C). The fact that this motility was not affected by abolishment of formins suggested that it was independent of actin polymerization.

To confirm this, we treated cells with Latrunculin B (LatB, Winder et al., 2003). We first determined that treatment with $20\mu\text{M}$ LatB for 10 min at RT was sufficient to remove all actin cables (not shown), confirming that cables were rapidly turning over. We then treated *bnr1Δ* cells (JYY24) cells with varying concentrations of LatB to specifically reduce formin-dependent polymerization activities. At LatB concentrations of 2-8 μM cables became progressively shortened until they completely disappeared at 16 μM . Strikingly, average cable extension rates, which now solely reflected cable motility, were successively increased, peaking at 2.4 $\mu\text{m/s}$ in 8

μM LatB (Fig. 2-8, table 2-3). These results confirmed that a polymerization-independent mechanism must exist to drive motility of actin cables at greater than $2\mu\text{m/s}$.

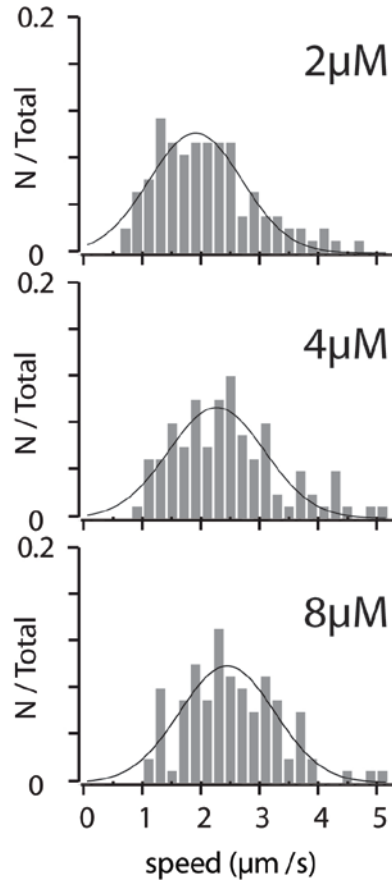


Figure 2-8

Fast cable motility is independent of formin mediated polymerization. Cable motility (extension rates) in UB cells in *bnr1Δ* mutant under the treatment of low-dose LatB. Cells were grown in YPD medium with incremental concentration of LatB at RT.

Table 2-3. Measurements of actin cable dynamics of UB cells in *bnr1Δ* mutant under the treatment of low-dose LatB.

Extension rates				
Strain (<i>bnr1Δ</i> UB)	Mean ($\mu\text{m/s}$)	SD	R ²	N (cables/cells)
2 μM LatB	1.90	1.13	0.87	100/20
4 μM LatB	2.26	0.55	0.77	100/20
8 μM LatB	2.44	0.52	0.78	100/20

2.3. Myo2 drives fast cable motility

2.3.1. Actin cable dynamics in *myo2* temperature sensitive mutants

The only previously reported process capable of generating movement at speeds close to the observed 2.5 $\mu\text{m/s}$ is intracellular transport driven by the type V myosin Myo2. Typical velocities of Myo2-dependent vesicle transport ranged between 2 and 3 $\mu\text{m/s}$ (Schott et al., 2002; Sheltzer and Rose, 2009). To this end, cable dynamics in UB cells of various Myo2 mutants were tested. First, the temperature sensitive (ts) mutant *myo2-66* (JYY32) was examined. As mentioned above, this mutant has a defect in its actin binding site (Johnston et al., 1991). Next, *myo2-16*, another ts mutant (JYY79) that has a defect in its globular tail (CTD) was tested. The mutations in *myo2-16* interfere with cargo binding (Schott et al., 1999) but not the motor function.

Neither mutant showed changes in the number of cables present at restrictive temperature (Fig. 2-9A). Strikingly, quantification of cable extension rates showed a specific loss of fast extensions without affecting slower events that presumably depended on Bni1 and Bnr1 (Fig. 2-8, 2-9B, C). Individual cables in cells with disrupted Myo2 function often exhibited tumbling motion (Fig. 2-9D) or were completely stuck for several seconds (Fig. 2-9E) – behaviours never observed in control cells, where cables always continuously moved along the cell cortex (Fig. 2-4C). These results suggested an active role of Myo2 in cable motility in UB cells. Consistent with this assumption, the fast-moving population of cables in a *bni1 Δ* strain (Fig. 2-7B) was completely absent, when Myo2 function was additionally abolished in a *bni1 Δ myo2-16* strain (JYY34). Only slow cable extension (0.7 $\mu\text{m/s}$) was observed that corresponded to Bnr1-mediated elongation. The average cable number was also drastically reduced (Fig. 2-9A, C, table 2-4).

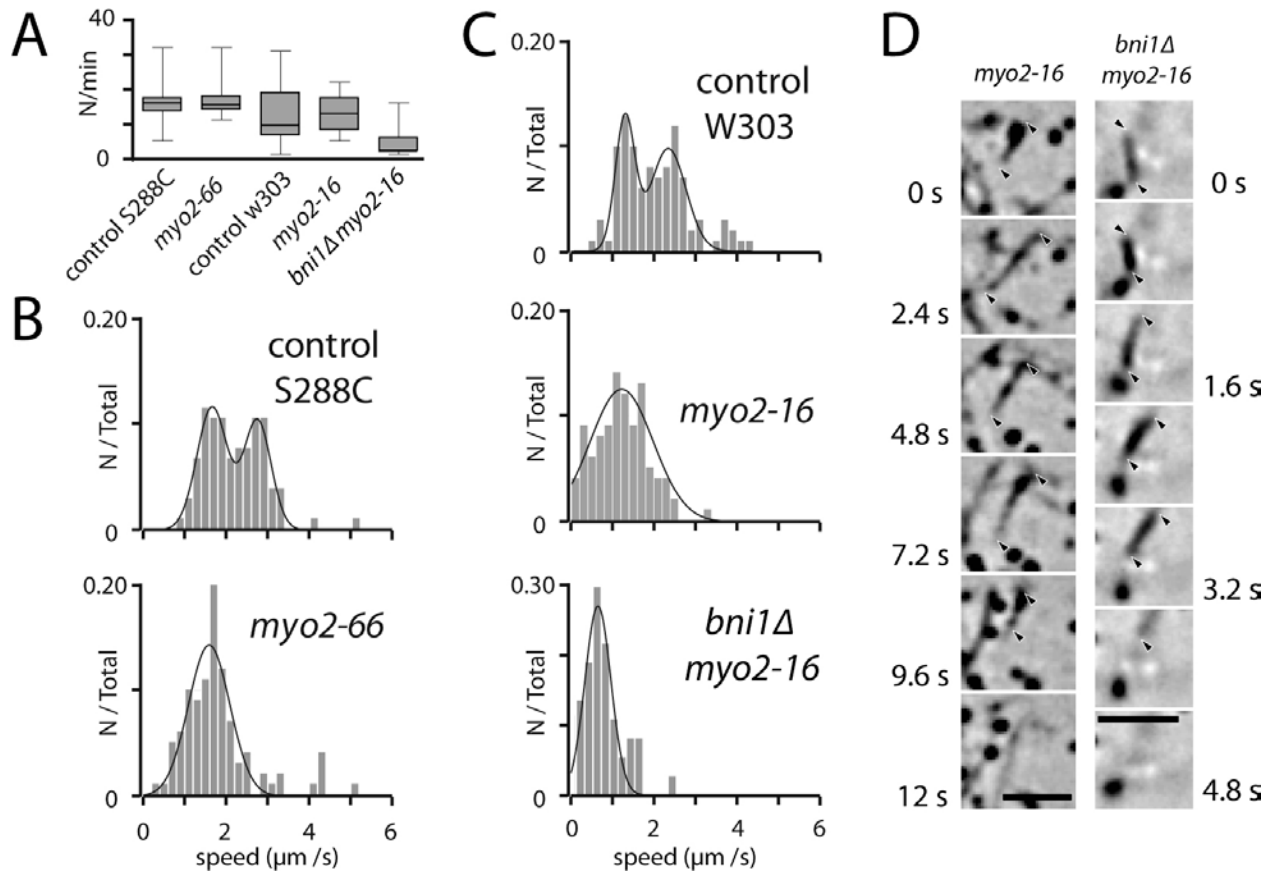


Figure 2-9

Actin cable dynamics in *myo2* ts mutants. (A) Cable numbers in control, *myo2-16* and *myo2-66* strains. Numbers are calculated as in Fig.2-7. (B) Histograms and Gaussian fits of cable extension rates in *myo2-66* cells and corresponding control cells. (C) Histograms and Gaussian fits of cable extension rates in *myo2-16* cells, *bni1Δ myo2-16* cells and corresponding control cells. (D) Abnormal actin cable behaviour in *myo2-16* and *myo2-16 bni1Δ* mutants. Left panel shows a stuck actin cable, which is immobile in the middle of the cell for 10 seconds. Right panel shows a cable exhibiting a rotation (arrowheads). All experiments performed at 36°C. Images were smoothed for better visualization.

Table 2-4. Measurements of actin cable dynamics in *myo2* ts mutants

Cable numbers (N/min/cell)						
Strain(at 36°C)	Mean	SEM		N (cells)		
control S288C	12.57	1.14		21		
<i>myo2-66</i>	4.4	1.06		15		
control W303	16.4	1.56		20		
<i>myo2-16</i>	16.3	1		20		
<i>myo2-16 bni1Δ</i>	13.3	2.11		20		
Extension rates						
Strain (at 36°C)	Mean 1 (μm/s)	SD 1	Mean 2 (μm/s)	SD 2	R ²	N (cables/cells)
control S288C	1.68	0.50	2.74	0.48	0.97	100/20
<i>myo2-66</i>	1.59	0.59	NA	NA	0.85	100/20
control W303	1.30	0.41	2.3	0.55	0.87	100/14
<i>myo2-16</i>	1.17	0.71	NA	NA	NA	100/20
<i>myo2-16 bni1Δ</i>	0.70	0.47	NA	NA	0.85	43/21

2.3.2. Speed of cable motility is dependent on Myo2 neck length

Both *myo2-16* and *myo2-66* are unable to support polarized transport, and therefore lead to serious physiological defects (Johnston et al., 1991; Schott et al., 1999). To rule out indirect effects on cable dynamics due to physiological defects in the myosin ts mutants, we wanted to directly link the speed of cable extension to the speed of Myo2. To this end, cable dynamics was measured in Myo2 mutants containing different numbers of IQ domains. As shown previously, removal of IQ domains lead to a reduction in myosin step size and hence speed of Myo2 (Schott et al., 2002). As expected, the proportion of fast moving cables was reduced and the overall speed progressively slowed down with the reduction of IQ repeats (Fig. 2-9F, table 2-5). In control cells (JYY148), extension rates exhibited the signature two-peak distribution. The average speed of fast cable motility was 2.54 μm/s. In *myo2-2IQ* mutant (JYY149), this peak collapsed and the average speed of the faster peak decreased to 1.57 μm/s. In *myo2-0IQ* mutant (JYY150), the high-speed peak was no longer detected. The overall average speed dropped below 1 μm/s, probably due to the slower myosin driven cable motility merging with the

polymerization peak. Taking together, these data confirm that Myo2 regulates actin dynamics by promoting rapid cable motility along the cell cortex in UB cells.

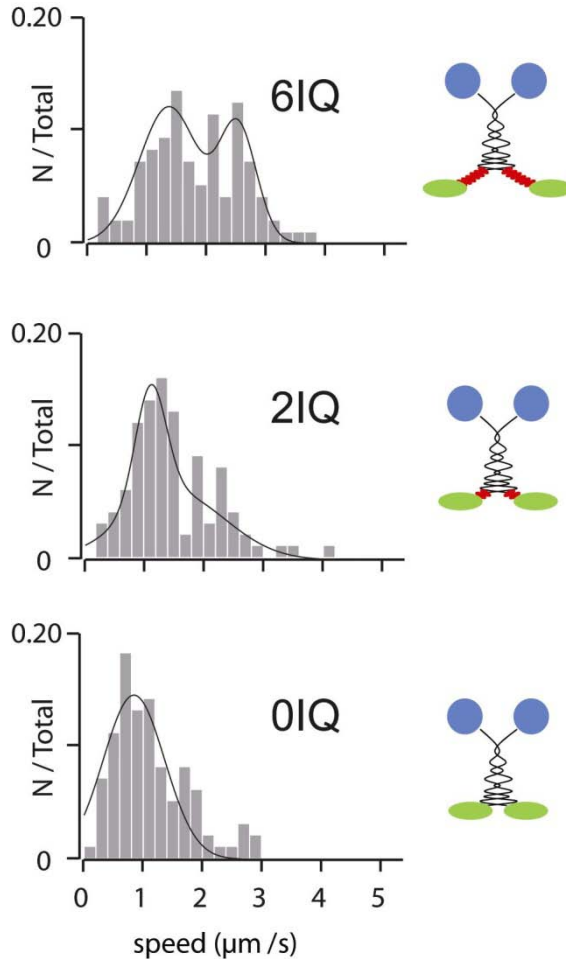


Figure 2-10

Speed of cable motility depends upon Myo2 lever arm length. Cable extension rate of UB cells in mutant under the treatment of LatB. Cable extension rates in Myo2-6IQ (6IQ), *myo2-2IQ* (2IQ) and *myo2-0IQ* (0IQ). Cells were grown in YPD medium containing 2 μ M LatB, which reduces the cable length, thereby increase proportion of cables undergoing translational motility

Table 2-5. Measurements of actin cable dynamics in UB cells of *myo2* IQ mutants

Extension rates						
Strain	Mean 1 (μ m/s)	SD 1	Mean 2 (μ m/s)	SD 2	R ²	N (cables/cells)
Myo2-6IQ	1.40	0.59	2.54	0.47	0.75	100/20
<i>myo2-2IQ</i>	1.17	0.43	1.57	0.79	0.82	100/20
<i>myo2-0IQ</i>	0.91	0.61	NA	NA	0.88	100/20

2.4. Interaction of actin cables with cortical Bni1 and Myo2

As actin cables are strictly cortical (Fig. 2-1), we assumed that the regulators of cable dynamics identified in UB cells must also reside on the cell cortex. However, there had been no previous report on cortical localization of either Bni1 or Myo2 apart from sites of polarized growth. To revisit this, endogenously tagged Bni1-GFP (JYY6) and Myo2-GFP (JYY8) were monitored by TIRFM. Strikingly, in UB cells both proteins localized to a large number of dynamic but clearly defined cortical dots. Both Bni1 and Myo2 cortical dots had average lifespan of 10-15 s (Fig. 2-11~15).

2.4.1. Bni1 and Myo2 dots are distinct from actin patches

Since both Bni1 and Myo2 dots had lifespans similar to actin patches (8-12 s, Kaksonen et al., 2003) we checked whether they colocalized. Actin cables and patches were labelled in the GFP tagged strains using Abp140 (1-214)-mRFPRuby (strains, JYY144 and JYY133, see section 5.1.1.). Actin cables were reduced by adding 2 μ M LatB. Cells were imaged using TIRFM as previously. Kymograph analyses showed that neither cortical Bni1 nor Myo2 dots colocalized with actin patches (Fig. 2-11). Therefore Bni1 and Myo2 cortical dots were distinct, novel structures that had not been previously identified.

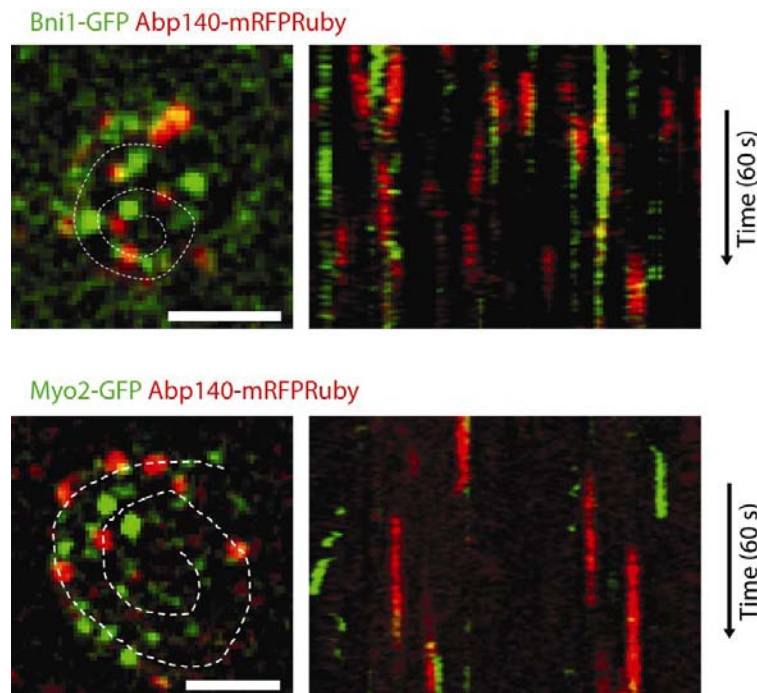


Figure 2-11

Cortical Bni1 and Myo2 dots are distinct from actin patches. Two-color TIRFM of cortical Bni1-GFP and Myo2-GFP dots together with actin patches labelled with Abp140(1-214)-mRFPRuby in 2 μ M LatB. Kymographs indicate minimal colocalization. Movies were acquired continuously with 100ms exposure time in the green channel and 300ms exposure in the red channel per frame.

2.4.2 Cortical Bni1 associates with actin cables

To drive actin cable dynamics, it is necessary for the cortical Bni1 and Myo2 patches to directly interact with actin cables. To test this, actin cables labelled with Abp140 [1-214]-mRFPRuby were colocalized with Bni1-GFP or Myo2-GFP.

Acquired images showed versatile interactions between actin cables and Bni1 dots. We found that actin cables frequently emerged from Bni1 dots on the cortex (Fig. 2-12A). Sometimes several cables grew out from a single Bni1 dot. Also, Bni1-GFP dots often moved short distances together with the trailing end of an emerging cable before disappearing (Fig. 2-12B). Furthermore, in a few cases, Bni1-GFP dots split in two with one part moving away with the cable and the rest remaining behind (Fig. 2-12C).

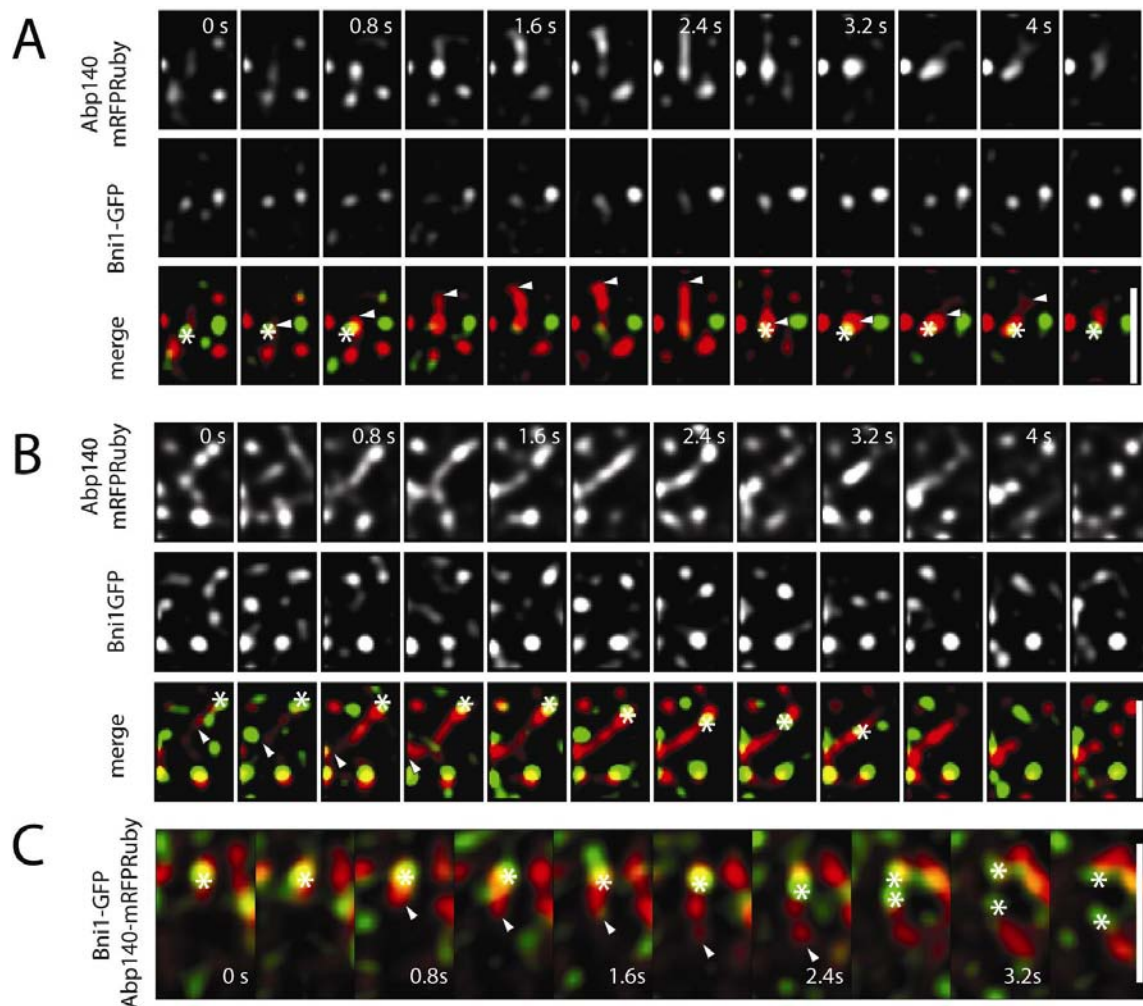


Figure 2-12

Cortical Bni1 dots interact with actin cables. (A) Actin cables labelled with Abp140 [1-214]-mRFPRuby (Arrowheads,) originate from a Bni1-GFP dot (Asterisks). (B) Bni1 dot (Asterisks) localizes to and moves along the trailing end of an actin cable before it disappears. (C) Short actin cable (arrowheads) originates from a Bni1 dot that splits into two (Asterisks). One dot remains at the original position, the other moves along the trailing end of the cable. Images were deconvolved with Huygens program to improve signal-to-noise ratio. Strain used JYY144.

2.4.3. Cortical Myo2 associates with actin cables

Next, colocalization of actin cables and Myo2 dots was tested. In unpolarized cells, actin cables were decorated with Myo2-GFP dots. Actin cables moved quickly along the cell cortex while the dots remained relatively static (Fig. 2-13A). As cables moved through one myosin dot, new dots were frequently formed along the path. These dots were mostly very faint, relatively short lived (< 4s) and usually undetectable in kymograph analyses. Less frequently, the more stable dots were picked up by motile cables. They then briefly moved along the respective cable and rapidly disappeared (Fig. 2-13B).

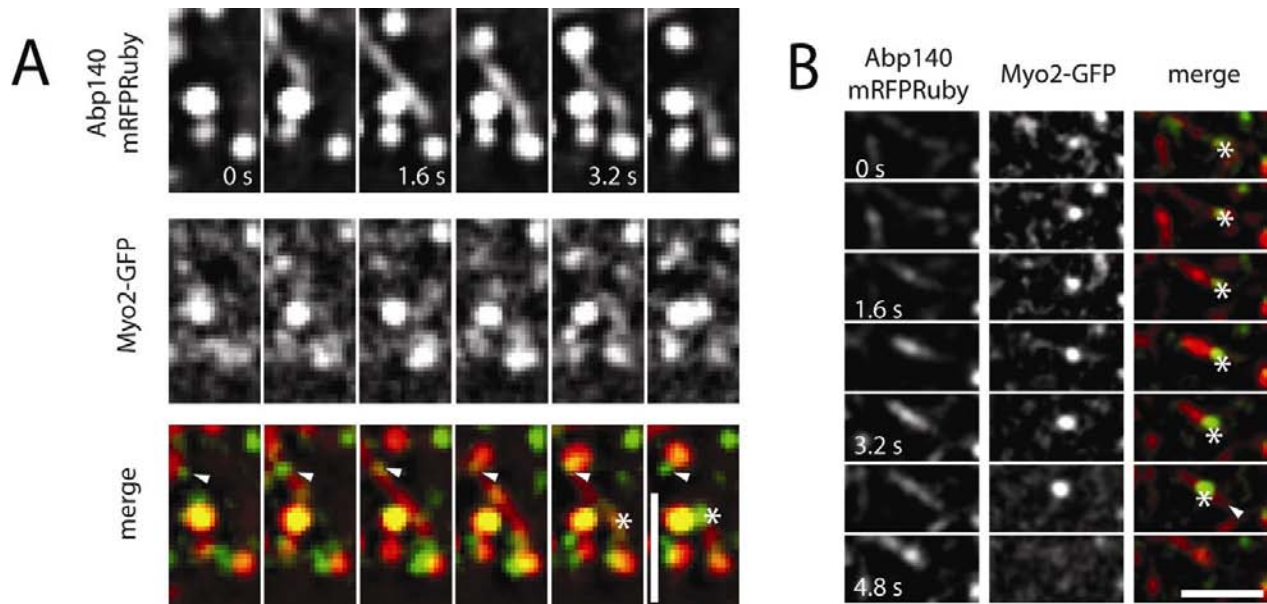


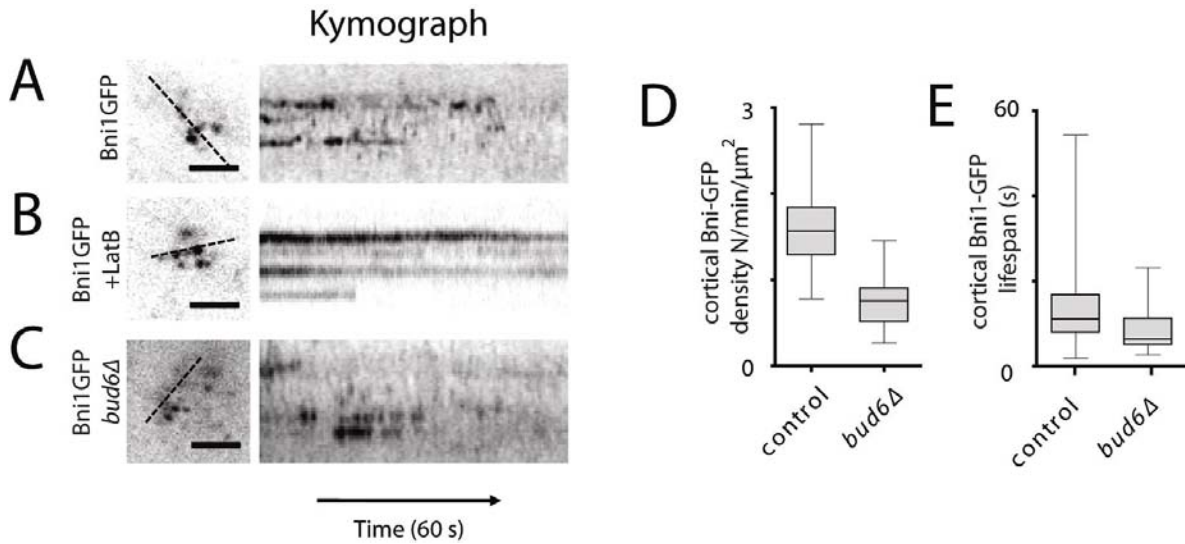
Figure 2-13

Cortical Myo2 dots interact with actin cables. (A) Motile actin cables interact with multiple Myo2 dots along the path. Arrowheads and asterisks indicate two different Myo2 dots which colocalize with actin cables along the path of translational movement. (B) A Myo2 dot is picked up by a passing cable, moves along the cable and disappears. Asterisks trace the dot; the arrowhead indicates its original position. Images were smoothed for better visualization.

In summary, Bni1 and Myo2 localize to the cortex of UB cells in distinct dynamic patches and associate with actin cables. The colocalization data were in agreement with the mechanism, whereby cortical Bni1 nucleates actin cables that are then moved along the plasma membrane via cortically anchored Myo2 molecules.

2.4.4. Dynamics of cortical Bni1 dots

In order to understand the molecular mechanism of Bni1-dependent actin dynamics, it was necessary to determine how exactly Bni1 associates with the cortex. One immediate question would be whether this association was dependent on actin cables. To answer this, actin cables in control cells (JYY6) were completely removed by treatment with 20 μ M LatB. Surprisingly, Bni1 dots seemed to become stabilized and remained on the cortex for often longer than to 60 s (Fig. 2-14A, B). In comparison, cortical Bni1-GFP dots in untreated UB cells had average lifespans of 13 s and in rare cases remained stable for up to 50s (table 2-6, Fig. 2-14E). Bud6 had been previously implied in recruiting Bni1 to the bud tip (Buttery et al., 2007). Consistent with a similar function in UB cells Bni1 patches in *bud6 Δ* mutant cells appeared at lower density and were shorter lived (JYY174, Fig. 2-14C-E). These results indicated that the formation of Bni1 cortical dots was independent of actin cables but dependent on Bud6. On the other hand, actin cables were most likely responsible for the removal of the Bni1 dots from the cortex, such as in the example shown in Fig. 2-12B

**Fig. 2-14**

Dynamics of cortical Bni1 dots. (A-C) Dynamics of cortical Bni1-GFP in control cells (A) control cells treated with 20 μM LatB (B) and *bud6Δ* cells (C). (D) Cortical Bni1 dot density. (E) Cortical Bni1 dot lifespan. All quantifications are presented as box plots as in Fig. 2-5.

Table 2-6. Measurements of cortical Bni1 dynamics

Lifetime of cortical Bni1 dots (UB cells)			
Strain	Mean (s)	SD	N (dots/cells)
control	13.74	9.28	100/11
<i>bud6Δ</i>	8.57	5	64, 13
Density of Bni1 dots (UB cells)			
Strain	Mean ($\mu\text{m}^{-2}/\text{min}^{-1}$)	SEM	N (cells)
control	1.6	0.12	18
<i>bud6Δ</i>	0.74	0.1	11

2.4.5. Dynamics of cortical Myo2 dots

Myo2-GFP formed dynamic dots on the cortex of UB cells with a lifespan similar to Bni1-GFP dots (Fig. 2-15A, table 2-6). Treatment with 20 μ M LatB in control cells (JYY8) also stabilized Myo2-GFP dots albeit to a lesser extent than for Bni1-GFP (Fig. 2-15B, F, G, table 2-6), indicating that Myo2 dots might also be removed from the cortex, by actin cables. Consistently, in *bni1 Δ* UB cells, which contained few actin cables, Myo2 dot densities and lifespans were increased (JYY161, Fig. 2-15F, G, table 2-6). Likewise, Myo2 dots were stabilized in a *myo2-66* mutant, which could no longer bind to actin (JYY130, Fig. 2-15C, F, G, table 2-7). On the other hand, when actin cables were stabilized in UB *bud14 Δ* cells, cortical Myo2-GFP dots exhibited reduced density and lifespan (JYY162, Fig. 2-15D, F, G). In these cells, most of the Myo2 was found in polar caps (Fig. 2-15H), similar to those formed by Bnr1-GFP (Fig. 2-7F). In summary, Myo2 cortical dots were stabilized when actin cables or actin-binding activity were disrupted whereas they became destabilized in the presence of stable actin cables.

The localization of Myo2 is dependent on both its head-domain and C-terminal cargo binding domain (CTD) domain (Johnston et al., 1991; Schott et al., 1999). The measurements of Myo2-66-GFP dynamics showed that the head-domain of Myo2 played no role in the formation of cortical dots. The localization function is therefore likely to depend on its CTD. To confirm this, the CTD-defective *myo2-16* was tagged with GFP (JYY87) and imaged. Strikingly, Myo2-16-GFP did not form cortical dots, but instead became enriched on actin cables (Fig. 2-15E, arrowheads)

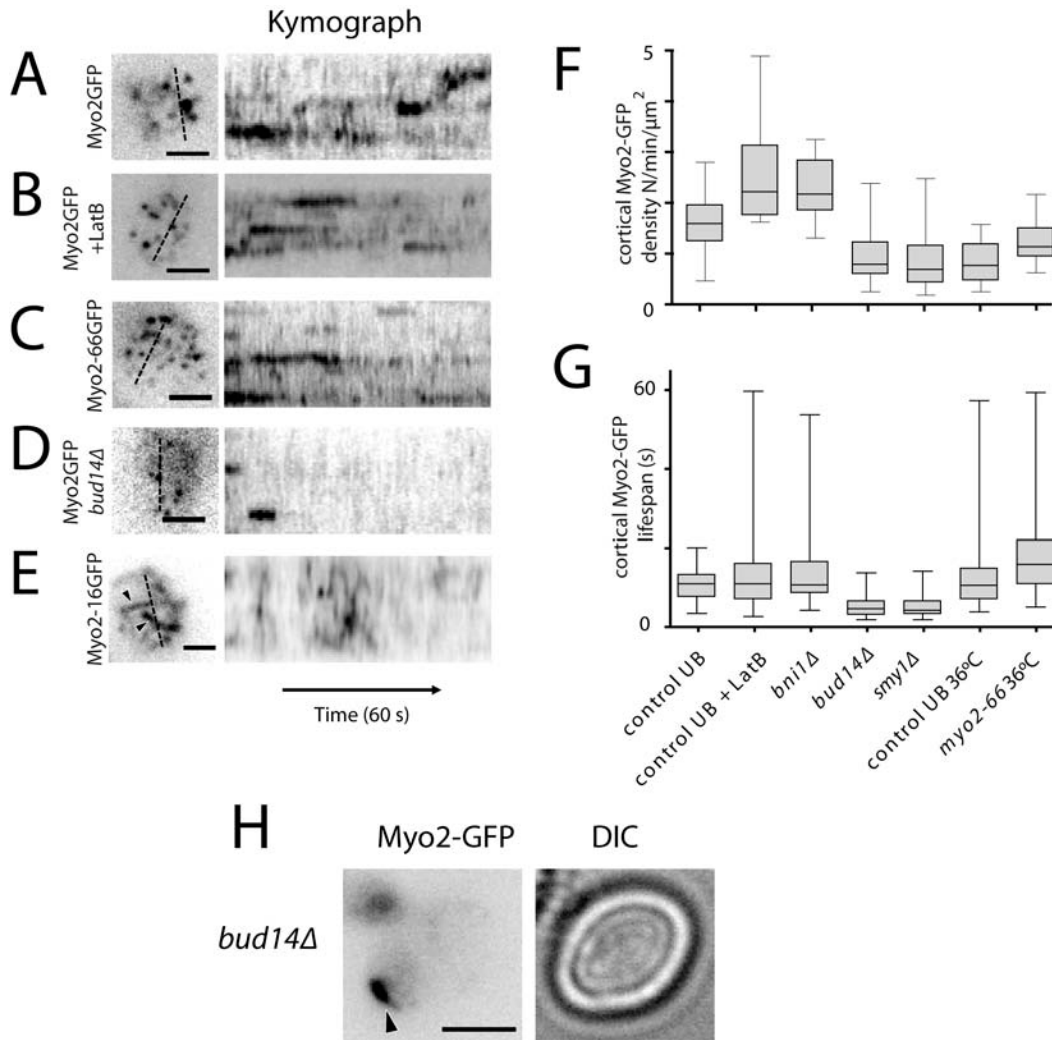


Figure 2-15

Dynamics of cortical Bni1 dots. Shown are individual time points and kymographs along indicated dotted lines. **(A)** Myo2-GFP, **(B)** Myo2-GFP in 20 μM LatB, **(C)** Myo2-66-GFP at 36°C, **(D)** Myo2-GFP in *bud14Δ* cell. **(E)** Myo2-16-GFP at 36°C. **(F)** Cortical Myo2 dot densities. **(G)** Cortical Myo2 lifespans. All quantifications are presented as box-whisker plots as in Fig.2-5. Scale bars 2 μm . **(H)** Localization of Myo2-GFP in *bud14Δ* UB cell. Arrow head indicate polarized cap structure of Myo2-GFP. Images were taken with 400ms exposure.

Table 2-7. Measurements of cortical Myo2 dynamics.

Lifetime of cortical Myo2 dots (UB cells)			
Strain	Mean (s)	SD	N (dots/cells)
control	11.12	4.33	100/20
control (MB)	10.14	9.43	100/20
control + 20 μM LatB	13.94	9.59	100/20
<i>bni1</i> Δ	14.24	10.15	100/20
<i>bud14</i> Δ	5.14	2.70	100/20
<i>smy1</i> Δ	5.02	2.63	100/22
control²	12.81	8.96	100/20
<i>myo2-66</i> ²	20.81	14.42	92/17
Density of Myo2 dots (UB cells)			
Strain	Mean ($\mu\text{m}^{-2}/\text{min}^{-1}$)	SEM	N (cells)
control	1.70	0.12	24
control (MB)	0.55	0.09	18
control + 20 μM LatB	1.06	0.12	21
<i>bni1</i> Δ	2.37	0.13	20
<i>bud14</i> Δ	1.06	0.11	21
<i>smy1</i> Δ	0.97	0.13	20
control²	0.94	0.09	20
<i>myo2-66</i> ²	1.32	0.09	17

2.4.6. Smy1 is a component of Myo2 dots

The recruitment of Myo2 to its organelle cargo is mediated via specific adaptor proteins that interact with the C-terminal tail (Pruyne et al., 2004). It is reasonable to postulate that a similar adaptor might link Myo2 to the plasma membrane. One candidate that has been previously shown to interact with the Myo2 tail is Smy1, a kinesin homologue that has lost its ability to bind to microtubules (Lillie and Brown, 1998). Smy1 overexpression suppresses the *myo2-16* and *myo2-66* mutations but its precise function is unknown (Lillie and Brown, 1992). TIRFM imaging showed that Smy1-GFP (JYY129) formed cortical patches similar to Myo2-GFP (Fig. 2-16A). When imaged by double-colour TIRFM, Smy1-GFP and Myo2-mRFPRuby was shown

² Experiments performed at 36°C

to colocalize in cortical patches over their whole lifespan (JYY139, Fig. 2-16B). Strikingly, a substantial reduction of Myo2 patch density and lifespan was observed in a *smy1Δ* strain (JYY131, Fig. 2-15F, G, L, table 2-7). These data demonstrated that Smy1 is a component of cortical Myo2 patches and important for the recruitment of Myo2 to the cell cortex probably via the globular tail domain of myosin.

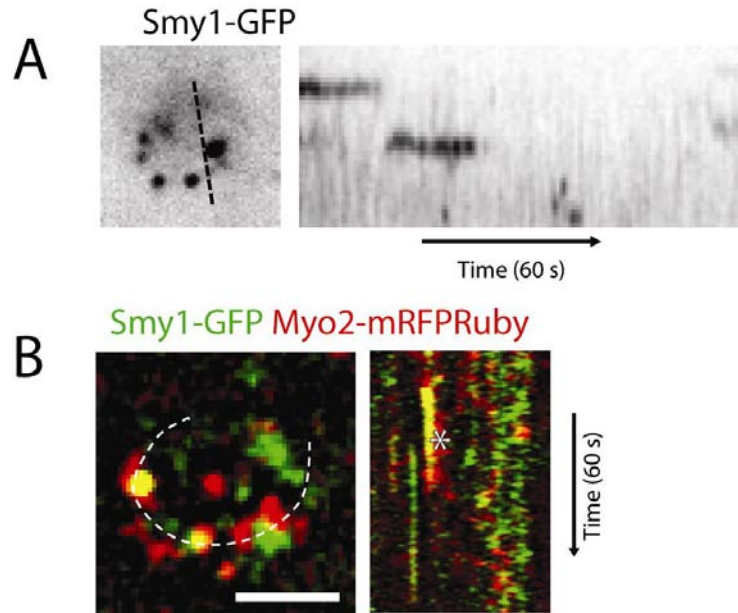


Figure 2-16

Myo2 colocalize with Smy1 on the cell cortex. (A) Dynamics of cortical Smy1-GFP dots in UB cell of control strain. A kymograph along the indicated dotted line is shown. (B) Colocalization of Smy1-GFP and Myo2-mRFPRuby in cortical dots. Images were taken with 400ms of exposure.

The results on cortical Myo2 dynamics demonstrated that Myo2 assembled into cortical dots via interaction with Smy1 through its CTD. The removal of the Myo2 dots was dependent on actin cables as well as the motor domain of Myo2.

The results on Bni1 and Myo2 dynamics paint a scenario of reciprocal interactions in cable regulation: Bni1 and Myo2 are recruited to the cortex of UB cells via interactions with Bud6 and Smy1, respectively. Once on the cortex they either polymerize cables or moved them along the

plasma membrane. In turn, actin cables destabilize cortical interactions of their own regulators and are involved in their removal from the cell cortex.

2.5. Actin cable dynamics in budded cells

2.5.1. Cable dynamics in polarized cells

Initial experiments in this work showed that cable dynamics in mother cells were strongly reduced during cell polarization (Fig. 2-5) and that cables exhibited more bundling and buckling (Fig. 2-6). We now wanted to understand the molecular basis for this change. As there were only few cases of cable extension $> 2 \mu\text{m/s}$ in MB cells, it was likely that fast translation of cables via Myo2 played a minor or no role in polarized cells. This hypothesis could not be tested directly since polarization was disrupted in the various Myo2 mutants (Johnston et al., 1991; Schott et al., 1999). Quantification showed that Myo2-GFP dots at the mother cell cortex of MB cells were slightly less dense and had shorter lifespans than in UB cells (Fig. 2-17A, table 2-6). Importantly, many Myo2-GFP dots moved along actin cables, occasionally over long-distance until it reaches the bud (Fig. 2-17B). This is the to date the first direct observation of Myo2 moving along actin cables, although such movements were suggested by indirect evidence from observing secretory vesicles (Schott et al., 2002; Sheltzer and Rose, 2009). As a result of polarized movement, Myo2 became concentrated at the bud tip (Fig. 2-17C).

Even more strikingly, Bni1-GFP almost completely disappeared from the mother cell cortex in MB cells, and instead became concentrated at the bud tip (Fig. 2-17C). However, Bni1 seemed to retain some activity as cable extension rates in MB *bni1Δ* cells were strongly reduced compared to control cells. All cables extended at speeds typical for Bnr1 activity or not at all (Fig. 2-17D, table 2-8). Importantly, deletion of Bni1 did not reduce the number of cables (Fig. 2-17E) but nearly all remaining cables were now polarized towards the bud neck, in keeping with a stable association of Bnr1 with the septin ring (Fig. 2-17F, Buttery et al., 2007). In contrast, when we examined cells deleted for Bnr1 we found that cables extended faster (Fig. 2-17D, table 2-8). Again, cable number was not altered (Fig. 2-17E) but half of the cables now were randomly oriented in the mother cells (Fig. 2-17F) and these extended significantly faster than the

polarized cables (Fig. 2-17G, table2-8). Removal of formin regulators also had the expected effects. In *bud6Δ* cells a reduction of Bni1-typical faster extension rates was observed (Fig. 2-17H). In *bud14Δ* cells, cables extended mostly with rates typical for Bnr1 at less than 1 $\mu\text{m/s}$ and similar to *bni1Δ* cells (Fig. 2-17H).

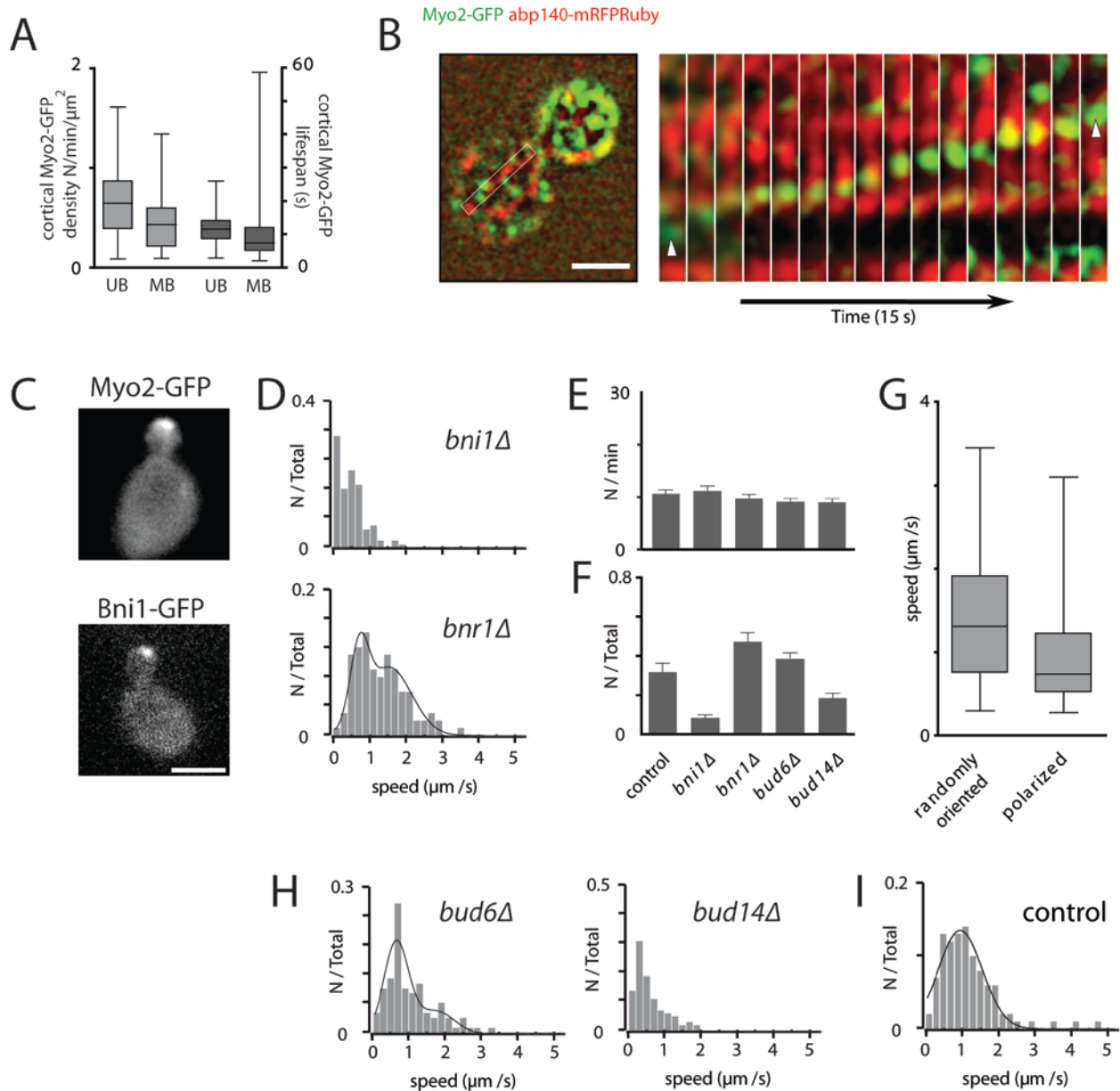


Figure 2-17

Dynamics of actin, Bni1 and Myo2 in polarized cells. (A) Quantification of cortical Myo2 densities and lifespans in control MB cells compared to UB cells (as in Fig. 2-15F, G). (B) Myo2 dot moves along a polarized actin cable. (C) Localization pattern of Bni1-GFP and Myo2-GFP in MB cells. (D) Cable extension rates in MB cells of *bni1Δ* and *bnr1Δ* cells. (E) Number of cable emerging within one minute of imaging in MB cells. (F) Ratio of randomly oriented cables in MB cells. (G) Extension rate of randomly oriented cables versus polarized cables. Measurements were done in MB cells of *bnr1Δ* mutant. (H) Cable extension rates in *bud6Δ* and *bud14Δ* MB cells. (I) Cable extension rates in control strain for comparison, identical to that in Fig 2-5A. Note that the data from *bni1Δ* and *bud14Δ* could not be fitted to a Gaussian distribution.

Table 2-8. Measurements of actin cable dynamics in MB cells

Cable numbers (N/min/cell)						
Strain	Mean	SEM	N (cells)			
control MB	10.9	0.81	21			
<i>bni1Δ</i> MB	10.1	0.69	18			
<i>bnr1Δ</i> MB	11.7	1	20			
<i>bud6Δ</i> MB	13.1	0.73	22			
<i>bud14Δ</i> MB	11.1	0.8	21			
Extension rates						
Strain	Mean 1 (μm/s)	SD 1	Mean 2 (μm/s)	SD 2	R ²	N (cables/cells)
control MB	0.96	0.65	NA	NA	0.95	100/19
<i>bni1Δ</i> MB	0.48	0.40	NA	NA	NA	100/20
<i>bnr1Δ</i> MB	0.69	0.64	1.50	0.64	0.95	100/20
<i>bnr1Δ</i> MB random	1.40	0.74	NA	NA	NA	46/20
<i>bnr1Δ</i> MB polarized	0.94	0.6	NA	NA	NA	63/20
<i>bud6Δ</i> MB	0.68	0.61	1.80	0.61	0.80	100/20
<i>bud14Δ</i> MB	0.59	0.45	NA	NA	NA	100/20

In summary, cable extension in polarized mother cells was driven by polymerization through both Bni1 and Bnr1. Bnr1 supported elongation around 0.5 μm/s and generated cables that were polarized towards the bud neck. Bni1 generated both polarized and randomly oriented cables at higher speeds of 0.9 μm/s and 1.4 μm/s, respectively. Myo2 seemed to play only minor role in actin cable dynamics at this cell cycle stage.

2.5.2. Cable dynamics large budded cells

As the bud grows bigger, cellular actin continues to reorganize, whereby the actin cables become less bundled and organized, while actin patches become re-distributed in the mother cells. These cells are categorized as large-budded (LB) cells. In LB cells of control strain, the dynamics of actin cables was in an intermediate stage, whereby the speed of cable extension recovered from the slow-down during cell polarization (Fig. 2-5). To test which of the above identified regulators were active during this stage, cable dynamics were measured in LB cells in different mutant backgrounds. The overall organizations of cables were similar to UB cells of each strain. In *bni1Δ* cells, cable numbers were reduced for 65% (Fig. 2-18A). Unlike MB cells, where only polarized cable bundles were observed (Fig. 2-7B), most cables in *bni1Δ* LB cells were short, randomly-oriented cables, similar to those in UB cells (Fig. 2-18B). Strikingly, significant number of fast moving cables ($> 2\mu\text{m}$) were seen (Fig. 2-18C). This suggested that Myo2 started to function as a motor that moves actin cables along the cortex in this cell cycle stage. The distribution of extension rate was similar to that in UB cells, except for a larger proportion of cables extending at rates below $1\mu\text{m/s}$, which probably represented Bnr1 activity. In LB cells of *bnr1Δ* strain, the cable number was reduced 26% (Fig. 2-18A), like in UB cells. However, unlike *bni1Δ* cells, many of the cables were still polarized towards the budneck (Fig. 2-18B). A small proportion of fast moving cables were also visible (Fig. 2-18D) but to a lesser extent. This could be because Myo2 is more likely to move shorter cables than longer, polarized ones.

Deletion of Bud6 or Bud14 also caused similar changes in LB cells as in UB cells. In *bud6Δ* cells both Bnr1-dependent and Bni1-dependent cable extensions decreased, whereas in *bud14Δ* a drastic slow-down of cable extension typical for over-activated Bnr1 was observed. Cable number was reduced 53% in *bud6Δ* cells and 15% in *bud14Δ* cells, similar to UB cells (Fig. 2-18A, E, F, table 2-8).

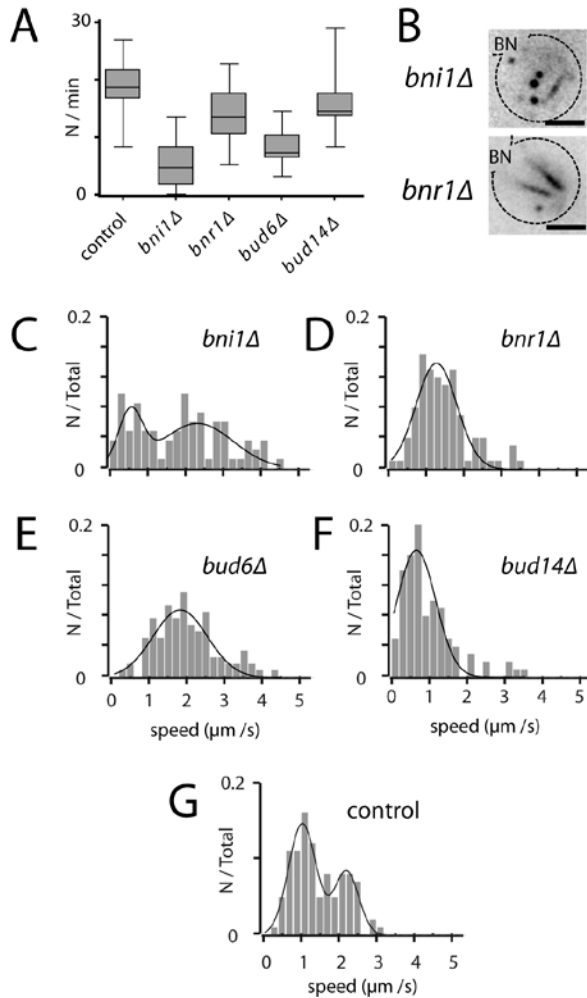


Fig. 2-18

Dynamics of actin cables in LB cells of *bni1Δ*, *bnr1Δ*, *bud6Δ* and *bud14Δ* mutants. (A) Number of cables that emerged in UB cells of the indicated strains within one minute of imaging. (B) Cable organization in *bni1Δ* and *bnr1Δ* cells (C-F) Extension rate of actin cables in (C) *bni1Δ* (D) *bnr1Δ* (E) *bud6Δ* and (F) *bud14Δ*. (G) Cable extension rates in control strain for comparison, identical to that in Fig 2-5A.

Table 2-9. Measurements of actin cable dynamics in MB cells

Cable numbers (N/min/cell)						
Strain	Mean	SEM	N (cells)			
control LB	17.8	0.94	21			
<i>bni1Δ</i> LB	4.9	0.77	28			
<i>bnr1Δ</i> LB	13.1	0.93	21			
<i>bud6Δ</i> LB	7.6	0.66	22			
<i>bud14Δ</i> LB	15.1	0.87	22			
Extension rates						
Strain	Mean 1 ($\mu\text{m/s}$)	SD 1	Mean 2 ($\mu\text{m/s}$)	SD 2	R ²	N (cables/cells)
control LB	1.04	0.51	2.21	0.48	0.93	100/20
<i>bni1Δ</i> LB	0.6	0.3	2.4	0.6	0.67	100/28
<i>bnr1Δ</i> LB	1.2	0.43	NA	NA	0.8	100/20
<i>bud6Δ</i> LB	1.8	0.51	NA	NA	0.84	100/24
<i>bud14Δ</i> LB	0.6	0.42	NA	NA	0.84	100/20

In summary, cable extension in depolarizing mother cells was also driven by polymerization through both Bni1 and Bnr1. Bni1 was the dominant formin at this stage, as Bud14 dependent Bnr1 deactivation seemed to be already occurring. Myo2 also started to play a role in driving fast cable motility, thereby increasing the speed of cable network remodelling. However, it was surprising that actin cables were polarized to a greater extent in *bnr1Δ* cells than in *bni1Δ* cells, given the opposite observation in MB cells (Fig. 2-17F). Also, the reduction of Myo2-dependent motility in *bni1Δ* cells called for explanation (see discussion section 3.2.).

2.6. The physiological role of fast cable motility

In this work, rapid actin cable remodelling in unpolarized cells was characterized for the first time. It was previously known that in polarized cells cables became oriented towards the bud neck, bundled and stabilized. All these changes are essential as they support polarized transport into the bud. However, it was surprising that cells invested so much energy to maintain high levels of cable dynamics in unpolarized cells. We therefore investigated the physiological consequences of rapid remodelling of the cable network. One possibility that we wanted to check was that cable reorganization enabled cells to efficiently establish polarity. Since the time window for polarization response in *S. cerevisiae* could be as short as 1 min, very fast remodelling would be required (Wedlich-Soldner and Li, 2004).

2.6.1. Physiological role Bni1-driven actin dynamics

To test the role of actin dynamics in cell polarization we monitored localization of a GFP fusion to the master polarity regulator Cdc42 in synchronized cells (Wedlich-Soldner et al., 2004). To render polarization more dependent on actin mediated recycling, the GDP dissociation inhibitor Rdi1 was deleted. This protein can extract Cdc42 from membranes (Tiedje et al., 2008) allowing it to polarize independently of actin (Wedlich-Soldner et al., 2004). The effect of Bni1 deletion on polarization in this strain was then monitored, as this mutation almost completely abolished polymerization of actin cables in UB cells (Fig. 2-7B). While deletion of either Rdi1 or Bni1 had no obvious effects, cell polarization was significantly delayed in the double mutant (experiments performed by Tina Freisinger, Fig. 2-19A). More strikingly, ~5 % of polarized cells exhibited a

remarkable phenotype: split caps or buds (Fig. 2-19B). These results indicated that the Bni1-driven fast cable polymerization is crucial for ensuring proper polarization of the cells.

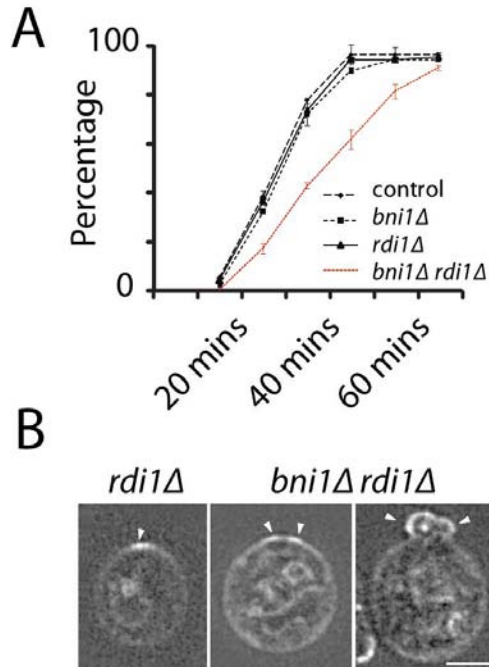


Fig. 2-19

Physiological role of Bni1-driven actin polymerization. Cell polarization was tracked using GFP-Cdc42. **(A)** Fraction of polarized cells in control, *bni1Δ*, *rdi1Δ* and *bni1Δ rdi1Δ* strains after G1 release. (error bars: SD., n = 3 experiments, 50 cells per data point). **(B)** Formation of multiple polarization sites in *bni1Δ rdi1Δ* mutant. Arrowheads indicate polarization caps.

2.6.2. Physiological role of Myo2-driven actin motility

In order to probe the role of fast cable motility in cell polarization, it was necessary to find a way to manipulate rapid cable movement specifically. Namely, the role of Myo2 as an essential transporter molecule had to be preserved, while its cable moving function was abolished or reduced. Deletion of Smy1 proved to be optimally suited to this task. Since it had been previously shown that Smy1 deletion did not affect Myo2 transport function (Lillie and Brown, 1994). As shown above, Smy1 deletion significantly reduced Myo2-cortical association (Fig. 2-15F, G). Quantification of cable dynamics in this strain consequently showed a selective reduction of fast cable motility (Fig. 2-20A). Furthermore deletion of Smy1 had only minimal effects on polarity establishment in synchronized cells (Fig. 2-20B).

It was previously shown that cell polarization in response to mating hormone, commonly known as shmooing, is particularly sensitive to actin perturbation (Sheltzer and Rose, 2009). Polarization assays performed under such conditions showed that *smy1Δ* cells formed mating projections with a previously observed aberrant morphology (Fig. 2-20C, D Bidlingmaier and Snyder, 2002) and a 30 min delay (Fig. 2-20E). These results indicated that a reduced speed of cable reorganization lead to defects in both temporal and spatial control of cell polarization.

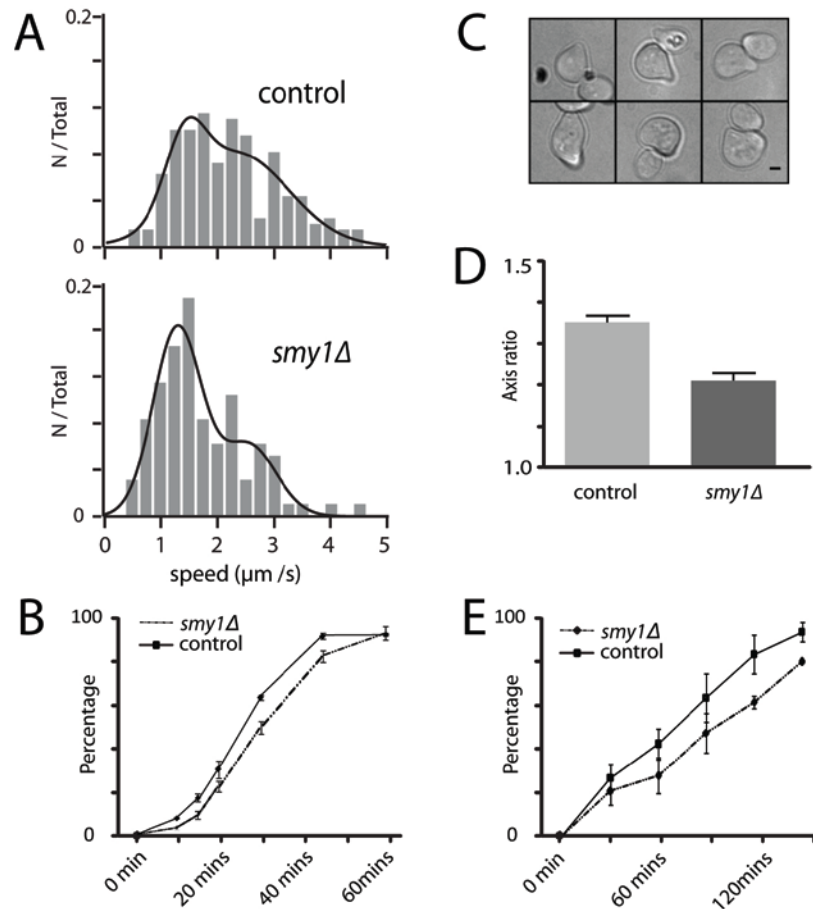


Fig. 2-20

Physiological role of Myo2-driven cable motility. (A) Fraction of polarized cells in control and *smy1Δ* strains after G1 release. (error bars: SD., n = 3 experiments, 50 cells per data point). (B) Cable extension rates in control and *smy1Δ* cells. (C, D) Shape of control and *smy1Δ* cells treated with 100 μM α-factor for 2 h. Axis ratio: length of axis through the middle of the mating projection over length of perpendicular axis (error bars: SEM., control: n=54, *smy1*: n=43). (E) Fraction of control or *smy1Δ* cells forming mating projections at indicated times after adding 100 μM α-factor (error bars: SD., n = 3 experiments, 200 cells per data point). Strains used JYY140. JYY141.

3. Discussion

3.1. Dynamics of actin cable network

The current work has led to a number of important mechanistic insights on the organization and dynamics of actin cables. These new insights, together with previous results, allow us to propose a schematic model for actin cable dynamics (Fig. 3-1).

In unpolarized G1 cells randomly oriented actin cables are generated by the formin Bni1 from dynamic dots at the cell cortex. Bud6 is important for recruitment of Bni1 to the cell cortex, while actin cables are involved in its removal. Although genetically redundant, the second formin Bnr1 only plays a minor role in unpolarized cells and is largely kept inactive by Bud14 (Chesarone et al., 2009). We demonstrated that the type V myosin Myo2 plays an unexpected role in cable dynamics. It associates with the cell cortex via its C-terminal cargo binding domain and Smy1 to directly slide actin cables along the plasma membrane at high speed. Importantly, Myo2 only transiently binds to the cortex and can be picked up by associated actin cables. This recycling ensures a constant decoration of actin cable with motors, which in turn ensures the continuity of movement (Fig. 3-1A).

During polarization, cable dynamics are strongly down-regulated. Cables become mostly oriented towards the bud neck while buckling and bundling are increased. Our results demonstrate that polarized cables are mostly generated by budneck localized Bnr1. These cables stay anchored to the bud neck for long times and are often bundled and bent. The bundling activity of actin cables can also be attributed to Bnr1 (Moseley and Goode, 2005). At the same time, Bni1 is removed from the mother cell cortex and preferentially recruited to the budtip, where Myo2 and Bud6 are also concentrated (Segal et al., 2000). Bni1-nucleated cables are likely to be generated predominantly in the bud and then released into the mother cell. The released cables become randomly oriented, probably via Myo2, which becomes polarized to the bud tip but partially remains on the mother cell cortex (Fig. 3-1B).

In large budded cells, the down-regulation of cable dynamics is reversed. Bundling of cables is reduced and cables become oriented more randomly. Both Bni1 and Bnr1 are found at the

budneck during cytokinesis. Bni1 is also redistributed into the mother cell, probably via retrograde transport towards the mother cell (Buttery et al., 2007). Presumably, the deactivation of Bnr1 via Bud14 occurs at this stage (Chesarone et al., 2009), allowing the acceleration of cable dynamics via Bni1 and Myo2 (Fig. 3-1C).

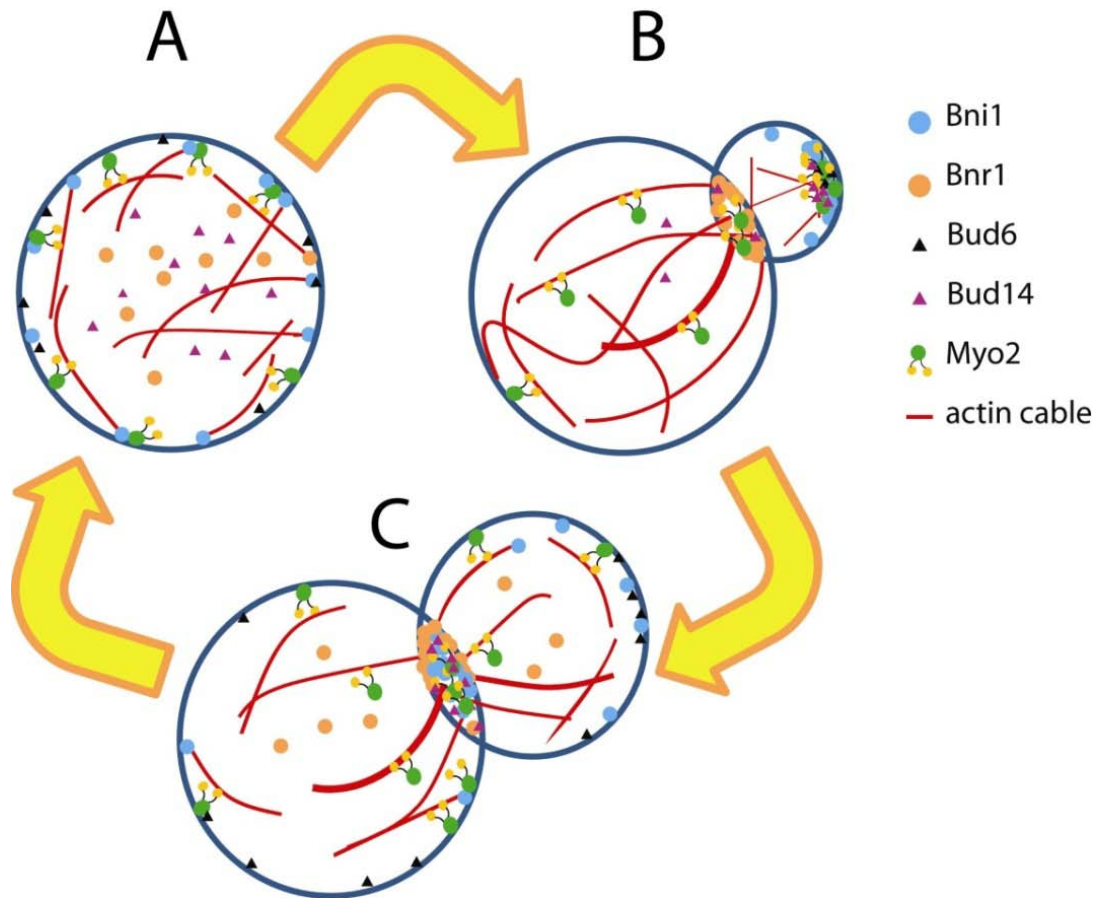


Fig. 3-1

Schematic model of actin cable dynamics in *S. cerevisiae* in unpolarized (UB), polarized (MB) and depolarizing (LB) cells. (A) In UB cells, Bni1 localizes to the cell cortex, where actin cables are assembled. Myo2 is also on the cortex, serving as motor for cable motility. **(B)** In MB cells both Bni1 and Myo2 are concentrated at the bud tip. Bnr1 is concentrated at bud neck. Myo2 moves along polarized cable bundles. Cable dynamics slow down drastically. **(C)** In LB cells, Bni1 and Myo2 are redistributed into the mother cell cortex. Concerted action of cortical Bni1 and Myo2 speeds up the cable remodelling again.

3.2. Interplay of two formins

Previous studies have already shown that the two yeast formins Bni1 and Bnr1 differ in their interaction partners and localization patterns (Buttery et al., 2007; Chesarone et al., 2009; Dong et al., 2003; Moseley and Goode, 2005). Results in the current study demonstrated that they drive assembly of temporally and kinetically separable cable populations. Bni1 was the dominant regulator of cable assembly in unpolarized cells, whereas Bnr1 only became localized and/or activated during bud formation. Strikingly, cable elongation by Bni1 was more than twice as fast as that by Bnr1 (0.9-1.7 $\mu\text{m/s}$ versus 0.4-0.7 $\mu\text{m/s}$, Fig. 2-7, 17, 18), indicating that the switch from one formin to another constitutes a major mechanism for cable regulation. Another major difference is that Bnr1 generated cables remained stably associated with their place of origin, while cables made by Bni1 frequently detached and – probably in conjunction with Myo2 dependent sliding – become randomly oriented. This fits well to the measured lower affinity of Bni1 to actin barbed ends compared to Bnr1 (Moseley and Goode, 2005). Bnr1 has also been shown to bundle actin filaments *in vitro*, which fits well to the increased bundling observed during polarization of cells or after Bud14 deletion.

Compared to previously published results on cable extension rates around 0.4 $\mu\text{m/s}$ (Yang and Pon, 2002), the speed determined here for Bni1-dependent cable polymerization was up to four folds higher, at 0.9 – 1.7 $\mu\text{m/s}$. Interestingly, this value is close to rates recently found in a variety of organisms. In *Arabidopsis* epidermal cells individual actin filaments were shown to polymerize at 1.7 $\mu\text{m/s}$ (Staiger et al., 2009). In *Dictyostelium*, formins have been proposed to reorganize filaments in the cortical actin network with speeds of 1-5 $\mu\text{m/s}$ (Diez et al., 2005). Finally, a fragment of the mouse formin mDial1 was shown to move at up to 2 $\mu\text{m/s}$ when expressed in *Xenopus* fibroblasts (Higashida et al., 2004). These studies indicate that formins are generally able to support fast assembly of actin filaments in cells and that yeast cables can serve as model system for fast actin dynamics.

Our results on Bni1 function also raise a few issues on the exact mechanism of actin dynamics. In this study, the highest measured speed of Bni1-based cable extension (1.7 $\mu\text{m/s}$) can be translated into a polymerization rate of 630 subunits/s (assuming 370 subunits/ μm). This is an extraordinarily high rate compared to *in vitro* data, where Bni1 FH1-FH2 mediated

polymerization at 20 subunits/s (with 1 μM actin, Kovar et al., 2003). Therefore the elongation rate of actin depends on the concentration of G-actin in a linear fashion as introduced above (Pollard, 1984). Based on this, a local G-actin concentration above 30 μM is expected to support the speed measured *in vivo*. Contradictorily, G-actin concentration in yeast was determined as around 0.01 μM (Pollard et al., 2000).

If we assume that all these measurements were correct, the cortical G-actin concentration must be 3000 folds higher than average concentration in the cytoplasm. It was shown G-actin is sequestered at the cell cortex by profilin-actin via interactions to phospho-inositol-biphosphate (PIP₂, Goldschmidt-Clermont et al., 1990) or the formin FH1 domains (Paul and Pollard, 2008). However, it is highly unlikely that such sequestration processes can achieve a 3000 fold increase in local concentration. Alternatively, a similar elongation rate was observed for formin mediated actin assembly in plant (Staiger et al., 2009). In this case, annealing of shorter filaments was suggested as the explanation for fast elongation. The results in the current work neither support nor exclude such an annealing mechanism. Intriguingly, although multiple short actin cables were observed radiating from a Bni1 dot, generation and elongation of longer cables were never associated directly with Bni1 dots despite careful observation of a large number of cells. This observation is in favour of the annealing hypothesis. In order to clarify these options, further detailed investigations are needed. While technically difficult, EM studies would help to understand the exact structure of actin cables. It would also be worthwhile to confirm or improve the earlier measurement of G-actin concentration in yeast cells, as it is unusually low compared to other cell types ($\sim 30\mu\text{M}$, Goode and Eck, 2007). Finally, alternative fluorescent markers (e.g. GFP tagged tropomyosins) should be developed which could provide insights on the molecular details of cable assembly

Whereas all results acquired in UB and MB cells supported our model in Fig. 3-1, data acquired in LB cells were less than unequivocal. In LB cells, the Myo2-dependent motility was hardly detectable in *bnr1Δ* cells but was apparent in *bni1Δ* cells (Fig. 2-18C, D). Also, actin cables in *bnr1Δ* appear more polarized than those in *bni1Δ* cells, which is opposite of what one would expect based on the data acquired in MB cells (Fig. 2-17F). These could be due to the scenario of formin activities in LB cells, whereby Bnr1 was becoming deactivated (Chesarone et al., 2009) with Bni1 still largely localized to bud tip and bud neck (Buttery et al., 2007). In *bni1Δ* LB cells,

formin activity would therefore become minimal, such that Myo2 became the dominant molecular motor in the cell. In this scenario, many actin cables would start to move rapidly in random orientations, as observed in Fig. 2-18B, C. In *bnr1Δ* LB cells, although Bnr1 was absent, polarized Bni1 can still maintain oriented cable bundles. However, this still does not explain the surprising reduction of Myo2-dependent peak in *bnr1Δ* cells (Fig. 2-18D, G). This discrepancy could be due to variable cell cycle stages among LB cells. As some cells might still be polarized whereas others already started depolarization and were entering cytokinesis. A closer investigation on LB cells at different cell cycle stages is required to finally clarify this. This will require a criterion much more sensitive than bud size for separating cell populations. Nonetheless, these discrepancies do not affect the conclusions on the functions of formins and Myo2 in different cell cycle stages.

3.3. A novel role for myosins

A role for myosins in the regulation of actin dynamics has been proposed in different systems. A previous study in yeast proposed that the type II myosin Myo1 was involved in retrograde flow of actin cables (Huckaba et al., 2006). However, kinetic measurements were restricted to polarized cable bundles making the exact mechanism for this function difficult to define. Myo1 could be associated with the bud neck cortex and pull actin filaments into the mother cell or it might be associated with cable bundles and slide filaments against each other. Type II myosins were also shown to regulate the reorganization of F-actin during cell migration, cell spreading and cytokinesis in various systems (Clark et al., 2007; Cramer and Mitchison, 1995; Matsumura, 2005; Wedlich-Soldner et al., 2003). In addition, Myosin X was suggested to organize actin filaments into filopodia via its motor and dimerization activities (Bohil et al., 2006; Tokuo et al., 2007). However, the mechanistic details for these interactions between actin and myosins were never identified.

Type V myosins are known for their role in polarized transport (see introduction section 1.4.3., Pruyne et al., 2004; Trybus, 2008). The current work demonstrated that, in addition to serving as an actin-based organelle transporter, plasma membrane-bound type V myosin Myo2 drives the motility of actin cables directly through its motor activity (Fig. 2-9, 10, 13). To date, this is the

first demonstration of such a function *in vivo*. The averaged speed of MyoV-dependent cable movement is ranged from 1.9 to 2.7 $\mu\text{m/s}$ with some reaching up to 5 $\mu\text{m/s}$. These speeds are comparable to the previous indirect measurements of MyoV driven transport (Schott et al., 2002). Despite this consistency, our results also show that the average speed of Myo2-driven actin movement differs significantly in different strains. This high level of variation may be due to the variable extent of Myo2 decoration on actin cables. Also, calibration of measurements showed that an error range of about 20% is to be expected for all speed measurements (see methods section 5.4.2, Fig. 5-2). In addition, the higher the speed of movement, the fewer frames in an image stack can be used for measurements, due to the small size of a yeast cells. Therefore measurements of cables moving at a speed $> 2\mu\text{m}$ are likely to be more error-prone than the slower measurements, which could result in the significant differences in average rates. However, although these errors do increase the data range, they do not affect the final conclusion on the Myo2 function in actin dynamics.

Based on our dynamics data and direct observation of actin-Myo2 interaction (Fig. 2-13, 15), a reciprocal regulation mechanism of actin cables and Myo2 can be proposed (Fig. 3-2): On the one hand Myo2 directly moves cables while its cargo binding domain anchors the molecule to the cell cortex. On the other hand actin cables frequently pick up cortical Myo2 dots. This dynamic regulation provides an elegant way to adapt to cell cycle specific requirements, shown in Fig. 3-1. In unpolarized cells sliding of cables and removal of Myo2 are balanced, such that cables are constantly decorated with Myo2 molecules, allowing continuous movement along the periphery of the cell. In polarized cells many cables are stably anchored to the bud neck and cannot be moved by Myo2. Instead, more myosin molecules are removed from the cortex and subsequently move along the stable cables to the bud, where they can further support polarized transport.

Smy1 is a kinesin-related which suppressed *myo2-66* and *myo2-16* mutant when over-expressed (Lillie and Brown, 1992; Schott et al., 1999). Smy1 could bind microtubules but cannot generate directed motion like kinesins (Hodges et al., 2009; Lillie and Brown, 1998). It was also shown that Smy1 binds actin and Myo2, and has genetic interactions with formins (Kikyo et al., 1999). Despite these results, the function of Smy1 *in vivo* was unknown. Here we show that Smy1 is involved in anchoring of Myo2 on the cell cortex. Disruption of Smy1 causes a partial loss of

Myo2-cortex interaction, leading to a moderate reduction of Myo2-driven actin motility (Fig. 2-20). In summary, the duality of Myo2, using actin filaments as its track, while at the same time actively participating in actin remodelling, adds a new layer of complexity to the regulation of cellular organization.

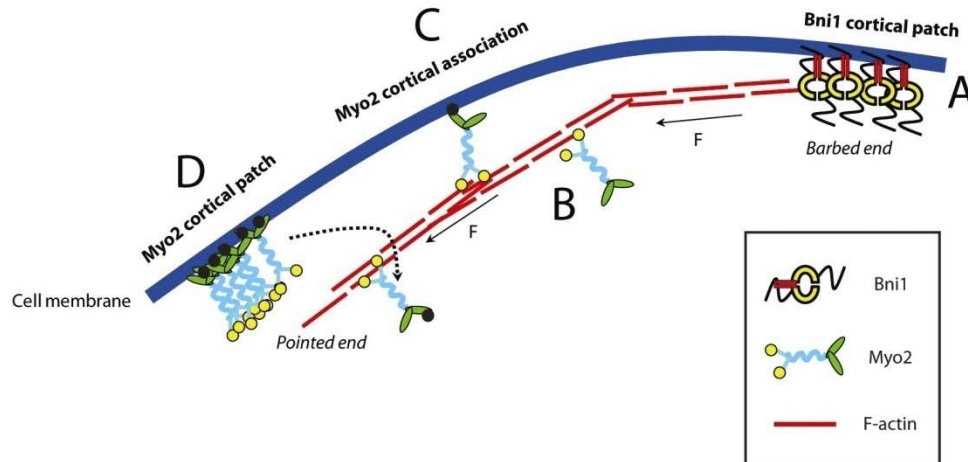


Fig. 3-2

Mechanism of fast actin cable dynamics in *S. cerevisiae*. (A) Actin cables are generated by cortical Bni1 molecules. Actin cables can serve as tracks for Myo2 movement (B) or be moved by static Myo2 molecules anchored to the cell cortex (C). Cortical Myo2 patches (D) serve as reservoir for active motors, which can be loaded onto actin cables nearby. Both Bni1 and Myo2 generate force towards the barbed ends, driving the fast extension / motility of actin cable.

3.4. Actin dynamics and cell polarization

As shown above, the *S. cerevisiae* cells maintain a high level of dynamics on cortical actin cables. The most surprising fact about this dynamics is that the highest speeds of polymerization and movements were detected in unpolarized cells, which can be considered a ground-state in the cell cycle. As we know that actin dynamics is tightly associated with the regulation of cell polarization (Pruyne et al., 2004, Wedlich-Soldner and Li, 2004), we reasoned that such fast dynamics could be involved in the accuracy polarity establishment, which in yeast happens within a few minutes. Indeed, our polarization assays showed that both Bni1-dependent

polymerization and Myo2-driven cable motility were crucial for the speed and fidelity of such a process (Fig. 2-19, 20).

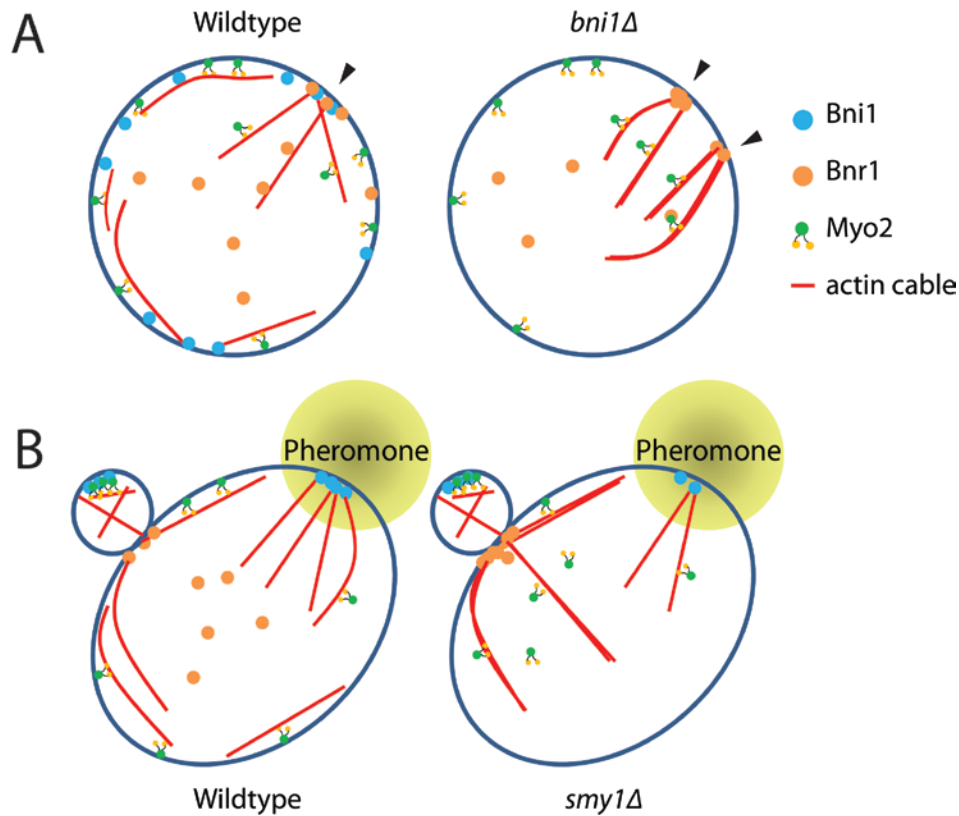
The central regulator of cell polarization is Cdc42 (for review, see Etienne-Manneville, 2004). During vegetative growth (budding), Cdc42 forms a single polarization cap, which directs the polarization of actin cytoskeleton and organelles. The polarization site then gradually develops into a bud. Cdc42 polarization was proposed to be regulated by two redundant pathways, namely the actin-dependent transport and the actin-independent recycling. The former pathway is driven by actin and Myo2-dependent transport, whereas the latter is dependent on the GTPase activity of Cdc42 and other recycling proteins (Li and Wedlich-Soldner, 2009; Wedlich-Soldner and Li, 2004). Redundancy in polarity regulation is not surprising, as correct polarization is essential for the propagation of *S. cerevisiae* cells. Multiple regulatory mechanisms ensure the robustness of the polarization process under various environmental conditions.

In this study, we showed that only when components from both pathways were deleted (*bni1Δrdi1Δ*) a delay in cell polarization could be observed (Fig. 2-19). This result further supported the model of dual regulation by actin-dependent and actin-independent pathways. Interestingly, a spit-bud or double-bud phenotype was also observed in *bni1Δrdi1Δ* cells, indicating erroneous decision-making in this usually highly fail-safe process. The question now is how such a phenotype could arise via perturbation of actin dynamics. One explanation is that in *bni1Δ* cells all cables generated during polarization would be stably anchored to the septin ring by Bnr1 (Pruyne et al., 2004) and serve as fixed vectors for delivery of Cdc42 containing vesicles (Wedlich-Soldner et al., 2003). In cases where cables happen to originate from opposite sides of the septin ring, separate Cdc42 caps could be formed, giving rise to the observed phenotype (Fig. 3-3A).

Another important polarization event in *S. cerevisiae* cells happens during sexual reproduction. In order to form a zygote, two cells of opposite mating type must form mating projections (shmoo) towards each other, which then fuse (for review see Elion, 2000). To form a shmoo, a polarization site separate from the budding site was usually selected. This implies that for a polarized (MB) cell, shmoo formation involves at two stages, namely the depolarization from the original budding site and the repolarization towards the newly selected shmooing site. It was

shown previously that shmoo formation requires Bni1-driven actin polymerization (Matheos et al., 2004). Therefore, it is reasonable to predict that this process would be more susceptible to changes in actin dynamics. Indeed, experiments carried out in this study showed that shmoo formation was disturbed in *smv1Δ* cells (Fig. 2-20), which exhibited only moderate defects in Myo2-driven actin motility. The exact mechanism of fast actin motility is still unknown. A possible explanation would be that the actin-moving function of Myo2 helps the cell to quickly reorganize its cortical actin, especially during the polarized stage of the cell cycle. Cells lacking the ability to move actin cables quickly would have a slower depolarization, which leads to a slower repolarization, observed as a delay in shmoo formation. In some cases, it could be that this process of depolarization cannot be completed in time before the shmooing starts. This might lead to multiple polarization sites in a shmooing cell, which in turn produces mating projections with aberrant morphology (Fig. 3-3B).

In summary, these examples illustrate the problems associated with overly static actin structures. Rapid remodelling of actin cables is necessary to enable a precise response during the highly dynamic process of polarity establishment (Brandman et al., 2005; Wedlich-Soldner et al., 2004).

**Fig. 3-3**

Fast actin dynamics ensures accurate cell polarization. (A) Proposed model for the role Bni1-driven actin polymerization in cell polarization during vegetative growth. Overly-static cable network in *bni1Δ* cells tend to polarize slower and produce multiple polar caps. Arrowheads indicate the polarization sites which will later development into buds. (B) Proposed model for the role of Myo2-driven actin motility in cell polarization during mating response. Reduction of Myo2-driven motility slows down the depolarization actin cables in polarized cells, resulting a delayed response to pheromone.

3.5. Outlook

We showed in this work that by combining TIRFM imaging technology with yeast genetics to introduce specific molecular perturbations, mechanisms of F-actin assembly and disassembly can now be investigated systematically *in vivo*. Using this approach, questions on the mechanisms of cable disassembly and bundling as well as on cable-actin patch interactions are now ready to be

addressed directly in living cells. One important question that remains unanswered is the mechanism of cable disassembly. Previous studies suggested that yeast Cofilin and Aip1 collaborate in the disassembly of actin cables (Lappalainen and Drubin, 1997; Okada et al., 2006). Conclusions in this respect were drawn mostly based on results of immuno-fluorescence images of fixed samples, as well as biochemical data. The TIRF-based assay can be applied here to directly visualize the process of cable disassembly and to pinpoint the molecules involved.

Another potentially fruitful area of investigation is the mechanism of lateral interaction or bundling of actin cables. The candidate molecules in this case include the yeast fimbrin Sac6 (Adams et al., 1991) and Scp1 (Winder et al., 2003). One can measure the frequency and extent of actin buckling and bundling in cells defective in these genes. By following the behaviours of individual cable bundles in cell, it is also possible to characterize exactly the mechanical properties of individual bundles. The data acquired can be used to attribute certain changes in the physical parameter of F-actin structure to individual genes.

Furthermore, although the data from polarization assays suggested the physiological functions of fast actin remodelling, it is still short of providing conclusive mechanisms linking these functions with behaviours of individual actin cables. In-depth studies on the roles of actin dynamics on various polarity components are required in order to firmly establish such links. Among many other possibilities, a detailed study of the actin dynamics in shmooing may be highly rewarding, as this process can be easily manipulated spatially with pheromone gradients generated through flow-chamber techniques (Moore et al., 2008). Combining this technical advance with the powerful imaging techniques developed here and subtle genetic manipulation available in *S. cerevisiae*, one can envision to study the dynamics of individual polarity proteins in real time with unprecedented spatial / temporal resolution, perhaps even on level of single molecules. These data will then be correlated with precise information on actin dynamics, which enable the construction of a quantitative predictive model for cellular decision-making during polarization.

4. Summary

The current work provided comprehensive analyses of cortical actin dynamics in yeast *Saccharomyces cerevisiae*. Using GFP labelled Abp140 and TIRFM, actin cable network could be visualized *in vivo* throughout the cell cycle. This network was limited to the cell cortex and was present in all cell cycle stages. It was randomly organized in unpolarized cells and became polarized during vegetative growth known as budding. Individual actin cables were linear filamentous structure that exhibit versatile dynamic behaviour such as extension, retraction, translational movement, bundling and buckling. The entire network underwent rapid remodelling, whereby the highest dynamics of remodelling was observed in unpolarized stage. Strikingly, at least two modes of cable extension could be clearly distinguished based on average speed.

Quantitative microscopy combined with genetic manipulations revealed the mechanisms that drive the cable dynamics. In unpolarized cells, fast polymerization of actin cables was dependent on formin Bni1, whereas the other formin Bnr1 only served auxiliary function. Formin regulators Bud6 promoted Bni1-dependent actin polymerization. The fast turnover of cables was dependent on the deactivation of Bnr1 via Bud14. However, the very fast cable motility was unaffected by the abolishment of actin polymerization. Further investigation showed that this fast cable motility was dependent on the type V myosin Myo2.

In unpolarized cells, both Bni1 and Myo2 formed distinct punctate structures on the cell cortex. The Bni1 and Myo2 dots were stabilized upon removal of F-actin. Double-colour TIRFM showed that actin cables originated from Bni1 dots, whereas Myo2 decorated mobile actin cables along their lengths. Both Bni1 and Myo2 could be picked up by actin cables before they disappeared from the cell cortex.

In polarized cells, Bnr1 became active for the assembly of bundled, polarized cables focused at the budneck. Myo2 moved mostly along these polarized bundled and ceased to be active in driving cable motility. Also, Bni1 dots could no longer be observed on the mother cell cortex. However, cable dynamics were slowed down drastically when either Bni1 or Bud14 was deleted. This further suggested that the switch from Bni1 to Bnr1 caused the massive slow-down of cable

turn-over in polarized cells. This slow-down was reversed as the daughter cell grew bigger. Cable network were depolarizing in these cells. Bni1 and Myo2 became active again on mother cell cortex and the dynamics of cable network sped up.

Finally, dynamics of cortical actin cables were shown to be crucial for the fidelity of cell polarization. Polarization assay performed on budding process of *bni1Δrdi1Δ* mutant cells showed a significant delay compared to single mutant cells. Cells also exhibited a remarkable double / split-bud phenotype. These data corroborated with the dual regulation model of cell polarization and illustrated the importance of Bni1-dependent cable polymerization in establishing cell polarity. Deletion of SMY1 caused a moderate reduction of Myo2-driven cable motility, which in turn caused a defective cellular morphogenesis during mating response. This result suggested that Myo2-driven cable motility was involved in regulating the polarization of cells during sexual reproduction, where even a slight perturbation of actin dynamics could have serious consequences in mating efficiency.

We revealed here a highly dynamic network of actin in *S. cerevisiae*, whose dynamics is driven by reciprocal regulation between actin cable and its regulators such as formins Bni1, Bnr1 and MyoV. This work also established the combination of high-resolution microscopy with yeast genetic as a systematic strategy to study cellular dynamics.

5. Materials and Methods

5.1. Materials

5.1.1. Strains

S. cerevisiae strains

Table 5-1 *S. cerevisiae* strains used in this work

Strain	Genotype	Selection Marker ³	Source
RWS24	MAT α MYO2::HIS3 <i>his3Δ200 ura3-52 leu2-3, 112 lys2-80 ade2-101</i>	H	(Schott et al., 1999)
RWS25	MAT α <i>myo2-16::HIS3 his3Δ200 ura3-52 leu2-3, 112 lys2-80 ade2-101</i>	H	(Schott et al., 1999)
RWS27	MAT α ABP140-GFP::kanR <i>myo2-0IQ::HIS3 his3Δ200 ura3-52 leu2-3, 112 lys2-801 ade2-101</i>	H	(Schott et al., 2002)
RWS28	MAT α ABP140-GFP::kanR <i>myo2-2IQ::HIS3 his3Δ200 ura3-52 leu2-3, 112 lys2-801 ade2-101</i>	H	(Schott et al., 2002)
RWS29	MAT α ABP140-GFP::kanR MYO2-6IQ::HIS3 <i>his3Δ200 ura3-52 leu2-3, 112 lys2-801 ade2-101</i>	H	(Schott et al., 2002)
RWS214	MAT α <i>his3Δ1 leu2Δ met15Δ lys2Δ</i>	-	Lab collection
RWS229	MAT α <i>myo2-66 his6Δ ura1Δ</i>	-	(Johnston et al., 1991)
RWS1021	MAT α pCDC42-GFPMYC-CDC42 <i>ade2-1 ura3 his3-11,15 trp1 leu2 can1-100, Gal+, Psi+ cln1::HisG cln2Δ cln3::HisG yip Lac204-MET-CLN2 (TRP1) bni1Δ::KanMX</i>	H, M, GEN	This study
RWS1022	MAT α pCDC42-GFPMYC-CDC42 <i>ade2-1 ura3 his3-11,15 trp1 leu2 can1-100, Gal+, Psi+ cln1::HisG cln2Δ cln3::HisG yip Lac204-MET-CLN2 (TRP1) rdi1Δ::LEU2, bni1Δ::KanMX</i>	H, L, M, GEN	This study
JYY6	MAT α BNI1-GFP::HIS3 <i>his3Δ1 leu2Δ met15Δ ura3Δ</i>	H	(Huh et al., 2003)

³ Selection markers: **GEN** – Geneticin resistance, **H** – HIS3, **HYG** – Hygromycin B resistance, **L** – LEU2, leucine auxotrophy, **M** – MET15, methionine auxotrophy, **NAT** – Nourseothricin resistance, **U** – URA3, uracil auxotrophy.

JYY7	MATa BNR1-GFP::HIS3 <i>his3Δ1 leu2Δ met15Δ ura3Δ</i>	H	(Huh et al., 2003)
JYY8	MATa MYO2-GFP::HIS3 <i>his3Δ1 leu2Δ met15Δ ura3Δ</i>	H	(Huh et al., 2003)
JYY14	MATa <i>bni1Δ::kanR ura3Δ leu2Δ his3Δ1 met15Δ</i>	GEN	(Winzeler et al., 1999)
JYY15	MATa <i>bnr1Δ::kanR ura3Δ leu2Δ his3Δ1 met15Δ</i>	GEN	(Winzeler et al., 1999)
JYY22	MATa ABP140-GFP::hphR <i>bni11Δ::kanR ura3Δ leu2Δ his3Δ</i>	HYG, GEN	This study
JYY24	MATa ABP140-GFP::hphR <i>bnr11Δ::kanR ura3Δ leu2Δ his3Δ1</i>	HYG, GEN	This study
JYY32	MATa ABP140-GFP::KanR <i>myo2-66 his6Δ ura1Δ</i>	GEN	This study
JYY34	MATa ABP140-GFP::kanR <i>myo2-16::HIS3 bni1Δ::NatR his3Δ200 ura3-52 leu2-3,112 lys2-801 ade2-101</i>	GEN, H, NAT,	This study
JYY44	MATa ABP140-GFP::kanR <i>his3Δ1 leu2Δ met15Δ lys2Δ</i>	GEN	(Huh et al., 2003)
JYY75	MATa ABP140-GFP::kanR MYO2::HIS3 <i>his3Δ200 ura3-52 leu2-3,112 lys2-801 ade2-101</i>	GEN, H,	This study
JYY79	MATa ABP140-GFP::kanR <i>myo2-16::HIS3 his3Δ200 ura3-52 leu2-3,112 lys2-801 ade2-101</i>	GEN, H	This study
JYY87	MATa MYO2-GFP::kanR <i>myo2-16::HIS3 his3Δ200 ura3-52 leu2-3,112 lys2-801 ade2-101</i>	GEN, H	This study
JYY128	MATa <i>smy1Δ::kanR ura3Δ leu2Δ his3Δ1 met15Δ</i>	GEN	Winzeler et al., 1999
JYY129	MATa SMY1-GFP::kanR <i>his3Δ1 leu2Δ met15Δ ura3Δ</i>	GEN	(Huh et al., 2003)
JYY130	MATa <i>myo2-66-GFP::kanMX his6Δ ura1Δ</i>	GEN	This study
JYY131	MATa <i>MYO-2GFP::natR smy1Δ::kanMX ura3Δ leu2Δ his3Δ1 met15Δ</i>	GEN, NAT	This study
JYY133	MATa MYO2-GFP::kanR <i>his3Δ1 leu2Δ met15Δ ura3Δ</i> pRS315-Abp140(1-214)-mRFPruby	GEN	This study
JYY139	MATa MYO2-mRFPruby::natR SMY1-GFP::kanR <i>his3Δ1 leu2Δ met15Δ ura3Δ</i>	GEN, NAT	This study
JYY140	MATa ABP140-GFP::hygR <i>smy1Δ::kanR ura3Δ leu2Δ his3Δ1 met15Δ</i>	HYG, GEN	This study
JYY141	MATa ABP140GFP::hygR <i>ura3Δ leu2Δ his3Δ1 met15Δ</i>	HYG	This study
JYY142	MATa <i>ura3Δ leu2Δ his3Δ1 met15Δ</i>	-	(Winzeler et al., 1999)

JYY143	MAT α MYO2GFP::hygR <i>ura3Δ leu2Δ his3Δ1 met15Δ</i>	HYG	This study
JYY144	MAT α BNI1-GFP::HIS3 <i>his3Δ1 leu2Δ met15Δ ura3Δ pRS315-Abp140(1-214)-mRFPruby :: LEU2</i>	H, L	This study
JYY148	MAT α ABP140-GFP::kanR MYO2-6IQ::HIS3 <i>his3Δ200 ura3-52 leu2-3,112 lys2 801 ade2-101</i>	GEN, H	This study
JYY149	MAT α ABP140-GFP::kanR <i>myo2-2IQ::HIS3 his3Δ200 ura3-52 leu2-3,112 lys2-801 ade2-101</i>	GEN, H	This study
JYY150	MAT α ABP140-GFP::kanR <i>myo2-0IQ::HIS3 his3Δ200 ura3-52 leu2-3,112 lys2-801 ade2-101</i>	GEN, H	This study
JYY158	MAT α <i>bud6Δ::kanR ura3Δ leu2Δ his3Δ1 met15Δ</i>	GEN	(Winzeler et al., 1999)
JYY159	MAT α <i>bud14Δ::kanR ura3Δ leu2Δ his3Δ1 met15Δ</i>	GEN	(Winzeler et al., 1999)
JYY160	MAT α ABP140-GFP::HygR <i>bud14Δ::kanR ura3Δ leu2Δ his3Δ1 met15Δ</i>	HYG, GEN	This study
JYY161	MAT α MYO2-GFP::HygR <i>bni1Δ::kanR ura3Δ leu2Δ his3Δ1 met15Δ</i>	HYG, GEN	This study
JYY162	MAT α MYO2-GFP::HygR <i>bud14Δ::kanR ura3Δ leu2Δ his3Δ1 met15Δ</i>	HYG, GEN	This study
JYY166	MAT α BNR1-GFP::HygR <i>bud14Δ::kanR ura3Δ leu2Δ his3Δ1 met15Δ</i>	HYG, GEN	This study
JYY168	MAT α ABP140-GFP::HygR <i>bud6Δ::kanR ura3Δ leu2Δ his3Δ1 met15Δ</i>	HYG, GEN	This study
JYY174	MAT α Bni1-GFP::HygR <i>bud6Δ::kanR ura3Δ leu2Δ his3Δ1 met15Δ</i>	HYG, GEN	This study
JYY180	MAT α <i>ura3 his3 leu2 lys2 pRS315-Abp140(1-60)-GFP::LEU2</i>	L	This study

All strains used in this study were haploids.

RWS24: Wildtype W303, in which MYO2 allele was replaced with another wildtype MYO2 allele using HIS3 cassette.

RWS25: W303 strain, in which MYO2 allele was replaced with a mutant version *myo2-16* (mutations: M1212T, L1471S, D1497V, Schott et al., 1999) using HIS3 cassette.

RWS27: W303 strain, in which MYO2 allele was replaced with a mutant version *myo2-0IQ* using HIS3 cassette, whereby all IQ repeats were deleted (Schott et al., 2002).

RWS28: W303 strain, in which MYO2 allele was replaced with a mutant version *myo2-2IQ* using HIS3 cassette, whereby four out of six IQ repeats were deleted (Schott et al., 2002).

RWS29: W303 strain, in which MYO2 allele was replaced with an intact version MYO2-6IQ using HIS3 cassette (Schott et al., 2002).

RWS214: Wildtype S288C strain.

RWS229: original *myo2-66* mutant from the genetic screen (Johnston et al., 1991).

RWS1021: *cln2-arrest* strain with BNI1 allele additionally deleted using KanMX cassette. CDC42 was tagged at the N-terminus with GFP.

RWS1022: *cln2-arrest* strain with BNI1 allele additionally deleted using KanMX cassette, RDI1 allele deleted using LEU2 cassette. CDC42 was tagged at the N-terminus with GFP.

JYY6: Strain from the GFP collection library, in which the allele BNI1 was tagged at C-terminus with GFP::HIS3.

JYY7: Strain from the GFP collection library, in which the allele BNR1 was tagged at C-terminus with GFP::HIS3.

JYY8: Strain from the GFP collection library, in which the allele MYO2 was tagged at C-terminus with GFP::HIS3.

JYY14: Strain from knock-out library, in which BNI1 allele was deleted using KanMX cassette.

JYY15: Strain from knock-out library, in which BNR1 allele was deleted using KanMX cassette.

JYY22: ABP140 allele in *bni1Δ* strain (JYY14) using hphR cassette, conferring the strain with hygromycin B resistance.

JYY24: ABP140 allele in *bnr1Δ* strain (JYY15) using hphR cassette, conferring the strain with hygromycin B resistance.

JYY32: ABP140 allele in *myo2-66* mutant strain (RWS229) was directed tagged with GFP at C-terminus using KanMX cassette, conferring the strain with geneticin resistance.

JYY34: *myo2-16* (RWS25) strain was crossed with *bni1Δ* labelled with Abp140 (JYY22). Diploid cells were then sporulated and analysed using a tetra-dissection. Spores that survived on SD-HIS + GEN were selected for microscopic analyses.

JYY44: Wildtype S288C strain (RWS214) with ABP140 allele tagged at C-terminus using KanMX cassette.

JYY75: ABP140 gene was tagged with GFP using KanMX cassette in W303 control strain (RWS24), conferring the strain with geneticin resistance.

JYY79: ABP140 gene was tagged with GFP using KanMX cassette in *myo2-16* strain (RWS25), conferring the strain with geneticin resistance.

JYY87: *myo2-16* mutant allele (RWS25) tagged with GFP using KanMX cassette, conferring the strain with geneticin resistance.

JYY128: Strain from knock-out library, in which SMY1 allele was deleted using KanMX cassette.

JYY129: Strain from the GFP collection library, in which the allele SMY1 was tagged at C-terminus with GFP::HIS3.

JYY130: *myo2-66* mutant allele (RWS229) tagged with GFP using KanMX cassette.

JYY131: MYO2 allele in *smylΔ* (JYY128) strain was tagged with GFP using NatR cassette, conferring the strain with ClonNAT resistance.

JYY133: Myo2-GFP strain (JYY8) transformed with plasmid pRS315-Abp140(1-214)-mRFPruby, which labels actin with red fluorescence. The plasmid uses LEU2 as selection marker.

JYY139: MYO2 allele in Smy1-GFP strain (JYY129) was tagged with mRFPRuby using NatR cassette, conferring the strain with clonNAT resistance.

JYY140: ABP140 allele in *smylΔ* strain (JYY128) was tagged with GFP using hphR cassette, conferring the strain hygromycin B resistance.

JYY141: ABP140 allele in S288C wildtype strain (JYY142) was tagged with GFP using HphR cassette, conferring the strain hygromycin B resistance.

JYY142: Wildtype S288C strain (BY4741, Winzeler et al., 1999) used in the knock-out library.

JYY143: MYO2 allele in wildtype S288C strain (JYY142) was tagged with GFP using HphR cassette, conferring the strain hygromycin B resistance.

JYY144: Bni1-GFP strain (JYY6) transformed with plasmid pRS315-Abp140(1-214)-mRFPruby, which labels actin with red fluorescence. The plasmid uses LEU2 as selection marker.

JYY148: ABP140 allele in Myo2-6IQ strain (RWS29) was tagged with GFP using KanMX cassette, conferring the strain with geneticin resistance.

JYY149: ABP140 allele in *myo2-2IQ* strain (RWS28) was tagged with GFP using KanMX cassette, conferring the strain with geneticin resistance.

JYY150: ABP140 allele in *myo2-0IQ* strain (RWS27) was tagged with GFP using KanMX cassette, conferring the strain with geneticin resistance.

JYY158: Strain from knock-out library, in which BUD6 allele was deleted using KanMX cassette.

JYY159: Strain from knock-out library, in which BUD14 allele was deleted using KanMX cassette.

JYY160: ABP140 allele in *bud14Δ* strain (JYY159) was tagged with GFP using hphR cassette, conferring the strain hygromycin B resistance.

JYY161: MYO2 allele in *bni1Δ* strain (JYY14) was tagged with GFP using hphR cassette, conferring the strain hygromycin B resistance.

JYY162: MYO2 allele in *bud14Δ* strain (JYY159) was tagged with GFP using hphR cassette, conferring the strain hygromycin B resistance.

JYY166: BNR1 allele in *bud14Δ* strain (JYY159) was tagged with GFP using hphR cassette, conferring the strain hygromycin B resistance.

JYY168: ABP140 allele in *bud6Δ* strain (JYY158) was tagged with GFP using hphR cassette, conferring the strain hygromycin B resistance.

JYY174: BNI1 allele in *bud6Δ* strain (JYY158) was tagged with GFP using hphR cassette, conferring the strain hygromycin B resistance.

JYY180: Wildtype S288C strain (RWS214) transformed with pRS315-Abp140(1-60)-GFP plasmid, which labels actin with green fluorescence

***Escherichia coli* strain**

The *E. coli* strain used for molecular cloning was the DH10B (Invitrogen) strain, which was derived from the original *E. coli* strain K12: *F endA1 recA1 galE15 galK16 nupG rpsLΔlacX74 Φ80lacZΔM15 araD139Δ(ara,leu)7697 mcrAΔ(mrr-hsdRMS-mcrBC) λ*.

5.1.2. Kits used

Agarose Gel Extraction Kit (Jena Bioscience) for isolation of DNA-fragments from agarose gel

ClonJET™ (Fermentas) for cloning of PCR products

EZNA™ (Omega Bio-Tek) Plasmid Mini Kit for plasmid-miniprep

QIAGEN® Plasmid Mini Kit (QIAGEN) for plasmid-miniprep

TOPO TA cloning ® (Invitrogen) for cloning of PCR products

5.1.3. Enzymes and proteins

Table 5-2 Enzymes and proteins used in this work

Name	Provider
Bovine Serum Albumin	Sigma
Concanavalin A	Roth
Pfu DNA Polymerase	Fermentas
Restriction enzymes	New England Biolabs
RNase A	Amersham
Taq DNA Polymerase	Biolabs
T4 DNA Ligase	Biolabs
Vent® (exo-) DNA Polymerase	Biolabs
Zymolyase	Biomolecule

5.1.4. Nucleate acids

For transformation of yeast with plasmid or PCR products, salmon sperm DNA (Invitrogen) was added as carrier DNA.

GeneRulers™ 1kb DNA Ladder and GeneRuler™ DNA ladder mix were used as size standards for the agarose-electrophoresis:

GeneRulers™ 1kb DNA Ladder	10000bp	3000bp	500bp
	8000bp	2500bp	250bp
	6000bp	2000bp	
	5000bp	1500bp	
	4000bp	1000bp	
	3500bp	750bp	
GeneRulers™ 1kb DNA Ladder mix	10000bp	2500bp	700bp
	8000bp	2000bp	600bp
	6000bp	1500bp	500bp
	5000bp	1200bp	400bp
	4000bp	1000bp	300bp
	3500bp	900bp	200bp
	3000bp	800bp	100bp

Table 5-3 Oligonucleotides used in this work

Name	Nucleotide sequence (5' → 3')	Usage ⁴
JY3	CTAAGAGAATAGTTGACCTTGTTGCCCAACAAGTCGTTCAA GACGGCCACCGTACGCTGCAGGTCGAC	PCR, TAG (MYO2)
JY4	ATTTCTTTTTTTAGCATTTCATGTACAATTTTGTTCCTCGCG CCATCAGTTATCGATGAATTCGAGCTCG	PCR, TAG (MYO2)
JY9	GGAAAGATCCATAGGTGAGGCTAGCACAGGTAACAGGCTAA GTTTCAAACGTACGCTGCAGGTCGAC	PCR, TAG (BNI1)
JY10	GGATGTTTGTTCGTTTGGTATTACTGTTGTCATAATTTTTTGGT TTAATATTATCGATGAATTCGAGCTCG	PCR, TAG (BNI1)

⁴ **SEQ**: Sequencing, **PCR**: polymerase chain reaction, **TAG**: PCR-based fluorescent tagging of proteins

JY13	CAACTAAAAATGTACCGCTGCTGGGTACAAGCTGTGTTTGA CGTTCCTCAACGTACGCTGCAGGTCGAC	PCR, TAG (ABP140)
JY14	CTTGTTTTATGATGAGAGAGGAGGTGGTACTTGTCTCAGAA CTTCATCGATGAATTCGAGCTCG	PCR, TAG (ABP140)
JY19	CTGCTGTGCGATTCGATACTAAC	PCR, HIS3 cassette internal 3'
JY20	CAAGGAGGGTATTCTGGGCC	PCR, HIS3 cassette internal 5'
JY21	CCCGACATCGGTTAGAGGAAG	PCR, Bni1 5' external
JY22	GCTGTTGTTGGGATGCATAGGTC	PCR, Bni1 5' internal
JY23	CTGAAGATTTACCATCGCCATC	PCR, Bni1 3' internal
JY24	GTGACTGTTTATCCACGCTCTC	PCR, Bni1 3' external
JY30	CGCGTCTGTGAGGGGAGCGTTTC	PCR, hygromycin cassette check
JY31	CACAAATCGCCCGCAGAAGCGCG	PCR, hygromycin cassette check
JY32	GAACCTTTTCAACAAACGAGAAGCAAGAAAGGAAGAGAAG GAAAGGAAATGCGTACGCTGCAGGTCGAC	PCR, BNI1 knock-out
JY51	GAGGTGAAATACACGTAGTTTTTTAGATAACATTCTCTGCTT GGTAAGAGAATGCGTACGCTGCAGGTCGAC	PCR, TAG (BUD14)
JY52	GATGCAAGTTCGTTGGATGAGAAAAAGACCAGGCTTTATTG TAAGGACAATATCAATCGATGAATTCGAGCTCG	PCR, TAG (BUD14)
JY53	GTTTTTGCAGAAATGGATGTGTTGATGAAACAATTGGATG AAATTATTCGTAAACGTACGCTGCAGGTCGAC	PCR, BUD14 knock-out
JY54	GTCCATTTCTTTATATAAGCTCCACAACACTACATAAAATACT AAGTCTTCACTAATCGATGAATTCGAGCTCG	PCR, TAG (BNR1)
JY55	CACGTTTTACTAGAGAGAACGCATGCTATGCTGAACGATAT TCAAATATACGTACGCTGCAGGTCGAC	PCR, TAG (BNR1)
RWS47	GATACTAACGCCGCCATC	PCR, SEQ, geneticin cassette check
RWS48	GTATTCTGGGCCTCCATG	PCR, SEQ, geneticin cassette check

RWS258	GATCGGATCCATGGGCAAGCTTACCATGG	PCR, Cloning of mRFPRuby
RWS581	CTCGAGAGCGCCTGTGCTATGTCTGCC	PCR, Cloning of mRFPRuby
RWS896	GTAATACGACTCACTATAGGG	SEQ, pJET1.2-5'
RWS1120	GAGTTGATGAATCTCGGTG	PCR, SEQ, clonNAT cassette check
RWS1121	GTATTCTGGGCCTCCATG	PCR, SEQ, clongNAT cassette check
T7 Primer	AATACGACTCACTATAG	SEQ

Table 5-4 Plasmids used in this work

Name	Description	Selection Marker ⁵	Annotation
RWC46	pFA6a-kanMX6	A, GEN	Plasmid used in one step tagging or deletion of genes. The selection marker is KanMX6, which confers transformants geneticin resistance (Longtine et al., 1998).
RWC48	pFA6a-His3MX6	A, H	Plasmid used in one step tagging or deletion of genes. The selection marker is His3MX6. Transformants of this cassette are able to grow on SD-His medium (Longtine et al., 1998).
RWC164	pRS305	A, L	General cloning vector for <i>S. cerevisiae</i> (Sikorski and Hieter, 1989). Selection marker, LEU2. Transformants are able to grow on SD-Leu medium.
RWC168	pRS315	A, L	General cloning vector for <i>S. cerevisiae</i> (Sikorski and Hieter, 1989). This plasmid contains centromere sequence (CEN), which limits the copy number of the plasmid to 2-3.

⁵ Selection markers: **A** – Ampicillin resistance, **GEN** – Geneticin resistance, **H** – HIS3 histidine auxotrophy, **HYG** – Hygromycin B resistance, **L** – LEU2, leucine auxotrophy, **NAT** – Nourseothricin resistance, **T**-TRP1, tryptophan auxotrophy, **U** – URA3,

RWC219	pFA6a-hphNT1	A, HYG	Plasmid used in one step tagging or deletion of genes. The original plasmid was pFA6a-hphMX4. The hphMX4 cassette of the original plasmid was replaced with hphNT1 using XhoI/SalI sites (Janke et al., 2004).
RWC220	pFA6a-natNT2	A, NAT	Plasmid used in one step tagging or deletion of genes. The original plasmid was pFA6a-NatMX4. The NatMX4 cassette of the original plasmid was replaced with NatNT2 using XhoI/SacI sites (Janke et al., 2004). Transformants of this cassette are clonNAT resistant.
RWC233	yeGFP-hphNT1	A, HYG	Plasmid used in one step tagging of genes with C-terminal yeGFP. The original plasmid was pFA6a-hphNT1. Yeast enhanced green fluorescent protein (yeGFP) was cloned in using SalI/BssHII sites (Janke et al., 2004).
RWC234	yeGFP-TRP1	A, T	Plasmid used in one step tagging of genes with C-terminal yeGFP. Selection marker of this plasmid is klTRP1, which allows transformants to grow on SD-Trp medium (Janke et al., 2004).
RWC235	EGFP-kanMX4	A, GEN	Plasmid used in one step tagging of genes with C-terminal EGFP. Selection marker of this plasmid is kanMX4, which confers transformants geneticin resistance (Janke et al., 2004).
RWC236	EGFP-HIS3MX6	A, H	Plasmid used in one step tagging of genes with C-terminal yeGFP. Selection marker of this plasmid is HIS3MX6, which allows transformants to grow on SD-His medium (Janke et al., 2004).
RWC311	mRFPRuby-hphNT1	A, HYG	Plasmid used in one step tagging of genes with C-terminal mRFPRuby. The original plasmid was pFA6a-hphNT1. mRFPRuby (a.k.a MARS) was cloned in using SalI/BssHII sites.
RWC312	mRFPRuby-natNT2	A, NAT	Plasmid used in one step tagging of genes with C-terminal mRFPRuby.
RWC316	pTOPO-Mars	A	Plasmid used as template for cloning of mRFPRuby. mRFPRuby was cloned into pCRII-TOPO vector using the TOPO TA cloning® kit.

RWC353	pRS305-pAbp140 ABP140(1-214)-EGFP	A, L	The first 642 bp of open reading frame of APB140 was cloned together with the 500 bp upstream of start codon (pABP140) replaced the pVrp1-BEE1 of the original pTL58. Sites used were PstI/BamHI. The expressed protein is the first 214 amino acids of ABP140 with a C-terminal EGFP tag.
RWC370	pRS305-pAbp140 ABP140(1-90)-EGFP	A, L	The first 270 bp of open reading frame of APB140 was cloned together with the 500 bp upstream of start codon (pABP140) replaced the pVrp1-BEE1 of the original pTL58. Sites used were PstI/BamHI. The expressed protein is the first 214 amino acids of ABP140 with a C-terminal EGFP tag.
-	pCRII-TOPO	A	PCR cloning vector used in the TOPO TA cloning® kit.
-	pJET1.2	A	PCR cloning vector used in the ClonJET™ kit.
-	pTL58 / pRS305-pVRP-BEE1- GFP	A, L	Promoter p-Vrp1 was cloned into the original plasmid pRS305 using BamHI/NotI sites. BEE1-EGFP was subsequently cloned in using NotI site.
-	pRS305-pAbp140- ABP140(1-214)- mRFPRuby	A, L	EGFP RWC353 was replaced with mRFPRuby from RWC316 using NotI/XhoI sites

5.1.5. Chemicals

Table 5-5 Chemicals used in this work

Name	Source
Acetic acid	Sigma
Agarose	Invitrogen
L-Alanin	VWR
Alexa Fluor 568 Phalloidine	Invitrogen
Ammonium chloride	Alfa Aesar

Ammonium hydrogen carbonate	Alfa
Ammonium nitrate	Carl Roth
Ampicillin sodium salt	Carl Roth
L-Arginin	VWR
L-Asparagin-Monohydrate	VWR
L-Aspartic acid	SIGMA
Calcium chloride	Serva
clonNAT	Werner
Chloroform	Roth
Concavalin A	Roth
L-Cysteine	VWR
Demthyl sulfoxide (DMSO)	Sigma
Deoxynucleotide Solution mix	BioLabs
Difco Bacto Agar	Becton Dickinson
Difco Bacto Peptone	Becton Dickinson
Difco Tryptone	Becton Dickinson
Difco Yeast Extract	Becton Dickinson
dNTP Set, 100mM solution	Fermentas
DTT	Fermentas
EDTA (Titrplex)	Merck
EGTA	Roth
Genticin	Roth
Glycerol	Roth
D(+)-Glucose	VWR
L-Glutamine	PAA
Glycerin 86% p.a.	Roth
HygromycinB	Merck
Kanamycin Sulfate	Invitrogen

Latrunculin B	Merck
Lectin from concanavalin A	Sigma
L-Leucin	VWR
Lithium acetate dihydrate	SIGMA
L-Lysin-Monohydrat	VWR
Magnesium chloride-Hexahydrate	Roth
Magnesium sulfate-Heptahydrate	Roth
Manganese chloride hydrate	Roth
2-Mercaptoethanol	Sigma
L-Methionine	VWR
Sodium azide	Sigma
Sodium chloride	Merck
Sodium dihydrogenphosphate	Roth
Sodium fluoride	Sigma
di-Sodium hydrogenphosphate	Sigma
Nicotinic acid	Alfa Aesar
dNTP Set, 100mM solutions	GE Healthcare
N-(3-triethylammoniumpropyl)-4-(4-(dibutylamino) styryl) pyridinium dibromide (Ethidium Bromide)	Invitrogen
Paraformaldehyd 37%	Alfa Aesar
L-Phenylalanine	VWR
Polyethyleneglycol (PEG3350)	SIGMA
Potassium hydride	Alfa Aesar
Rhodamine phalloidine	Invitrogen
ROTI-Phenol/Chloroform/Isoamyl	Carl Roth
Rubidiumchloride	Sigma
Salmon Sperm DNA	Invitrogen
SDS	Roth

L-Serine	VWR
Salmon Sperm DNA	Eppendorf
Sodium azide	Sigma
Sodium bicarbonate solution	Sigma
Sodium carbonate	Sigma
Sodium hydride	Sigma
Sodium sulfate anhydrous	Alfa
D(-)-Sorbitol	VWR
L-Threonine	VWR
Tris, HCl	Merck
TritonX 100	Roth
L-Tryptophan	VWR
L-Tyrosine	VWR
L-Valine	VWR
Yeast Nitrogen Base	Becton Dickinson

5.1.6. Other materials

Table 5-6 Other materials used in this work.

Name	Source
Coverslip	Menzel Gäser
Filter paper 3MM	Whatman
Glassbeads	Sigma
Glassslide	Menzel Gäser
Lense paper	Assistent
Petri dishes	Greiner
Plastic cuvettes	Brand
Pipet Tips	Qiagen

5.1.7. Buffers and solutions

Table 5-7 Buffers and solutions used in this work

Description	Recipe
Ampicilin solution	10 mg/mL Ampicilin In double distilled sterile H ₂ O
clonNAT solution	20 % (w/v) clonNAT In double distilled sterile H ₂ O
Concavalin A coating solution	0.5 mg/ml Concanavalin A 10 mM Potassium Phosphate buffer pH 6.0 1 mM CaCl ₂ 0.02% NaN ₃
6x DNA Loading buffer	50 % (w/v) sucrose 0.25% (w/v) bromopheno-blue In TE buffer
DNA precipitation buffer	3 M NaOAc pH = 4.8
EDTA solution pH 8.0	0.5M EDTA Na ₂ EDTA*2H ₂ O pH = 8.0
Geneticin solution	200 mg/ml geneticin In double distilled sterile H ₂ O
Hygromycin B solution	50 mg/ml hygromycin In sterile PBS
10x Ligase buffer	50 mM MgCl ₂ 660 mM Tris-HCl 10 mM DTT 10 mM ATP pH = 7.5
Lysis buffer	2% (v/v) Triton X-100 1% (w/v) SDS 100 mM NaCl 10mM Tris-HCl 1mM EDTA
MOPS	20 mM MPOS 8 mM NaOAc 1 mM EDTA pH6.8
Sodium phosphate buffer	1M NaH ₂ PO ₄ 1M Na ₂ HPO ₄ pH = 7.0

10x PBS buffer	92 mM Na ₂ HPO ₄ 147 mM KH ₂ PO ₄ 27 mM KCL 1.39 M NaCl pH = 7.2
10x Pfu buffer	200 mM Tris-HCl 100 mM KCl 100 mM (NH ₄) ₂ SO ₄ 20 mM MgSO ₄ 1 % Triton X-100 1 mg/ml BSA pH = 8.8
PEG mix	100mM LiOAc 10mM Tris-HCl pH8 1mM EDTA 40% (v/v) PEG 3350
Phenol/chloroform	50% Phenol 50% Chloroform
Potassium phosphate buffer (10x)	1M KH ₂ PO ₄ 1M K ₂ HPO ₄ pH = 7.0
RF1	100 mM RbCl 50 mM MnCl ₂ 30 KOAc 10 mM CaCl ₂ 15% (w/v) Glycerol pH = 5.8
RF2	10 mM MOPS 10 mM RbCl 75 mM CaCl ₂
Rhodamine-Phalloidine staining solution	6.6 μM Rhodamine Phalloidine In Methanol
SORB	100 mM LiOAc 10 mM Tris – HCl 1 mM EDTA 1 M Sorbitol
50x TAE buffer	2M Tris – Base 2M Acetic Acid 50 mM EDTA pH = 8.0

10x TBE buffer	440 mM Tris Base 440 mM Boric Acid 10 mM EDTA pH = 8.0
10x TBS buffer	50 mM Tris – HCl 150 mM NaCl pH = 7.5
10x TE buffer	10 mM Tris-Base 1 mM EDTA pH = 8.0
10x Thermopol buffer	500 mM KCl 15 mM MgCl ₂ 100 mM Tris-HCl pH = 8.3
1M Tris buffer	619 mM Tris – HCl 381 mM Tris Base pH = 8.0
VALAP	33% Valine (w/w) 33% Lanoline (w/w) 33% Parafin (w/w)

5.1.8. Media

Table 5-8 Media used in this work

Name	Source
<i>S. cerevisiae</i> media	
SD-Medium (liquid)	0.67% (w/v) Bacto-yeast nitrogen base without amino acid 0.2% (w/v) drop-out powder
SD-plates	0.67% (w/v) Bacto-yeast nitrogen base without amino acid 0.2% (w/v) drop-out powder 0.8% (w/v) Bacto agar
Sporulation medium (liquid)	0.1% (w/v) Bacto yeast extract 1% (w/v) KCl 0.05% (w/v) D(+)- Glucose

Sporulation plates	0.1% (w/v) Bacto yeast extract 1% (w/v) KCl 0.05% (w/v) D(+)- Glucose 0.8% (w/v) Bacto agar
YPD-Medium (liquid)	2% (w/v) Bacto peptone 1% (w/v) Bacto yeast extract 2% (w/v) D(+)- Glucose
YPD plates	2% (w/v) Bacto peptone 1% (w/v) Bacto yeast extract 2% (w/v) D(+)- Glucose 0.8% (w/v) Bacto agar
YPD plates + Geneticin	YPD plates 300 µg/ml Geneticin
YPD plates + Hygromycin B	YPD plates 300 µg/ml Hygromycin B
YPD plates + clonNAT	YPD plates 100 µg/ml clonNAT
<i>E. coli</i> media	
LB-medium (liquid)	1% (w/v) Bacto Tryptone 0.5% (w/v) Bacto Yeast-Extrakt 0.5% (w/v) NaCl
LB plates	1% (w/v) Bacto Tryptone 0.5% (w/v) Bacto Yeast-Extrakt 0.5% (w/v) NaCl 0.8% (w/v) Bacto agar
YT-medium (liquid)	0.8% (w/v) Bacto Tryptone 0.5% (w/v) Bacto Yeast-Extrakt 0.5% (w/v) NaCl
YT plates	0.8% (w/v) Bacto Tryptone 0.5% (w/v) Bacto Yeast-Extrakt 0.5% (w/v) NaCl 0.8% (w/v) Bacto agar

In synthetic drop-out (SD) media different combinations of drop-out powder were added. The amino acid concentration in the synthetic complete (SC) medium, the final amounts of amino acids are:

Adenine sulfate	20 mg/L
Uracil	20 mg/L
L-tryptophan	20 mg/L
L-histidine	20 mg/L
L-arginine	40 mg/L
L-methionine	20 mg/L
L-tyrosine	50 mg/L
L-leucine	60 mg/L
L-isoleucine	60 mg/L
L-lycine	50 mg/L
L-phenylalanine	50 mg/L
L-aspartic	100 mg/L
L-glutamic acid	100 mg/L
L-valine	150 mg/L
L-threonine	200 mg/L
L-serine	400 mg/L

5.2. Microbiological and genetic methods

5.2.1. *Escherichia Coli*

Culturing of *E. coli*

E. coli strains were cultured at 37°C either in liquid with 200rpm shaking or on plates. Overnight cultures grown in LB or YT liquid media were used for extraction of plasmids. Strains were either stored at 4°C on plates or -80°C in 25% glycerol.

Measurement of cell density of *E. coli* culture

The cell densities of liquid cultures were measured photometrically at 600nm wavelength using plastic cuvettes and a GeneSys spectrophotometer (Thermo Electron Corporation). Culture media were used as blank solutions. OD₆₀₀ = 1.0 corresponds roughly 10⁹ cells/ml.

Preparation of competent *E. coli* using rubidium chloride

DH10B *E. coli* cultures were grown in small volume of LB medium (5-10 ml) overnight at 37°C, and inoculated in 500ml LB medium. Inoculated cultures were grown till OD₆₀₀ = 0.5, and were cooled on ice for 15 mins. The cooled cultures were transferred to centrifuge tubes and spun at 4500rpm in a Biofuge Primo R (Thermo Scientific) for 10 mins. Supernatants were poured out and the pellets were resuspended in 30ml solution RF1 (see 5.1.7.). The suspension was cooled on ice for 15mins, and then centrifuged for 5 mins at 4000rpm. The pellets were resuspended in RF2 on ice and aliquoted into 100µl vials and stored at -80°C.

Chemical transformation of competent *E. coli*

50µl-100µl vial of competent cells was thawed on ice. 1-10µl of Plasmid solution (1-5ng DNA) or ligation reactions was added to the cells and the mixture was incubated on ice for 20-25 mins. The reaction was then heatshocked at 42°C for 60-120 secs, before being cooled on ice for 2 mins. The reaction could be directly plated on LB or YT medium containing 100µg/ml ampicillin. Alternatively, 900µl of liquid LB or YT media was added into the mixture. The mixture was then recovered at 37°C on a heating block for 30 mins and plated.

5.2.2. *S. cerevisiae*

Culturing *S. cerevisiae*

S. cerevisiae strains were cultured at 30°C or RT either in liquid with 200rpm shaking or on plates. Overnight cultures grown in YPD or SD liquid media were used inoculation or storage. Strains were either stored at RT up to 6 weeks or at -80°C in 25% glycerol.

Measurement of cell density of *S. cerevisiae* culture

The cell densities of liquid cultures were measured photometrically at 600nm wavelength using plastic cuvettes and a GeneSys spectrophotometer (Thermo Electron Corporation). Culture media were used as blank solutions. $OD_{600} = 1.0$ corresponds roughly 10^7 cells/ml.

Transformation of *S. cerevisiae*

S. cerevisiae strains were grown in appropriate media to saturation ($OD_{600} > 1$) at 30°C in small volumes (5-10ml). The cultures were then diluted in 50 ml liquid media $OD_{600} < 0.1$ and grown at 30°C until $OD_{600} = 0.4-0.8$. Cells were transferred into centrifuge tubes and centrifuged at 1000 rpm for 5mins in a Biofuge Primo R (Thermo Scientific). Supernatants were discarded and pellets were resuspended in 25ml sterile ddH₂O, before being re-centrifuged at 1000 rpm for 5 mins. The pellets were then resuspended in 10 ml SORB solution and aliquoted in 45 μ l vials.

For transformation, it was usually required that the competent cells were prepared freshly as above. 5 μ l of Salmon Sperm DNA was added to the 45 μ l competent cells as carriers. For transformation of plasmids, 1 μ l of plasmid solution was needed. For transformation using PCR amplified homologous-recombination cassettes, 5-10 μ l of the PCR reaction was added. The cells together with DNA were then mixed with a vortex cell mixer (VWR) together with 6 volumes of PEG Mix (306 μ l for transformation with plasmid, 330-360 μ l for transformation with PCR reaction). The mixture was incubated at 30°C or RT for 30mins-1hr. 1/9 volume of DMSO was then added. Heatshock was carried out at 42°C for 15-30 mins. Cells were then sedimented at 2000rpm for 1 mins, and resuspended in 100-200 μ l ddH₂O. If the transformants were expected to carry an antibiotic-resistance, 900 μ l of corresponding medium without antibiotics was added to the cells. Cells were recovered at 30°C or RT overnight, before being plated on antibiotic

containing medium. If the expected transformants did not contain any anti-biotic resistance, cells were plated directly after resuspension in H₂O.

Genetic manipulation in *S. cerevisiae*

One of the greatest advantages of using *S. cerevisiae* as a model system is the availability of powerful genetic techniques. In last decades, a highly effective system of genetic manipulation was established based on homologous recombination of DNA. This technique is a PCR-mediated technology, whereby PCR reactions are directly used to either tag or delete the target gene. In order to manipulate a gene, primers were designed in a way such that flanking sequences of a target gene were amplified together with the selection markers as well as promoters and tags (Fig 5-1A). Amplification was carried out using a special PCR programme (Fig 5-1B) which ensures sufficient amount of DNA would be available for transformation. Subsequently, PCR products were directly added into the transformation reaction as described above. For tagging of the protein at N-terminus, PCR products contain the flanking sequences around the start codon (ATG) of the target ORF, selection marker, introduced promoter and the tag. For tagging at C-terminus, PCR products contain flanking sequences around the stop codon of the target ORF, the tag and the selection marker. For deletion of the gene, PCR product contain only the flanking sequences before the start codon and after the stop coden together with the selection marker (Fig 5-1C). Homologous recombination occurs during DNA replication. The net results of successful reactions were either insertion of amplification cassettes before or behind the gene, or the replacement of the gene with the deletion cassette.

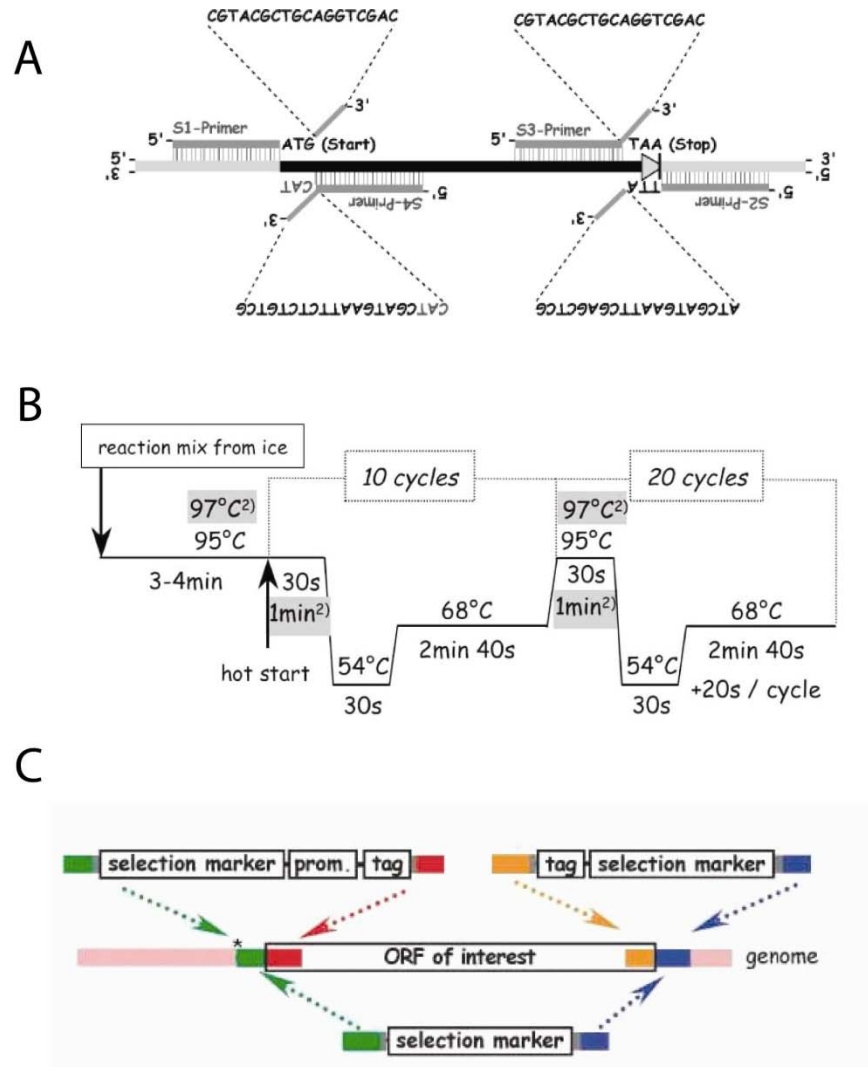


Figure 5-1.

Scheme for PCR-based genetic manipulation in *S. cerevisiae*. (A) Primer design scheme for amplification of insertion/deletion cassettes. For N-terminal tagging, S1 and S4 primers were used. For C-terminal tagging, S2 and S3 primers were used. For gene deletion, S1 and S2 primers were used. (B) PCR cycles for amplification of insertion/deletion cassettes. (C) Simplified scheme of insertion and deletion based on homologous recombination.

Selection of transformants

Selection of transformants was typically carried out 2-5 days after transformation. Medium-sized colonies were picked and streaked on a selective medium identical to the medium used for plating, and incubated at 30°C or RT for 1-2 days. Individual colonies arising from the re-streaked cells were then picked and incubated in 1 ml liquid medium overnight, before being tested.

Testing of the positive clones was carried out in two different ways depending on the requirement of the experiments. Strains intended for fluorescent tagging were tested for fluorescence using a Zeiss Axio Imager A1 microscope. Strains tested for gene knock-out were probed with colony-PCR pairs of primers that bind to the flanking sequence of the deleted gene as well as the deletion cassette. Gene sequencing was performed in cases where confirmation of correct tagging was required.

Mating

Colonies from two strains of *S. cerevisiae* of different mating types were mixed thoroughly in 50µl ddH₂O and then incubated at 30°C for 2hrs. Cells were then picked in small quantity and spread into a single layer on the edge of a plate containing selective media. Conjugating cells (a.k.a. Mexican hats) were picked out using a tetrad dissection microscope and in the central area of the plate. The mating culture was incubated at 30°C for 2-5 days. Colonies that survived are diploid cells which could be sporulated to generate haploid strains of the desired genotype.

Sporulation and tetrad dissection

Diploid cells were first grown in 1 ml YPD medium overnight. Cells were sedimented at 2000 rpm for 2 mins, and the pellet were washed three times using 1.5 ml ddH₂O. Pellet was then resuspended in 1 ml sporulation liquid medium and incubated at 30°C for 2-3 days with shaking. Tetrad formation was confirmed under a microscope. A small amount of cells (50-100µl) were sedimented and incubated in 40 µl 1x potassium phosphate buffer together with 10µl Zymolyase (5 µg/ml) at 30°C for 5-10 mins. The incubation reaction was then streaked on a plate containing YPD medium and dried for 10 mins. Tetrads were broken by the dissection needle and spread

into the rows of four on a grid. The plate was incubated at 30°C for two days, before replica plating to determine the segregation of selection markers.

5.3. Molecular biological methods

5.3.1. Handling and isolation of DNA

DNA precipitation

DNA can be concentrated and purified from aqueous solutions by precipitation procedures. DNA precipitation buffer (3M NaOAc, pH = 4.8) was added in 1/10 of sample volume, followed by 2x sample volume of 100% ethanol. The sample was then placed on ice for 1-2 hr, before being sedimented at 14000 rpm in a table centrifuge (Galaxy 16DH, VWR) for 10-15 mins. Supernatant was removed carefully by vacuum. Pellet was washed twice using 70% ethanol, in order to remove the salt thoroughly. After removal of ethanol, pellet was air-dried for 30-45 in RT, before being dissolved in appropriate volume of TE buffer.

Mini-preparation of plasmid DNA from *E. coli*

The mini-preparation of plasmid DNA was carried out following the instructions provided in EZNA™ Plasmid Mini Kit for plasmid-miniprep kit and QIAGEN® Plasmid Mini Kit.

Isolation of genomic DNA from *S. cerevisiae*

Genomic DNA of *S. cerevisiae* cells were needed as template for gene amplification and sequencing. Cells were grown overnight at 30°C in 2-5ml liquid YPD medium. Cultures were centrifuged at 2000 rpm for 2 mins. Supernatants were removed. Pellets were resuspended in 200µl lysis buffer. 200µl of TE buffer and 200 µl of phenol/chloroform were then added into the sample, followed by equal volume of glass-beads. Cells were broken up by vortex in this mixture for 5-10 mins. The mixtures were then sedimented at 14000 rpm in a table centrifuge for 10 mins. The mixtures were clearly separated into three layers. The aqueous top layer was transferred into a fresh 1.5 ml tube. DNA was then purified using precipitation procedure described above. Dried pellets were dissolved in TE buffer containing 10µg/ml RNase A.

5.3.2. *in vitro* modification of DNA

Restriction digestion of DNA

The digestion of double- stranded DNA was carried out using Type II – restriction endonucleases (New England Biolabs) together with recommended buffer conditions. The digestion reactions were typically incubated at 37°C for 1hr before being evaluated using TAE or TBE-Agarose gel electrophoresis.

Ligation of DNA fragments

Double-stranded DNAs were joined covalently using T4 DNA ligase. In this work, all ligation reactions were carried out in order to introduce a linear insert into a digested vector. The usual molar ratios of vector : insert were 1 : 3 and 1 : 1. A typical reaction make-up is as following:

100ng linearized vector

3 times of equal molar amount of insert DNA

1 U T4 DNA ligase

1 µl 10x ligase buffer

10 µl total volume made up by sterile ddH₂O

The reaction was incubated either 1-2 hr in RT or 4°C overnight. Before being transformed into competent *E. coli*.

5.3.3. Analyses of DNA

Agarose electrophoresis

DNA fragments can be separated according to their sizes by applying an electric field. Generally, agarose gels were prepared using 1% agarose dissolved in electrophoresis buffer (1x TAE or TBE). The mixture was heated to boiling using a microwave cooker, until all agarose powder dissolved in the buffer. The solution was then poured into a sealed gel tray, on which a comb was placed. 0.5µg/ml of ethidium bromide was added in the gel as the solution cooled to about 60°C. After complete cooling, the comb was removed, producing wells for sample loading. The solidified gel was then mounted onto an electrophoresis tank and submerged completed into

electrophoresis buffer. DNA samples were mixed with 0.2 volumes of 6x DNA loading buffer and loaded into the gel. DNA was then separate by applying an electric field between two electrode for 30 – 45 mins at 100-120 V. Gels after eletrophoresis were then placed into a GeneFlash gel imaging system (Syngene Bio Imaging) to be photographed.

DNA sequencing

Plasmid DNA was sequenced using an ABI-3730 (Perkin Elmers) sequencer and ABI Big Dye 3.1 sequencing chemistry. The reactions were carried out by the Core Facility of Max-Planck Institute of Biochemistry.

5.3.4. Polymerase chain reaction (PCR)

Standard PCR

DNA fragments can be selectively amplified by PCR reactions. Two primers which bind to the 5' and 3' ends of the amplification target were needed. The reaction was carried out using a PXE 0.2 Thermal Cycler (Thermo Electro Corporation). Other than amplification of homologous recombination cassettes described in 5.2.2. (Fig. 5-1), the PCR reactions were typically made up as following:

1 µl	Template DNA (10 ng/µl)
0.5 µl	Forward primer (binds 5' end)
0.5 µl	Reverse primer (binds reverse complementary strand at 3' end)
1 µl	dNTP mix
1 µl	Taq or Pfu DNA-polymerase (1 U/µl)
5 µl	10 x PCR buffer (Thermopol or Pfu buffer)
2.5 µl	25 mM MgCl ₂ (optional)

Add sterile ddH₂O to 50 µl.

The optimal temperature set-up for the reaction depends on the nature of the template DNA and the melting temperature of the primers. One of the most important parameter for a successful PCR reaction is the determination of primer annealing temperature. In some cases, enzyme were

added “hot start” after the initial denaturation step, in order to maximize to polymerization efficiency.

A typical program for stand PCR is as following

Stage	Repeats	Temperature	Duration
1	1x	95°C	5 mins
2	30-35x	95°C	30 secs
		55°C	1 min
		72°C	1-5 mins (~1000 bp per min)
3	1x	72°C	10 mins
4	1x	4°C	∞

Colony PCR of *S. cerevisiae*

In order to quickly check the success of genetic manipulation of a large number of *S. cerevisiae* colonies, entire colonies were sometimes used for PCR analyses without isolation of genomic DNA. Individual colonies sized 0.5-1.0 mm were resuspended in 100 µl of PBS buffer containing 0.02M NaOH. Samples were heated at 95°C for 10 mins in order to break yeast cells. Cell debris was sedimented at 5000 rpm for 2 mins. 10 µl of the supernatant was typically used instead of the template DNA in a PCR reaction as described above.

It is important to ensure that the colonies picked for analysis were not over-sized, since too much material affects the reliability of results. In my experience, amplification of DNA fragments of 300-1500 bp could be performed reproducibly using this procedure. Detection of longer or shorter fragments should be performed on isolated genomic DNA or plasmid DNA. It is highly recommended to perform this test using two or more pairs of primers. Genomic DNA based tests or DNA sequencing should be performed to confirm positive colonies acquired in colony PCR analyses.

5.4. Microscopy

5.4.1. Epifluorescent microscopy

Fixation and staining with rhodamine phalloidine

S. cerevisiae cells were grown to OD₆₀₀ 0.5-0.8 in 1 ml liquid medium. 130 µl of 37% paraformaldehyde was added directly in to the medium. Cells were incubation on with 1-2rpm rotation at RT for 45 mins. The reactions were then centrifuged at 2000 rpm. The supernatants were removed and pellets were washed twice with 500 µl PBS. The final pellets were resuspended in 30 µl of PBS containing 0.1% Triton X-100. 3µl of rhodamine phalloidine (final concentration 0.6 µM) staining solution was added into the reaction. The samples were incubated at RT for 45 mins. Staining solution was removed by centrifugation, followed by washing three times with 500 µl PBS. Finally, fixed cells were resuspended in 20 µl PBS and stored at 4°C. Samples can be stored for up to a week in PBS without additives. Observation within 1-2 days post staining is strongly recommended. Otherwise anti-fade solution should be added in the sample.

Widefield microscopy

Widefield imaging of both fixed samples and live cells were performed using an imaging system based on a Zeiss upright microscope. The set-up of the system is as following:

Component	Description	Provider
Microscope	Zeiss Imager A1	Carl Zeiss
Objective lense	Olympus 1.3 NA 100x	Olympus
Motor	Visitron MS-2000 Nanodrive	Visitron Systems GmbH
Halogen lamp	X-Cite	Visitron Systems GmbH
Shutter Control	Uniblitz VCM-1®	Vincent Associates
Camera	Andor iXON EM CCD	Andor
Software	Metamorph 7.0	Molecular Devices

Samples were mounted onto a glass slide in small volume (2.5-4 μ l). Coverslips were put over the samples without coating. For imaging rhodamine phalloidine fixed samples, camera gain was set to minimum, and the exposure time was < 50ms. The microscope is equipped with a filter sets with allow the excitation and detection of green, red, blue and yellow fluorescence. For live- cell imaging, camera gain was typically set to maximum. Exposure time was 100ms-500ms depending on the intensity of the fluorescent marker. For 4D micrososcopy, Z sections of the same cells were taken with 2 s intervals. Exposure time was 100 ms, each Z stack contains 5-7 individual frames.

5.4.2. TIRF microscopy

ConA coating of coverslips

Concanavalin A (ConA) is a lectin that binds to polysaccharide molecules on the yeast cell walls, which physically fixes cells on a coverslip, allowing long-term fluorescent imaging of the same cell. For coating, glass coverslips were first cleaned by soaking in 1 M NaOH in a petri dish for 4 hrs or overnight with 2 rpm shaking. These were then washed with ddH₂O three times, each time 5 mins with shaking. ConA coating solution was then added to the petri dish, and incubated at RT for 30 mins with shaking. Coverslips were then rinsed briefly with ddH₂O and placed on paper tissues in enclosed petri dishes to air dry, and storage at RT. To use, the upper surface of the coverslips should be in contact with the sample.

Sample preparation

S. cerevisiae cultures were grown overnight and diluted to OD₆₀₀ < 0.2. Diluted cultures were grown 4-6 hrs to OD₆₀₀ 0.5-0.8. For mounting, 2.5-3 μ l of liquid sample was added in the centre of a glass slide. A ConA coated coverslip was carefully placed on top of the liquid drop, avoiding bubble formation. The sample is placed at RT for 5-10 mins before mounting to the microscope. This was to ensure the proper adsorption of cells on the coverslip. For imaging at 36°C, cells were typically incubated in a shaker at 36°C for 30 mins, while the climate control unit was switched on for equilibration.

Total Internal Reflection Microscopy (TIRFM)

Dynamics of cortical protein and cytoskeletal dynamics were probed using custom-made TIRFM set-up based on an iMIC modular microscopic unit:

Component	Description	Provider
Microscopic unit	iMic standing unit	TiLL photonics
Objective lens	Olympus 1.45 NA 100x	Olympus
Control unit	ICU	TiLL photonics
TIRF angle control	Galvanometer-drive 2-axis scan head	TiLL photonics
Excitation laser 1	DPSS laser with 75 mW at 488 nm	Coherent Sapphire
Excitation laser 2	DPSS laser with 75mW at 561 nm	Cobolt Jive
Light source for DIC imaging	LED lamp	TiLL photonics
Lamp source for epifluorescence	Polychrome unit	TiLL photonics
Laser shutter	AOTF unit	TiLL photonics
Camera 1	Imago QE CCD	TiLL photonics
Camera 2	Andor iXON DU-897 EM CCD	Andor
Climate control	Temperature control unit with heating block	Workshop in MPI of Biochemistry
Software	Live-Acquisition	TiLL photonics

Samples were mounted onto the microscope in an inverted manner. Target cells for imaging were first identified using live streaming with DIC imaging. TIRF angles were adjusted such that total reflection. Sometimes, the TIRF angles were set slightly below the critical angle for total reflection, such that part of the excitation light was passed through with an extremely low angle across the sample. This kind of low-angle imaging was termed oblique illumination. Oblique illumination increases the area of sample illumination by TIRF set-up at the same time does not cause as much photo-bleaching as wide-field imaging (Tokunaga et al., 2008).

5.4.3. Image processing and analyses

Imaging smoothing

Unless otherwise specified, images presented in this work were raw images. Inversion of whole images was done to ease visualization. Image smoothing was performed using built-in journal

functions of Metamorph (Version 7.0, Molecular Devices). For smoothening, images were first processed with “equalize light” function in Metamorph to minimize the effect of photobleaching and intensity fluctuations. The processed images were then processed further with “flatten background” function and then passed through a Gaussian filter with the kernel (1 3 1; 3 7 3; 1 3 1).

Image deconvolution

Image deconvolution was performed using Huygens deconvolution package (Scientific Volume Imaging). Point spread function was measured separately for green and red channels using 50nm or 100nm fluorescent beads as described before (Yoo et al., 2006).

Measurement of cable extension and retraction rate

Before the measurements, pixel sizes of each microscope set-up were determined using micro-grids. For Imago QE CCD, the pixel size was 0.065 $\mu\text{m}/\text{pixel}$. For Andor EM CCD camera on TIRFM, the pixel size was 0.086 $\mu\text{m}/\text{pixel}$. Individual actin cables were then tracked through time. The lengths of trajectory of the leading of the cables were used to calculate the cable extension rate, whereas those of the trailing ends were used to calculate cable retraction rate:

$$V = D * \frac{r}{F * t}$$

Where V is the extension/retraction rate, D is the length of trajectory in pixels, r is the pixel size (0.085 $\mu\text{m}/\text{pixel}$), F is the number of frames, t is the frame rate in seconds. Typically, 100 cables were measured in 20 cells for a particular condition. Data were then plotted into histogram using speed as the x axis, with binning of 0.2 $\mu\text{m}/\text{s}$. Calibration of measurements was done by tracking the ends of actin cable frame by frame. The error rate of the measurement is around 20% for all measurements (see Fig.5-2 for an example).

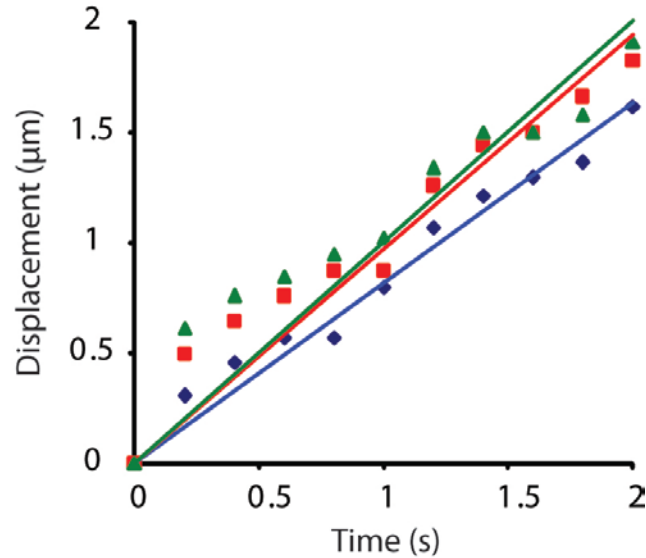


Figure 5-2

Calibration of measurements for actin cable extension/retraction rate. Shown is an example for a calibration procedure. The extension of the same cable was measured three times by tracking its leading end frame by frame. The position of the end at each frame was registered and displacement from the original position was calculated and plotted against elapsed time. Data were then fitted with linear regression to obtain the extension rate. Here, the calculated rate were $1 \mu\text{m/s}$ (data points represented by green triangles, $R^2 = 0.84$), $0.97 \mu\text{m/s}$ (red rectangular, $R^2 = 0.92$) and $0.82 \mu\text{m/s}$ (blue diamonds, $R^2 = 0.97$)

Non-linear regression

Histograms of cable extension/retraction rates were fitted using non-linear least-squares:

$$y = \frac{1}{\delta_1 \sqrt{2\pi}} e^{-\frac{(x-\mu_1)^2}{2\delta_1^2}} + \frac{1}{\delta_2 \sqrt{2\pi}} e^{-\frac{(x-\mu_2)^2}{2\delta_2^2}}$$

in MatLab™ (The Math Works), where σ^2 is the variance and μ the mean. The goodness of the fit was evaluated by calculating the R^2 . As rule, each dataset was fitted to either single or double Gaussian distribution. The distribution that gave a higher R^2 value was used in the final result presentation.

Measurement of lifespan of cortical dots

Measurements of lifespans of cortical dots were performed using kymographs of image stacks. Kymographs were typically generated on the whole visible area of the cell in TIRFM. Cortical dots were then randomly picked up on the kymographs for measurement. Vertical lines spanning the dwelling time of dots were then drawn on the kymograph. The lifespans were calculated as:

$$T = d \cdot t$$

where T is the lifespan, d is the length of the vertical line, t is frame rate in ms.

Bar graphs and box-whisker plots

Bar graphs and box-whisker plots presented in the figures were based on statistical analyses done using Graphpad Prism 4 (Graphpad) software. P-values were calculated using One-way ANOVA with post hoc Bonferroni's test.

5.5. Cell biological methods

5.5.1. Polarization assay

S. cerevisiae strains contain *cln2-arrest* allele were grown in 2 ml SD-Met medium at 30°C overnight. The cultures were diluted to $OD_{600} = 0.4$. Diluted cultures were incubated at 30°C for 2 hrs with shaking and sedimented at 2000 rpm for 2 mins. Cell pellets were resuspended in 2 ml arrest medium, which consisted of synthetic complete (SC) medium containing 3mM Methionine and 2% of glucose. Arrest cultures were incubated at 30°C for 4 hrs. Cells were then sedimented and washed thoroughly twice with ddH₂O. Cell cycle release was initiated by resuspension in SD-Met medium. Counting of polarized cells was started 15 mins post release with 10 mins

intervals. Cells were considered polarized once a concentrated GFP-Cdc42 fluorescence was observed on the cell periphery. Experiment was performed three times independent. Each data point represents 50 counts. Data was plotted against time using Excel sheet.

5.5.2. Mating projection (shmoo) assay

For the assay of shmoo formation MATa cells were grown overnight in YPD medium at 30°C with shaking. Cultures were diluted to $OD_{600} < 0.1$ and re-grown till $OD_{600} = 0.5-0.8$. Cells were then treated with 100 μ M alpha factor (Winder et al., 2003). Polarization was monitored at the 30 mins interval post alpha factor addition. Experiment was performed three times independent. Each data point represents 200 counts. Data was plotted against time using Excel sheet. Axis ratio calculation was performed on images taken 2 hrs post alpha factor addition.

6. Literature

- Adams, A.E., Botstein, D., and Drubin, D.G. (1991). Requirement of yeast fimbrin for actin organization and morphogenesis in vivo. *Nature* 354, 404-408.
- Alberts, B. (2007). *Molecular Biology of the Cell*.
- Altmann, K., Frank, M., Neumann, D., Jakobs, S., and Westermann, B. (2008). The class V myosin motor protein, Myo2, plays a major role in mitochondrial motility in *Saccharomyces cerevisiae*. *J Cell Biol* 181, 119-130.
- Amberg, D.C. (1998). Three-dimensional imaging of the yeast actin cytoskeleton through the budding cell cycle. *Mol Biol Cell* 9, 3259-3262.
- Amberg, D.C., Zahner, J.E., Mulholland, J.W., Pringle, J.R., and Botstein, D. (1997). Aip3p/Bud6p, a yeast actin-interacting protein that is involved in morphogenesis and the selection of bipolar budding sites. *Mol Biol Cell* 8, 729-753.
- Axelrod, D., Thompson, N.L., and Burghardt, T.P. (1983). Total internal inflection fluorescent microscopy. *J Microsc* 129, 19-28.
- Bamburg, J.R. (1999). Proteins of the ADF/cofilin family: essential regulators of actin dynamics. *Annu Rev Cell Dev Biol* 15, 185-230.
- Beningo, K.A., Lillie, S.H., and Brown, S.S. (2000). The yeast kinesin-related protein Smy1p exerts its effects on the class V myosin Myo2p via a physical interaction. *Mol Biol Cell* 11, 691-702.

- Bi, E., Maddox, P., Lew, D.J., Salmon, E.D., McMillan, J.N., Yeh, E., and Pringle, J.R. (1998). Involvement of an actomyosin contractile ring in *Saccharomyces cerevisiae* cytokinesis. *J Cell Biol* *142*, 1301-1312.
- Bidlingmaier, S., and Snyder, M. (2002). Large-scale identification of genes important for apical growth in *Saccharomyces cerevisiae* by directed allele replacement technology (DART) screening. *Funct Integr Genomics* *1*, 345-356.
- Bohil, A.B., Robertson, B.W., and Cheney, R.E. (2006). Myosin-X is a molecular motor that functions in filopodia formation. *Proc Natl Acad Sci U S A* *103*, 12411-12416.
- Brandman, O., Ferrell, J.E., Jr., Li, R., and Meyer, T. (2005). Interlinked fast and slow positive feedback loops drive reliable cell decisions. *Science* *310*, 496-498.
- Brockerhoff, S.E., Stevens, R.C., and Davis, T.N. (1994). The unconventional myosin, Myo2p, is a calmodulin target at sites of cell growth in *Saccharomyces cerevisiae*. *J Cell Biol* *124*, 315-323.
- Buttery, S.M., Yoshida, S., and Pellman, D. (2007). Yeast formins Bni1 and Bnr1 utilize different modes of cortical interaction during the assembly of actin cables. *Mol Biol Cell* *18*, 1826-1838.
- Carballido-Lopez, R. (2006). The bacterial actin-like cytoskeleton. *Microbiol Mol Biol Rev* *70*, 888-909.
- Carballido-Lopez, R., Formstone, A., Li, Y., Ehrlich, S.D., Noirot, P., and Errington, J. (2006). Actin homolog MreBH governs cell morphogenesis by localization of the cell wall hydrolase LytE. *Dev Cell* *11*, 399-409.
- Carrier, M.F. (1991). Nucleotide hydrolysis in cytoskeletal assembly. *Curr Opin Cell Biol* *3*, 12-17.
- Catlett, N.L., and Weisman, L.S. (1998). The terminal tail region of a yeast myosin-V mediates its attachment to vacuole membranes and sites of polarized growth. *Proc Natl Acad Sci U S A* *95*, 14799-14804.
- Chesarone, M., Gould, C.J., Moseley, J.B., and Goode, B.L. (2009). Displacement of formins from growing barbed ends by bud14 is critical for actin cable architecture and function. *Dev Cell* *16*, 292-302.
- Clark, K., Langeslag, M., Figdor, C.G., and van Leeuwen, F.N. (2007). Myosin II and mechanotransduction: a balancing act. *Trends Cell Biol* *17*, 178-186.
- Cramer, L.P., and Mitchison, T.J. (1995). Myosin is involved in postmitotic cell spreading. *J Cell Biol* *131*, 179-189.
- Diez, S., Gerisch, G., Anderson, K., Muller-Taubenberger, A., and Bretschneider, T. (2005). Subsecond reorganization of the actin network in cell motility and chemotaxis. *Proc Natl Acad Sci U S A* *102*, 7601-7606.

- Dong, Y., Pruyne, D., and Bretscher, A. (2003). Formin-dependent actin assembly is regulated by distinct modes of Rho signaling in yeast. *J Cell Biol* *161*, 1081-1092.
- Dunn, B.D., Sakamoto, T., Hong, M.S., Sellers, J.R., and Takizawa, P.A. (2007). Myo4p is a monomeric myosin with motility uniquely adapted to transport mRNA. *J Cell Biol* *178*, 1193-1206.
- Elion, E.A. (2000). Pheromone response, mating and cell biology. *Curr Opin Microbiol* *3*, 573-581.
- Estrada, P., Kim, J., Coleman, J., Walker, L., Dunn, B., Takizawa, P., Novick, P., and Ferro-Novick, S. (2003). Myo4p and She3p are required for cortical ER inheritance in *Saccharomyces cerevisiae*. *J Cell Biol* *163*, 1255-1266.
- Etienne-Manneville, S. (2004). Cdc42--the centre of polarity. *J Cell Sci* *117*, 1291-1300.
- Evangelista, M., Klebl, B.M., Tong, A.H., Webb, B.A., Leeuw, T., Leberer, E., Whiteway, M., Thomas, D.Y., and Boone, C. (2000). A role for myosin-I in actin assembly through interactions with Vrp1p, Bee1p, and the Arp2/3 complex. *J Cell Biol* *148*, 353-362.
- Evangelista, M., Pruyne, D., Amberg, D.C., Boone, C., and Bretscher, A. (2002a). Formins direct Arp2/3-independent actin filament assembly to polarize cell growth in yeast. *Nat Cell Biol* *4*, 260-269.
- Evangelista, M., Pruyne, D., Amberg, D.C., Boone, C., and Bretscher, A. (2002b). Formins direct Arp2/3-independent actin filament assembly to polarize cell growth in yeast. *Nat Cell Biol* *4*, 32-41.
- Evangelista, M., Zigmund, S., and Boone, C. (2003). Formins: signaling effectors for assembly and polarization of actin filaments. *J Cell Sci* *116*, 2603-2611.
- Frankel, S., and Mooseker, M.S. (1996). The actin-related proteins. *Curr Opin Cell Biol* *8*, 30-37.
- Fujiwara, T., Tanaka, K., Mino, A., Kikyo, M., Takahashi, K., Shimizu, K., and Takai, Y. (1998). Rho1p-Bni1p-Spa2p interactions: implication in localization of Bni1p at the bud site and regulation of the actin cytoskeleton in *Saccharomyces cerevisiae*. *Mol Biol Cell* *9*, 1221-1233.
- Geli, M.I., and Riezman, H. (1996). Role of type I myosins in receptor-mediated endocytosis in yeast. *Science* *272*, 533-535.
- Goldschmidt-Clermont, P.J., Machesky, L.M., Baldassare, J.J., and Pollard, T.D. (1990). The actin-binding protein profilin binds to PIP2 and inhibits its hydrolysis by phospholipase C. *Science* *247*, 1575-1578.
- Goode, B.L., and Eck, M.J. (2007). Mechanism and function of formins in the control of actin assembly. *Annu Rev Biochem* *76*, 593-627.

- Goodman, A., Goode, B.L., Matsudaira, P., and Fink, G.R. (2003). The *Saccharomyces cerevisiae* calponin/transgelin homolog Scp1 functions with fimbrin to regulate stability and organization of the actin cytoskeleton. *Mol Biol Cell* *14*, 2617-2629.
- Govindan, B., Bowser, R., and Novick, P. (1995). The role of Myo2, a yeast class V myosin, in vesicular transport. *J Cell Biol* *128*, 1055-1068.
- Hayashi, T., and Ip, W. (1976). Polymerization polarity of actin. *J Mechanochem Cell Motil* *3*, 163-169.
- Higashida, C., Miyoshi, T., Fujita, A., Ocegüera-Yanez, F., Monypenny, J., Andou, Y., Narumiya, S., and Watanabe, N. (2004). Actin polymerization-driven molecular movement of mDial1 in living cells. *Science* *303*, 2007-2010.
- Hodges, A.R., Bookwalter, C.S., Kremntsova, E.B., and Trybus, K.M. (2009). A Nonprocessive Class V Myosin Drives Cargo Processively When a Kinesin-Related Protein Is a Passenger. *Curr Biol*.
- Hoepfner, D., van den Berg, M., Philippsen, P., Tabak, H.F., and Hettema, E.H. (2001). A role for Vps1p, actin, and the Myo2p motor in peroxisome abundance and inheritance in *Saccharomyces cerevisiae*. *J Cell Biol* *155*, 979-990.
- Huckaba, T.M., Gay, A.C., Pantalena, L.F., Yang, H.C., and Pon, L.A. (2004). Live cell imaging of the assembly, disassembly, and actin cable-dependent movement of endosomes and actin patches in the budding yeast, *Saccharomyces cerevisiae*. *J Cell Biol* *167*, 519-530.
- Huckaba, T.M., Lipkin, T., and Pon, L.A. (2006). Roles of type II myosin and a tropomyosin isoform in retrograde actin flow in budding yeast. *J Cell Biol* *175*, 957-969.
- Huh, W.K., Falvo, J.V., Gerke, L.C., Carroll, A.S., Howson, R.W., Weissman, J.S., and O'Shea, E.K. (2003). Global analysis of protein localization in budding yeast. *Nature* *425*, 686-691.
- Hwang, E., Kusch, J., Barral, Y., and Huffaker, T.C. (2003). Spindle orientation in *Saccharomyces cerevisiae* depends on the transport of microtubule ends along polarized actin cables. *J Cell Biol* *161*, 483-488.
- Janke, C., Magiera, M.M., Rathfelder, N., Taxis, C., Reber, S., Maekawa, H., Moreno-Borchart, A., Doenges, G., Schwob, E., Schiebel, E., *et al.* (2004). A versatile toolbox for PCR-based tagging of yeast genes: new fluorescent proteins, more markers and promoter substitution cassettes. *Yeast* *21*, 947-962.
- Jansen, R.P., Dowzer, C., Michaelis, C., Galova, M., and Nasmyth, K. (1996). Mother cell-specific HO expression in budding yeast depends on the unconventional myosin myo4p and other cytoplasmic proteins. *Cell* *84*, 687-697.

- Johnston, G.C., Prendergast, J.A., and Singer, R.A. (1991). The *Saccharomyces cerevisiae* MYO2 gene encodes an essential myosin for vectorial transport of vesicles. *J Cell Biol* *113*, 539-551.
- Kaksonen, M., Sun, Y., and Drubin, D.G. (2003). A pathway for association of receptors, adaptors, and actin during endocytic internalization. *Cell* *115*, 475-487.
- Kaksonen, M., Toret, C.P., and Drubin, D.G. (2005). A modular design for the clathrin- and actin-mediated endocytosis machinery. *Cell* *123*, 305-320.
- Kamasaki, T., Arai, R., Osumi, M., and Mabuchi, I. (2005). Directionality of F-actin cables changes during the fission yeast cell cycle. *Nat Cell Biol* *7*, 916-917.
- Karpova, T.S., McNally, J.G., Moltz, S.L., and Cooper, J.A. (1998). Assembly and function of the actin cytoskeleton of yeast: relationships between cables and patches. *J Cell Biol* *142*, 1501-1517.
- Kikyo, M., Tanaka, K., Kamei, T., Ozaki, K., Fujiwara, T., Inoue, E., Takita, Y., Ohya, Y., and Takai, Y. (1999). An FH domain-containing Bnr1p is a multifunctional protein interacting with a variety of cytoskeletal proteins in *Saccharomyces cerevisiae*. *Oncogene* *18*, 7046-7054.
- Kovar, D.R., Kuhn, J.R., Tichy, A.L., and Pollard, T.D. (2003). The fission yeast cytokinesis formin Cdc12p is a barbed end actin filament capping protein gated by profilin. *J Cell Biol* *161*, 875-887.
- Lammers, M., Rose, R., Scrima, A., and Wittinghofer, A. (2005). The regulation of mDial1 by autoinhibition and its release by Rho*GTP. *Embo J* *24*, 4176-4187.
- Lappalainen, P., and Drubin, D.G. (1997). Cofilin promotes rapid actin filament turnover in vivo. *Nature* *388*, 78-82.
- Li, F., and Higgs, H.N. (2003). The mouse Formin mDial1 is a potent actin nucleation factor regulated by autoinhibition. *Curr Biol* *13*, 1335-1340.
- Li, R., and Wedlich-Soldner, R. (2009). Bem1 complexes and the complexity of yeast cell polarization. *Curr Biol* *19*, R194-195; author reply R195.
- Lillie, S.H., and Brown, S.S. (1992). Suppression of a myosin defect by a kinesin-related gene. *Nature* *356*, 358-361.
- Lillie, S.H., and Brown, S.S. (1994). Immunofluorescence localization of the unconventional myosin, Myo2p, and the putative kinesin-related protein, Smy1p, to the same regions of polarized growth in *Saccharomyces cerevisiae*. *J Cell Biol* *125*, 825-842.
- Lillie, S.H., and Brown, S.S. (1998). Smy1p, a kinesin-related protein that does not require microtubules. *J Cell Biol* *140*, 873-883.

- Lippincott, J., and Li, R. (1998). Sequential assembly of myosin II, an IQGAP-like protein, and filamentous actin to a ring structure involved in budding yeast cytokinesis. *J Cell Biol* *140*, 355-366.
- Longtine, M.S., DeMarini, D.J., Valencik, M.L., Al-Awar, O.S., Fares, H., De Virgilio, C., and Pringle, J.R. (1996). The septins: roles in cytokinesis and other processes. *Curr Opin Cell Biol* *8*, 106-119.
- Longtine, M.S., McKenzie, A., 3rd, Demarini, D.J., Shah, N.G., Wach, A., Brachat, A., Philippsen, P., and Pringle, J.R. (1998). Additional modules for versatile and economical PCR-based gene deletion and modification in *Saccharomyces cerevisiae*. *Yeast* *14*, 953-961.
- Matheos, D., Metodiev, M., Muller, E., Stone, D., and Rose, M.D. (2004). Pheromone-induced polarization is dependent on the Fus3p MAPK acting through the formin Bni1p. *J Cell Biol* *165*, 99-109.
- Matsumura, F. (2005). Regulation of myosin II during cytokinesis in higher eukaryotes. *Trends Cell Biol* *15*, 371-377.
- McConnell, R.E., and Tyska, M.J. (2007). Myosin-1a powers the sliding of apical membrane along microvillar actin bundles. *J Cell Biol* *177*, 671-681.
- Mermall, V., Post, P.L., and Mooseker, M.S. (1998). Unconventional myosins in cell movement, membrane traffic, and signal transduction. *Science* *279*, 527-533.
- Moore, T.I., Chou, C.S., Nie, Q., Jeon, N.L., and Yi, T.M. (2008). Robust spatial sensing of mating pheromone gradients by yeast cells. *PLoS One* *3*, e3865.
- Moseley, J.B., and Goode, B.L. (2005). Differential activities and regulation of *Saccharomyces cerevisiae* formin proteins Bni1 and Bnr1 by Bud6. *J Biol Chem* *280*, 28023-28033.
- Moseley, J.B., and Goode, B.L. (2006). The yeast actin cytoskeleton: from cellular function to biochemical mechanism. *Microbiol Mol Biol Rev* *70*, 605-645.
- Moseley, J.B., Sagot, I., Manning, A.L., Xu, Y., Eck, M.J., Pellman, D., and Goode, B.L. (2004). A conserved mechanism for Bni1- and mDial1-induced actin assembly and dual regulation of Bni1 by Bud6 and profilin. *Mol Biol Cell* *15*, 896-907.
- Munchow, S., Sauter, C., and Jansen, R.P. (1999). Association of the class V myosin Myo4p with a localised messenger RNA in budding yeast depends on She proteins. *J Cell Sci* *112 (Pt 10)*, 1511-1518.
- Nicholson-Dykstra, S., Higgs, H.N., and Harris, E.S. (2005). Actin dynamics: growth from dendritic branches. *Curr Biol* *15*, R346-357.
- Okada, K., Ravi, H., Smith, E.M., and Goode, B.L. (2006). Aip1 and cofilin promote rapid turnover of yeast actin patches and cables: a coordinated mechanism for severing and capping filaments. *Mol Biol Cell* *17*, 2855-2868.

- Paul, A.S., and Pollard, T.D. (2008). The role of the FH1 domain and profilin in formin-mediated actin-filament elongation and nucleation. *Curr Biol* *18*, 9-19.
- Pirani, A., Vinogradova, M.V., Curmi, P.M., King, W.A., Fletterick, R.J., Craig, R., Tobacman, L.S., Xu, C., Hatch, V., and Lehman, W. (2006). An atomic model of the thin filament in the relaxed and Ca²⁺-activated states. *J Mol Biol* *357*, 707-717.
- Pollard, T.D. (1984). Polymerization of ADP-actin. *J Cell Biol* *99*, 769-777.
- Pollard, T.D. (1986). Assembly and dynamics of the actin filament system in nonmuscle cells. *J Cell Biochem* *31*, 87-95.
- Pollard, T.D. (2007). Regulation of actin filament assembly by Arp2/3 complex and formins. *Annu Rev Biophys Biomol Struct* *36*, 451-477.
- Pollard, T.D., Blanchoin, L., and Mullins, R.D. (2000). Molecular mechanisms controlling actin filament dynamics in nonmuscle cells. *Annu Rev Biophys Biomol Struct* *29*, 545-576.
- Pollard, T.D.E., W.C. (2008). *Cell Biology* (Saunders Elsevier).
- Pring, M., Evangelista, M., Boone, C., Yang, C., and Zigmond, S.H. (2003). Mechanism of formin-induced nucleation of actin filaments. *Biochemistry* *42*, 486-496.
- Pruyne, D., Legesse-Miller, A., Gao, L., Dong, Y., and Bretscher, A. (2004). Mechanisms of polarized growth and organelle segregation in yeast. *Annu Rev Cell Dev Biol* *20*, 559-591.
- Pruyne, D.W., Schott, D.H., and Bretscher, A. (1998). Tropomyosin-containing actin cables direct the Myo2p-dependent polarized delivery of secretory vesicles in budding yeast. *J Cell Biol* *143*, 1931-1945.
- Quinlan, M.E., Heuser, J.E., Kerkhoff, E., and Mullins, R.D. (2005). *Drosophila* Spire is an actin nucleation factor. *Nature* *433*, 382-388.
- Riedl, J., Crevenna, A.H., Kessenbrock, K., Yu, J.H., Neukirchen, D., Bista, M., Bradke, F., Jenne, D., Holak, T.A., Werb, Z., *et al.* (2008). Lifeact: a versatile marker to visualize F-actin. *Nat Methods* *5*, 605-607.
- Romero, S., Le Clainche, C., Didry, D., Egile, C., Pantaloni, D., and Carlier, M.F. (2004). Formin is a processive motor that requires profilin to accelerate actin assembly and associated ATP hydrolysis. *Cell* *119*, 419-429.
- Rossanese, O.W., Reinke, C.A., Bevis, B.J., Hammond, A.T., Sears, I.B., O'Connor, J., and Glick, B.S. (2001). A role for actin, Cdc1p, and Myo2p in the inheritance of late Golgi elements in *Saccharomyces cerevisiae*. *J Cell Biol* *153*, 47-62.
- Sagot, I., Klee, S.K., and Pellman, D. (2002a). Yeast formins regulate cell polarity by controlling the assembly of actin cables. *Nat Cell Biol* *4*, 42-50.

- Sagot, I., Rodal, A.A., Moseley, J., Goode, B.L., and Pellman, D. (2002b). An actin nucleation mechanism mediated by Bni1 and profilin. *Nat Cell Biol* 4, 626-631.
- Schott, D., Ho, J., Pruyne, D., and Bretscher, A. (1999). The COOH-terminal domain of Myo2p, a yeast myosin V, has a direct role in secretory vesicle targeting. *J Cell Biol* 147, 791-808.
- Schott, D.H., Collins, R.N., and Bretscher, A. (2002). Secretory vesicle transport velocity in living cells depends on the myosin-V lever arm length. *J Cell Biol* 156, 35-39.
- Segal, M., Bloom, K., and Reed, S.I. (2000). Bud6 directs sequential microtubule interactions with the bud tip and bud neck during spindle morphogenesis in *Saccharomyces cerevisiae*. *Mol Biol Cell* 11, 3689-3702.
- Sheltzer, J.M., and Rose, M.D. (2009). The class V myosin Myo2p is required for Fus2p transport and actin polarization during the yeast mating response. *Mol Biol Cell* 20, 2909-2919.
- Sikorski, R.S., and Hieter, P. (1989). A system of shuttle vectors and yeast host strains designed for efficient manipulation of DNA in *Saccharomyces cerevisiae*. *Genetics* 122, 19-27.
- Staiger, C.J., Sheahan, M.B., Khurana, P., Wang, X., McCurdy, D.W., and Blanchoin, L. (2009). Actin filament dynamics are dominated by rapid growth and severing activity in the Arabidopsis cortical array. *J Cell Biol* 184, 269-280.
- Stevens, R.C., and Davis, T.N. (1998). Mlc1p is a light chain for the unconventional myosin Myo2p in *Saccharomyces cerevisiae*. *J Cell Biol* 142, 711-722.
- Sun, Y., Martin, A.C., and Drubin, D.G. (2006). Endocytic internalization in budding yeast requires coordinated actin nucleation and myosin motor activity. *Dev Cell* 11, 33-46.
- Tiedje, C., Sakwa, I., Just, U., and Hofken, T. (2008). The Rho GDI Rdi1 regulates Rho GTPases by distinct mechanisms. *Mol Biol Cell* 19, 2885-2896.
- Tokunaga, M., Imamoto, N., and Sakata-Sogawa, K. (2008). Highly inclined thin illumination enables clear single-molecule imaging in cells. *Nat Methods* 5, 159-161.
- Tokuo, H., Mabuchi, K., and Ikebe, M. (2007). The motor activity of myosin-X promotes actin fiber convergence at the cell periphery to initiate filopodia formation. *J Cell Biol* 179, 229-238.
- Trybus, K.M. (2008). Myosin V from head to tail. *Cell Mol Life Sci* 65, 1378-1389.
- Tyska, M.J., and Warshaw, D.M. (2002). The myosin power stroke. *Cell Motil Cytoskeleton* 51, 1-15.

- Vibert, P., Craig, R., and Lehman, W. (1993). Three-dimensional reconstruction of caldesmon-containing smooth muscle thin filaments. *J Cell Biol* *123*, 313-321.
- Wedlich-Soldner, R., Altschuler, S., Wu, L., and Li, R. (2003). Spontaneous cell polarization through actomyosin-based delivery of the Cdc42 GTPase. *Science* *299*, 1231-1235.
- Wedlich-Soldner, R., and Li, R. (2004). Closing the loops: new insights into the role and regulation of actin during cell polarization. *Exp Cell Res* *301*, 8-15.
- Wedlich-Soldner, R., Wai, S.C., Schmidt, T., and Li, R. (2004). Robust cell polarity is a dynamic state established by coupling transport and GTPase signaling. *J Cell Biol* *166*, 889-900.
- Weisman, L.S. (2006). Organelles on the move: insights from yeast vacuole inheritance. *Nat Rev Mol Cell Biol* *7*, 243-252.
- Wen, K.K., and Rubenstein, P.A. (2009). Differential regulation of actin polymerization and structure by yeast formin isoforms. *J Biol Chem* *284*, 16776-16783.
- Winder, S.J., Jess, T., and Ayscough, K.R. (2003). SCP1 encodes an actin-bundling protein in yeast. *Biochem J* *375*, 287-295.
- Winzeler, E.A., Shoemaker, D.D., Astromoff, A., Liang, H., Anderson, K., Andre, B., Bangham, R., Benito, R., Boeke, J.D., Bussey, H., *et al.* (1999). Functional characterization of the *S. cerevisiae* genome by gene deletion and parallel analysis. *Science* *285*, 901-906.
- Xu, C., Craig, R., Tobacman, L., Horowitz, R., and Lehman, W. (1999). Tropomyosin positions in regulated thin filaments revealed by cryoelectron microscopy. *Biophys J* *77*, 985-992.
- Xu, Y., Moseley, J.B., Sagot, I., Poy, F., Pellman, D., Goode, B.L., and Eck, M.J. (2004). Crystal structures of a Formin Homology-2 domain reveal a tethered dimer architecture. *Cell* *116*, 711-723.
- Yanagida, T. (2007). Muscle contraction mechanism based on actin filament rotation. *Adv Exp Med Biol* *592*, 359-367.
- Yang, H.C., and Pon, L.A. (2002). Actin cable dynamics in budding yeast. *Proc Natl Acad Sci U S A* *99*, 751-756.
- Yoo, H., Song, I., and Gweon, D.G. (2006). Measurement and restoration of the point spread function of fluorescence confocal microscopy. *J Microsc* *221*, 172-176.
- Young, M.E., Cooper, J.A., and Bridgman, P.C. (2004). Yeast actin patches are networks of branched actin filaments. *J Cell Biol* *166*, 629-635.
- Zhou, M., and Wang, Y.L. (2008). Distinct pathways for the early recruitment of myosin II and actin to the cytokinetic furrow. *Mol Biol Cell* *19*, 318-326.

Zot, H.G., and Pollard, T.D. (1993). Motility of myosin I on planar lipid surfaces. *Methods Cell Biol* 39, 51-63.